ORIGIN AND SULFUR ISOTOPE GEOCHEMISTRY OF THE GRUM DEPOSIT, ANVIL RANGE, YUKON TERRITORY, CANADA

BY

JANET S. MODENE

A thesis submitted in partial fulfillment

of the requirements for the degree of

MASTER OF SCIENCE

(Geology)

at the

UNIVERSITY OF WISCONSIN—MADISON

1982

TABLE OF CONTENTS

ACKNOWLEDGEMENTS

Original proposition of this project, guidance during it, valuable discussion and editing of the manuscript were given by W.C. Shanks. This project was funded by Cyprus Anvil Mining Corporation. Introduction to Anvil Range geology and extensive assistance by D.S. Jennings and other Cyprus Anvil geologists is greatly appreciated. Work and discussion with D.S. Jennings, D.J. Hanson, P. Nakai, R.S. Tolbert and G.A. Gorzynski improved my understanding of the Grum deposit. L.G. Woodruff and R.A. Zierenberg provided discussion and editing of the manuscript. E.N. Cameron greatly increased my background in economic geology through course work at the University of Wisconsin.

Permission to collect samples from Grum deposit drill core and to present company information was given by Cyprus Anvil Mining Corporation.

D. Fadness prepared thin and polished sections used in this study The scanning electron microscope and X-ray diffractometer at the University of Wisconsin were used and instruction in their use by R.A. Zierenberg is appreciated. S.W. Bailey assisted in interpretation of some XRD patterns.

Sulfur isotope geochemistry was done in the laboratories run by W.C. Shanks at the University of Wisconsin. Instruction and assistanc in laboratory procedures and mass spectrometric analysis were given by L.G. Woodruff. Instruction in initial stages of sample preparation was given by D.A. Mako. Some lab work was done by J.I Pounder during the summer of 1981.

Special thanks to L.G. Woodruff and R.A. Zierenberg for patience, support and distraction during this project.

* * * * *

All materials referenced in this thesis are on repository at the University of Wisconsin-Madison, Department of Geology, under file number U.W. 1743. See Appendix III for list of specimens on file.

LIST OF FIGURES

Figure

LIST OF TABLES

LIST OF PLATES

Plate

ORIGIN AND SULFUR ISOTOPE GEOCHEMISTRY OF THE GRUM DEPOSIT, ANVIL RANGE, YUKON TERRITORY, CANADA

Janet S. Modene

Abstract

The Grum deposit is one of several Zn-Pb-Ag mineral deposits located in the Anvil Range, south central Yukon Territory. The Anvil deposits are sediment-hosted stratiform sulfide deposits similar to well known deposits in Australia, Germany and western Canada. Lower Cambrian pelitic host sediments were deposited near the western flank of the Selwyn Basin, a Paleozoic epicontinental trough or extensional basin within a trailing continental margin miogeoclinal wedge. The sulfide deposits are associated with lenses of graphitic metapelite which occur at the transition between noncalcareous metapelites of the Hadrynian to Lower Cambrian Mt. Mye Formation and calcareous metapelites of the Lower Cambrian to Lower Ordovician Vangorda Formation. Mafic volcanic rocks are not directly associated with the deposits. The sulfide deposits and conformable host rocks have undergone greenschist to amphibolite grade metamorphism and complex deformation related to intrusion of the Cretaceous Anvil Batholith.

The Grum deposit consists of four sulfide horizons which occur in a fold nose that has been refolded into second phase recumbent S shaped folds. The lower two horizons are in the Mt. Mye Formation; the upper two horizons are in the Vangorda Formation. Steep and low angle faults disrupt the southeastern near surface end of the deposit.

Ore mineralogy in the Grum deposit consists of sphalerite and galena. Pyrite is the predominant iron sulfide and is abundant throughout the deposit. Chalcopyrite, tennantite-tetrahedrite, pyrrhotite, arsenopyrite and magnetite occur in minor amounts. Textures of the Grum ores reflect greenschist grade metamorphism. Ore minerals have been metamorphically recrystallized and coarsened, erasing syngenetic and early diagenetic features.

Lithofacies variations common to all the Anvil deposits tend to occur in a characteristic stratigraphic succession or "Anvil Cycle". A graphitic quartzitic sulfide bearing facies is usually basal or marginal and interfingers with unmineralized graphitic phyllite. Pyritic quartzitic ore occurs centrally and is overlain by massive pyritic sulfides. A massive sulfide plus barite facies commonly caps each cycle. Sericitic alteration zones, which are variably mineralized and silicified, inconsistently surround the sulfide horizons and are sometimes best developed in the footwall.

Sulfur isotope studies indicate that the lithofacies variations are reflected by variations in sulfide sulfur isotopic composition. Upward increasing $\delta^{34}S$ values could be explained by increasing temperature of the incoming fluids and mixing with sulfate-bearing seawater overlying an anoxic depositional basin. Inorganic reduction of sulfate carried by subsurface fluids took place within the sedimentary pile at temperatures above 250°C.

INTRODUCTION

Large, stratiform, shale-hosted, massive sulfide mineral deposits such as McArthur River, Mt. Isa and Broken Hill in Australia, Rammelsberg and Meggen in western Germany and Sullivan in British Columbia, have received a great deal of recent study. Similar, recently discovered deposits of the Selwyn Basin, northwestern Canada belong to the same class of deposits. Although they possess features similar to volcanogenic massive sulfides, these deposits have only a weak genetic linl with volcanism. They usually occur in intracratonic fault-controlled sedimentary basins (Gustafson and Williams, 1981; Krebs, 1978). Laminated pyrite-sphalerite-galena ores often occur as tabular to lensoidal bodies interlaminated with carbonaceous and calcareous shales and siltstones. Tuffaceous material and turbidite horizons are sometimes present. Altered, silicified or mineralized zones can occur beneath the deposits and are related to ore fluid influx. Metal zoning can be present in such zinc-lead-silver ores and barite is a common gangue mineral (Carne and Cathro, 1980). Shale-hosted, stratiform massive sulfide deposits, which range in age from Mid-Proterozoic to Mid-Paleozoic (Table 1) are extremely important sources of lead and zinc, containing on the order of 25% of the western world's zinc reserves (Large, 1980). Furthermore, some of the deposits contain significant copper (Mt. Isa and Rammelsberg) or barite (Meggen) orebodies (Large, 1980).

The Selwyn Basin of northwestern Canada (Fig. 1) is a major metallogenic province for lead, zinc, silver and tungsten (Mining Journal, 1980). In addition to the Mactung tungsten deposit, vein-type silver

DEPOSIT	AGE m.y.	Mt	Pb %	Zn %	Cu %	Ag gm/mt	B[1]	FWA[2]	REFERENCES
Broken Hill New South Wales	L.-M.Prot 1700	180	11.3	9.8	0.2	175			Lambert, 1976 Gustafson and Williams, 1981
Mt. Isa (Pb-Zn) Queensland	M.Prot 1650	88	7.1	6.1	0.06	7		X	Mathias and Clark, 1981 Gustafson and Williams, 1981 Finlow-Bates, 1979
McArthur River Northern Territories	M.Prot 1650	237	4.1	9.2	0.2	41	X		Lambert, 1976 Gustafson and Williams, 1981
Sullivan British Columbia	M.Prot 1430	155	6.6	5.7		68		X	Thompson and Panteleyev, 1976
Anvil Yukon	L.Camb	250	3.7	5.7		46	X	X	Cyprus Anvil Mining Corp.
Howard's Pass Yukon	L.Sil	100	1.5	6.0					Morganti, 1979
Rammelsberg West Germany	M.Dev	22	10.0	19.0	2.0	120	X	X	Large, 1980 Krebs, 1976
Meggen West Germany	M.Dev	60	1.3	10.0	0.02	1	X	X	Krebs, 1976; 1978
Tom Yukon	U.Dev	9	8.6	8.4		84	X	X	Carne, 1979

[1] B = barite
[2] FWA = footwall alteration

TABLE 1. Economic geology of stratiform, shale-hosted Zn-Pb sulfide deposits.

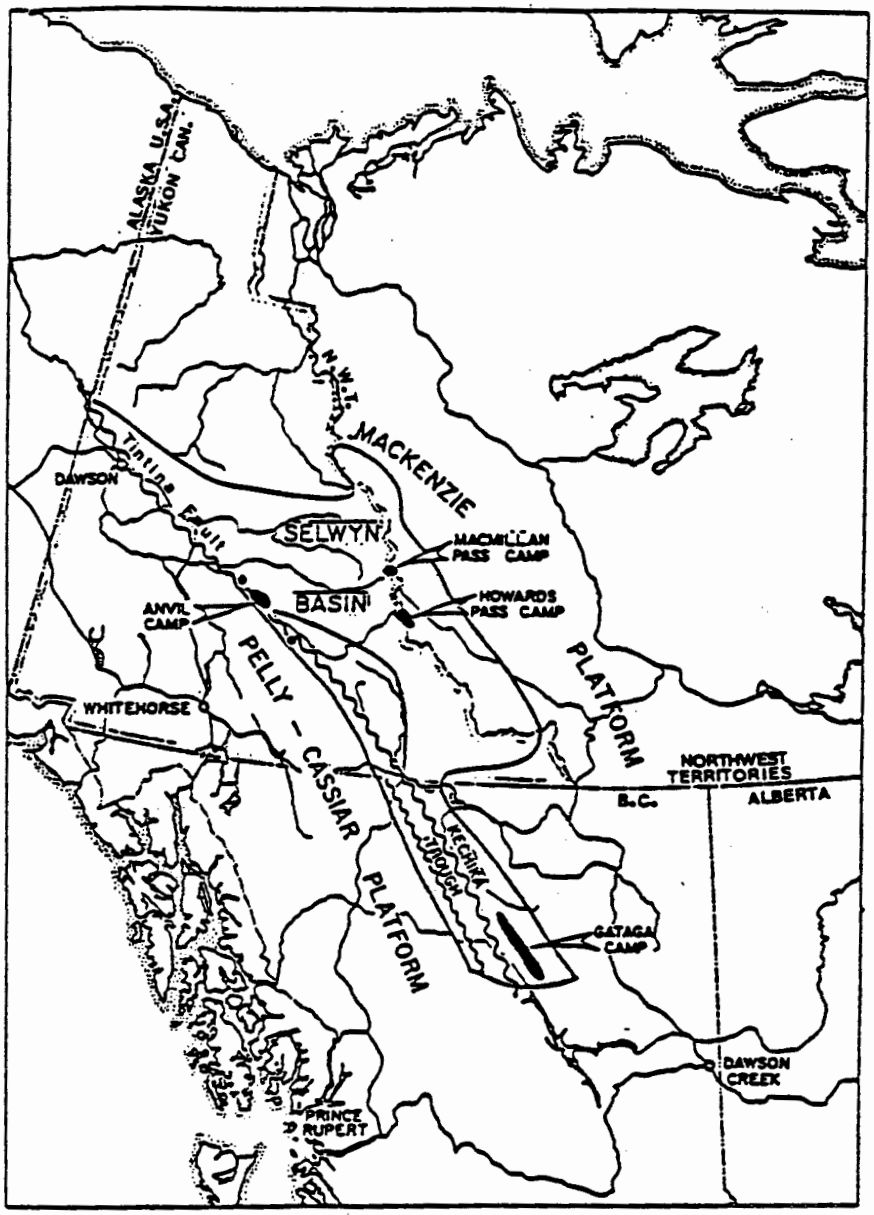

Fig. 1. Selwyn Basin location map showing the four principal camps of stratiform shale-hosted sulfide mineralization (modified after Carne and Cathro, 1980).

mineralization at Keno Hill and carbonate-hosted lead-zinc mineralization near the Mackenzie Platform, the Selwyn Basin contains large, shale-hosted stratiform zinc-lead-silver deposits of three different ages located primarily in four different camps (Fig. 1). Although prospecting techniques resulted in initial discovery of two of the camps in the early 1950's, many of the deposits have been discovered within the last decade. Minimum recoverable resources have been estimated at 43 Mt zinc, 20 Mt lead, and 25,000 mt silver (Carne and Cathro, 1980).

Lower Cambrian zinc-lead-silver-barite deposits of the Anvil district, including Grum, constitute the oldest shale-hosted mineralization in the Selwyn Basin. The XY and Anniv deposits of Howard's Pass Camp contain zinc-lead mineralization of Lower Silurian age. The Tom and Jason deposits of MacMillan Pass Camp, located 50 miles north of Howard's Pass along the Yukon-Northwest Territories border, contain Upper Devonian zinc-lead-silver-barite mineralization. Similar Upper Devonian mineralization is found in the Cirque and Driftpile deposits of the Gataga Camp in northeastern British Columbia. Barite is a major constituent of Upper Devonian mineralization and occurs without sulfides at the same stratigraphic level throughout the Selwyn Basin (Carne and Cathro, 1980).

Such large, shale-hosted stratiform massive sulfide deposits have been called submarine exhalative, sedimentary exhalative or SEDEX deposits because they are thought to have formed in active tectonic environments, precipitating at the sea floor from metalliferous, geothermally or magmatically heated brines that migrated upward along deep seated fault zones (Carne and Cathro, 1980; Large, 1980). Present

thinking is that the ore fluids consisted of recirculated seawater and/or convecting subsurface waters, which scavenged metals from underlying bedrock. Exhalation into anaerobic basins or subbasins and cooling allows metals to react with sulfide from reduced sulfate to precipitate sulfide minerals (Fig. 2).

LOCATION

The Anvil Range, southcentral Yukon Territory, contains 8 shale-hosted zinc-lead-silver massive sulfide deposits which have been discovered since 1953. The deposits occur along a northwesterly trend in the southern Anvil Range just north of the Pelly River between the towns of Carmacks and Ross River (Fig. 3). The town of Faro, built in 1969 as townsite for the Anvil Mine, is located about 25 kilometers northwest of Ross River and about 200 kilometers northeast of Whitehorse. A well-maintained dirt road runs north from the Robert Campbell Highway to Faro and to the mine, 15 kilometers north of town. The Grum deposit is located 8 kilometers northeast of Faro, near Vangorda Creek. A trailer camp on the Grum deposit site serves as a core storage facility and exploration headquarters.

EXPLORATION HISTORY

Initial discovery of the district occurred in 1953 when Ross River Indians and prospector Alan Kulan found a gossan outcrop of the Vangorda deposit in Vangorda Creek (Sirola, 1975). Prospector Airways optioned the property and diamond drilled the deposit between 1953 and 1955 (Brock, 1973). Kerr Addison Mines Ltd. of Toronto, Ontario, eventually acquired Prospector Airways but falling metal prices postponed

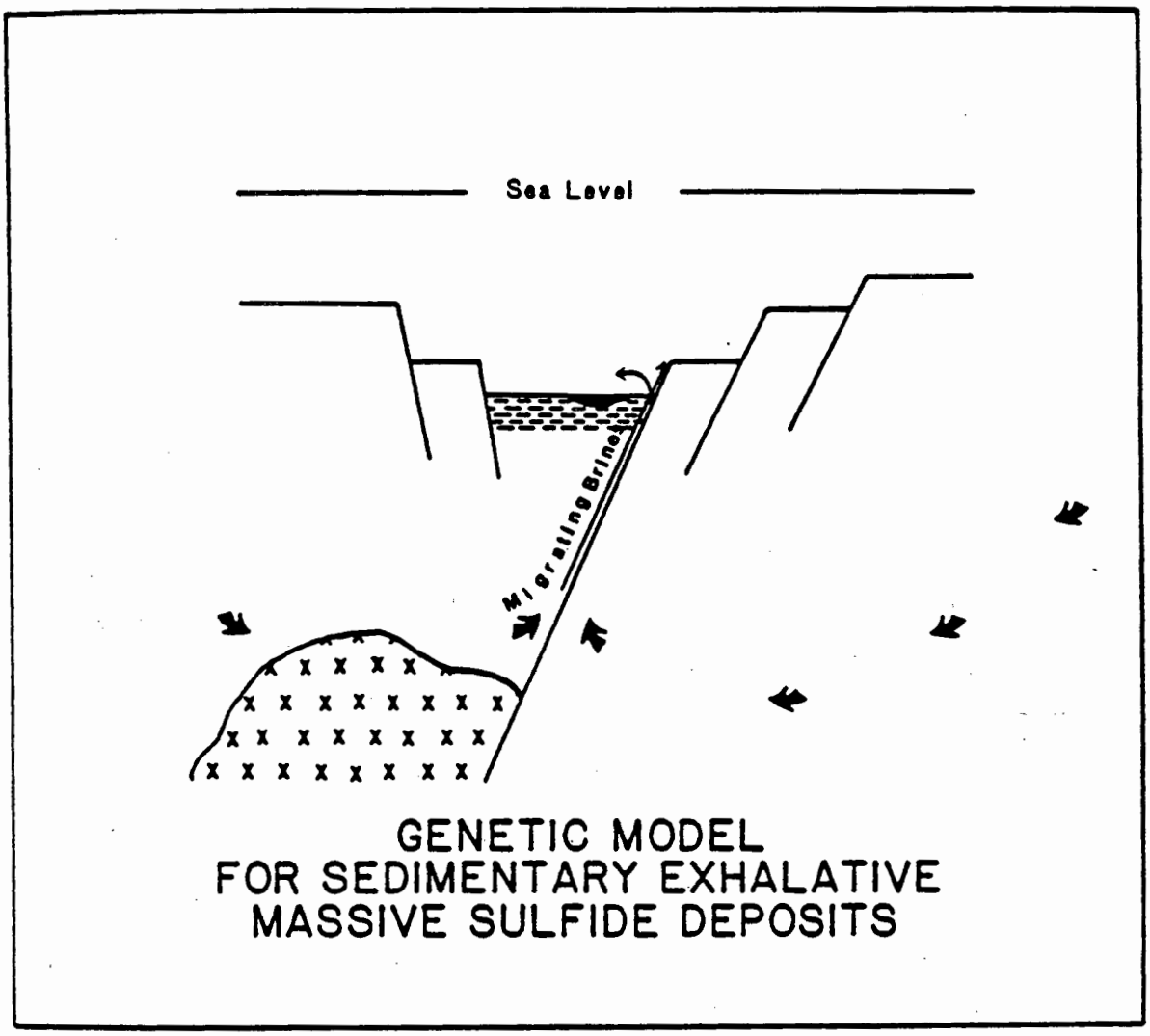

Fig. 2. Genetic model for "sedimentary exhalative" massive sulfide deposits. Heated metal-bearing subsurface brines migrate upward along deep seated faults and are exhaled into subbasins. Metals combine with sulfur from reduced sulfate to precipitate sulfide minerals at the sea-floor (modified after Carne and Cathro, 1980).

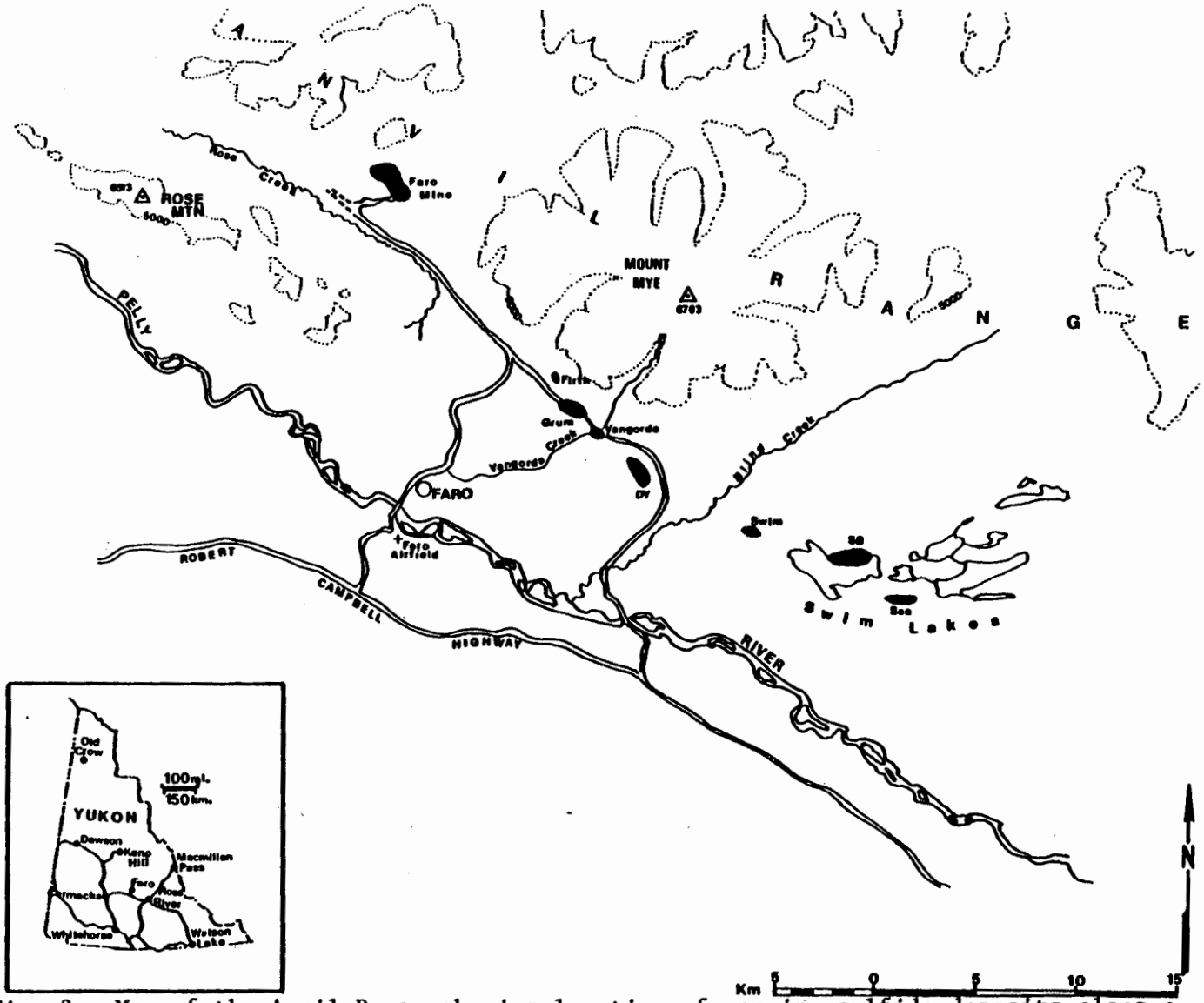

Fig. 3. Map of the Anvil Range showing location of massive sulfide deposits along a 35 km curvilinear trend on the southwest flank of the range.

the project (Pazour, 1979). In 1964, two years after resuming exploration, Kerr Addison Mines discovered the Swim deposit by drilling a geophysical anomaly 10 kilometers southeast of Vangorda. Swim was drilled in 1965 and 1966.

Aro Aho of Dynasty Exploration Ltd. began exploration in the Anvil Range in 1964 and, in a joint venture with Cyprus Mines Corporation of the United States, discovered the Faro orebody in 1965 through combined geochemical and geophysical methods (Brock, 1973). The joint venture staked 1800 claims in the area and by the end of 1965, Anvil Mining Corporation Ltd. was incorporated (Pazour, 1979). Concentrated drilling outlined the large Faro orebody and two subsidiary orebodies. In 1969, the town of Faro was built, as was a road between Carmacks and Ross River, so that mining and milling could begin.

In 1973, AEX Minerals Corporation discovered the Grum deposit while drilling a coincident gravity anomaly and high Turam response area on claims owned by Kerr Addison Mines in the Vangorda Creek area (Sirola, 1975). By July 1974, AEX Minerals had drilled 16 holes totalling 4000 meters on the Grum deposit. A joint venture to be managed by Kerr Addison Mines was formed, and by the end of 1974, 60 holes totalling 17,000 meters had been drilled at 60 meter spacing on sections 120 meters apart (Sirola, 1975; Cyprus Anvil Mining Corp., 1980). The size of the deposit outlined by this initial drilling program warranted additional underground exploration. Underground workings were developed by Kerr Addison in 1975-76. These consist of a 900 meter decline from the surface and two ramps which follow the plunge of the deposit and are connected by crosscuts every 120 meters. Ring drilling in the

plane of previously drilled sections was done at 60 meter intervals from the ramps, resulting in 15,000 meters of additional core. 2900 meters of openings comprise the underground workings, which are now flooded. During underground exploration, an additional 24,000 meters of surface holes completed a 60 meter grid with some fill-in holes at 30 meter spacing (Cyprus Anvil Mining Corp., 1980; Sirola, 1975). Kerr Addison geologists interpreted the structure and stratigraphy of the deposit in a general way using surface holes, underground holes, and data from underground mapping. They distinguished two ore types and three host rock types. Metallurgical testing of Grum ore and development of a computer based mine model were also done by Kerr Addison.

In 1974, Dynasty Exploration Ltd. merged with Anvil Mining Corporation to form Cyprus Anvil Mining Corporation (Pazour, 1979). The new corporation discovered the DY deposit in 1976 by drilling a stratigraphic target at depths greater than 300 meters. In 1978, Cyprus Anvil acquired the Kerr Addison interests, including Grum.

Taking advantage of a greater understanding of district and deposit geology resulting from detailed regional mapping and development of the Faro orebodies, Cyprus Anvil geologists initiated an extensive program of relogging and resampling of the 56,000 meters of Grum drill core in 1980. In addition, limited new drilling was completed in 1981. This program is leading to a significantly better understanding of the Grum deposit and to reinterpretation of deposit geometry. The structural picture emerging for the Grum deposit is proving to be an aid in interpretation of the other less intensively drilled deposits.

Tonnage and grade estimates for five of the Anvil deposits are

shown in Table 2. Presently, mining of the Faro deposit continues. Vangorda and Grum deposits are close to production, and the DY and Swim deposits are still being explored. Mining of the Faro open pit is by truck haulage. Ultimate dimensions of the pit will be 4700 feet by 3200 feet by 986 feet deep (Pazour, 1979). One of the subsidiary Faro orebodies has already been mined out and mining of the third zone is underway. Milling operations, which exist at the mine site, can process 10,000 tons per day, producing bulk concentates as well as lead and zinc concentrates by crushing, grinding, flotation circuits and drying (Pazour, 1979). Concentrates are trucked to Whitehorse, transported to Skagway, Alaska by railroad and then shipped to Japanese and West German markets. Mining and milling continues year-round.

The DY deposit is both large and high grade, but the 300 meter depth of the deposit creates problems for continuing exploration. Vangorda, though small, has the advantage of being a near surface deposit. Swim is also small but faulted extensions to the deposit may exist. Firth appears to be uneconomic. SB and Sea are in preliminary stages of exploration.

The Grum ore body, which is the second or third largest of the Anvil district deposits, has an areal extent of approximately 1200 by 400 meters and is roughly 300 meters thick. It is buried beneath 20 to 40 meters of overburden in the southeastern corner, and 150 meters of overburden and Vangorda Formation lithologies in the northwestern corner. Total tonnage is 60 to 80 Mt, reserves are 30.78 Mt and grade, above a 4% combined lead-zinc cut-off, is 4.9% zinc, 3.1% lead, and 49 gm/mt silver. Copper values are about 0.2%.

TABLE 2. Tonnage, reserves, grade and discovery of Anvil Range deposits (from Cyprus Anvil Mining Corporation report, November, 1981).

	Tonnage[1] mt x 10^6	Reserves[2] mt x 10^6	Zn %	Pb %	Ag gm/mt		Discovery
Faro[3]	64-68	57.6	5.7	3.4	35	1965	Dynasty Exploration and Cyprus Mines; geophysics and geochemistry
Grum	60-80	30.8	4.9	3.1	49	1973	AEX Syndicate; geophysics
Vangorda	22	4.9	4.3	3.3	48	1953	Al Kulan; prospecting
DY	80-100	20.3	7.0	5.7	82	1976	Cyprus Anvil Mining Corporation; stratigraphic drilling
Swim	8	4.7	4.7	3.8	42	1964	Kerr Addison; geophysics
Total Anvil District	234-278	113.6	5.7	3.7	46		

[1] Estimated total sulfide resource

[2] Reserves calculated above 4% Pb+Zn cutoff for Grum and Vangorda, 5% for Faro, 6% for Swim, 9% for DY

[3] Tonnage and reserve for Faro reported prior to mining

PREVIOUS GEOLOGIC WORK

Excellent understanding of Anvil Range geology and of the Anvil deposits has resulted from largely unpublished field investigations by David Jennings, Gregg Jilson and several other Cyprus Anvil Mining Corporation geologists. In 1972, Templeman-Kluit of the Geological Survey of Canada published a study of the Faro, Vangorda and Swim deposits based largely on his examination of drill core belonging to Anvil Mining Corporation and Kerr Addison Mines Ltd. In 1974, Campbell and Ethier published a study of sulfur isotopes and iron content of sphalerites in the Faro deposit. In conjunction with Cyprus Anvil geologists, Barry Ryan, formerly of the University of British Columbia, has recently studied lead isotope systematics of ore samples from Anvil district deposits. Also in conjunction with Cyprus Anvil, W.C. Shanks of the University of Wisconsin is currently undertaking a stable isotope study of the DY deposit. Two fairly extensive company reports dealing with the Grum deposit were written during ownership by Kerr Addison Mines. Carson (1977) studied the metallurgy of the ores, and Paxton and Po (1978) described and interpreted the geology as observed in drill core and in underground workings of Grum.

SULFUR ISOTOPE SYSTEMATICS AND STRATIFORM SULFIDE DEPOSITS

Recent sulfur isotope studies have placed constraints upon several aspects of the genesis of stratiform, sediment-hosted sulfide deposits. In particular, sulfur isotope systematics in conjunction with careful geologic observations can place firm constraints on the source of sulfate, the mechanism and locus of sulfate reduction, the nature of the

depositional basin and the nature of the ore fluid.

Because sulfate reduction reactions are thought to be important in the genesis of many stratiform sulfide deposits, the source of sulfate is an important consideration. Three possible sources of sulfate are: (1) contemporary seawater sulfate within the depositional basin, (2) contemporary seawater sulfate recirculated to depths, or (3) sulfate of other origins carried by subsurface waters within underlying sedimentary formations. Sulfate carried by subsurface waters could have been leached from evaporites within the sequence. Sangster (1968, 1976) inferred a seawater sulfate source for many stratiform sulfide deposits by comparison of sulfur isotopic compositions with an age curve for seawater sulfate composition (Fig. 4). However, Gustafson and Williams (1981) have re-examined such data and conclude that there is little correlation.

Sulfur isotope systematics can place constraints upon the mechanism and locus of sulfate reduction. The exact mechanism of sulfate reduction controls the reaction rates and therefore the degree of ^{34}S depletion in H_2S and sulfide minerals relative to sulfate (Fig. 5). At temperatures above 250°C, sulfate can be reduced to form H_2S by reaction with ferrous iron bearing minerals in the wall rocks (Shanks et al., 1981; Ohmoto and Rye, 1979), but reaction rates for inorganic sulfate reduction are known to be geologically slow at temperatures below 250°C (Sakai and Dickson, 1978; Shanks et al., 1981). Studies of oil field brines indicate that sulfate bearing waters can undergo sulfate reduction reactions if brought into contact with organic-rich sedimentary sequences at temperatures above 80-120°C (Orr, 1974, 1975).

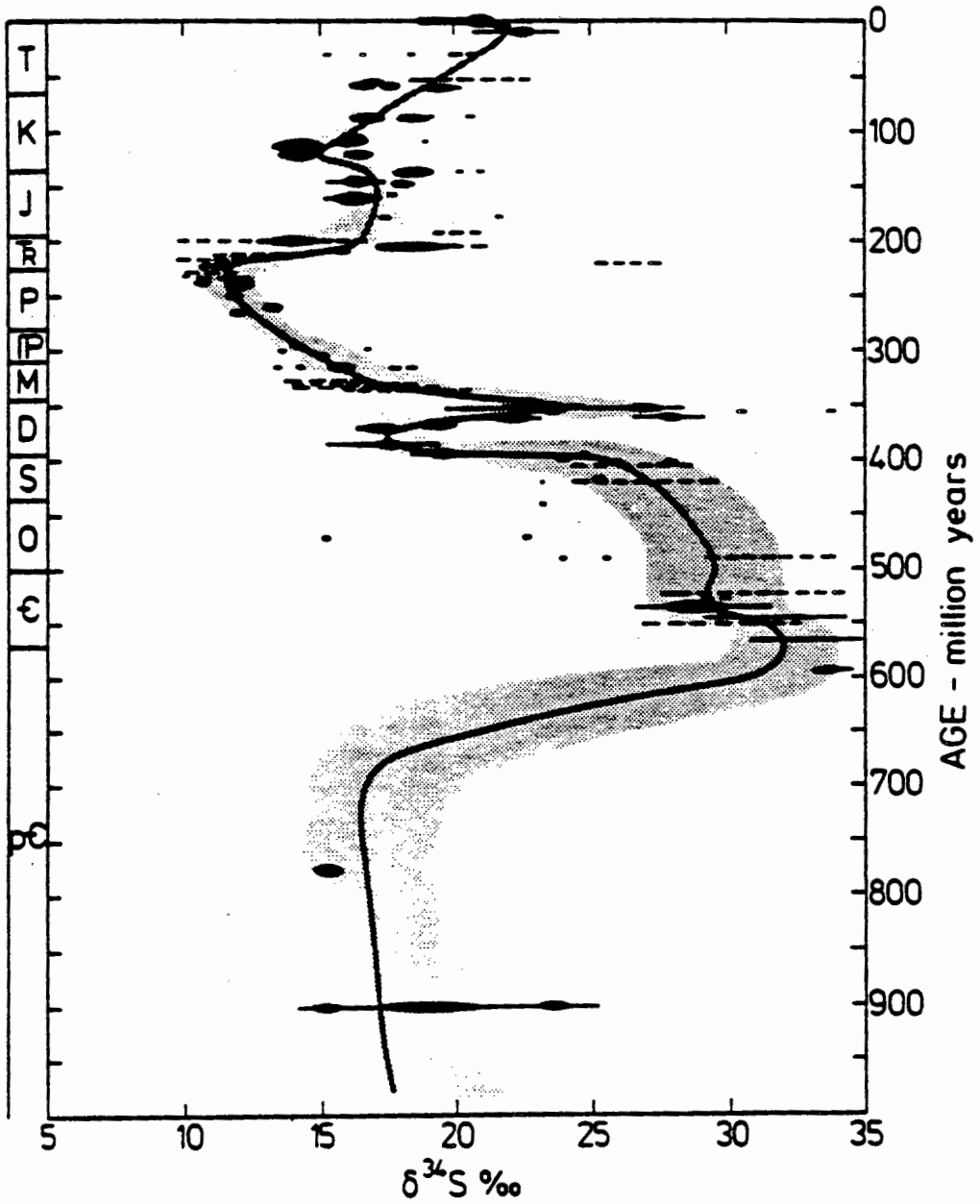

Fig. 4. Summary sulfur isotope age curve for marine sulfate (from Claypool et al., 1980).

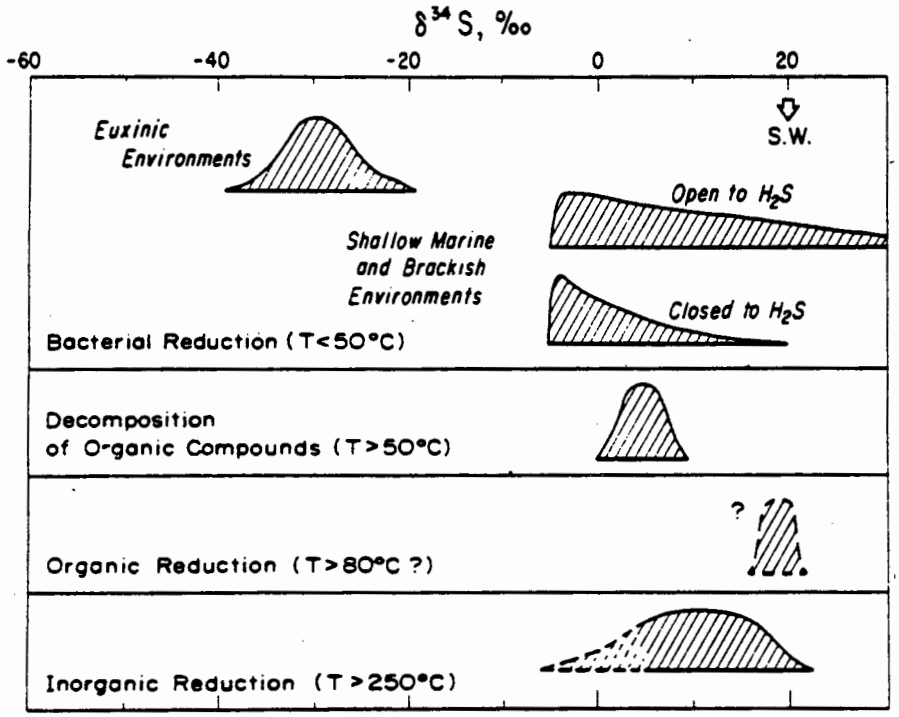

Fig. 5. Distribution pattern for $\delta^{34}S$ values of H_2S and sulfide minerals when sulfate of $\delta^{34}S$ = 20 o/oo is reduced by various mechanisms. S.W. is seawater (from Ohmoto and Rye, 1979).

Sulfate reducing bacteria are known to mediate reactions at temperatures below 50°C (Kaplan and Rittenberg, 1964). Bacterial sulfate reduction is the mechanism most often called upon to explain sulfate reduction which takes place during or after deposition. However, if the temperature of the incoming fluids is hot enough, inorganic sulfate reduction can account for reduction of contemporary seawater sulfate at the site of deposition.

A second possible locus of sulfate reduction is at depth. Recirculated seawater or sulfate-bearing subsurface waters could be heated geothermally or by intrusive bodies to temperatures of organic or inorganic sulfate reduction. In this case, the $S_{oxidized}/S_{reduced}$ ratio in the fluid and the isotopic composition of the source sulfate would control sulfur isotopic composition of precipitated sulfide minerals. It is possible that both sulfate reduction at depth and sulfate reduction at deposition could have been involved in the formation of a single stratiform sulfide deposit.

Sulfur isotopic variation within a deposit can perhaps place constraints upon the nature and evolution of the depositional processes. In particular, the $\delta^{34}S$ of H_2S is dependent upon the mole ratio of total sulfate to total sulfide species in the system which is in turn a function of fO_2, pH, and temperature (Ohmoto and Rye, 1979). Trends in the value of $\delta^{34}S$ through some deposits have been related to changes in these parameters through time.

Sulfur isotope systematics are effected by the mixing behavior of the ore fluid and the nature of the bottom waters. If sulfate reduction occurs at deposition, mixing of the ore fluid with oxygenated or

sulfate bearing seawater will effect the $\delta^{34}S$ of precipitating sulfides. The degree of mixing with seawater will be a function of temperature and salinity of the incoming fluid. Studies of brine behavior indicate that a cool, highly saline fluid will produce bottom hugging currents which extablish a stratified brine/seawater interface (Sato, 1972; Turner and Gustafson, 1978). Higher temperature and less saline fluids could rise up as bouyant plumes, mixing with seawater immediately upon exhalation. If, however, bottom waters are anoxic and sulfate free, then mixing may have little effect on sulfur isotope systematics.

Because many massive sulfide deposits have undergone post-depositional deformation and metamorphism, the effect of metamorphism upon sulfur isotope distribution is an important consideration. Rye and Ohmoto (1974) conclude from detailed studies of Homestake, Bathhurst, and Ducktown that metamorphism causes small scale changes in sulfur isotopic composition, such as redistribution among coexisting minerals and local variations related to structure. Large scale variations such as isotopic signatures of formations seem to be preserved. This observation implies that large amounts of sulfur were not added to or subtracted from these systems during metamorphism (Rye and Ohmoto, 1974) and that stratigraphic variations of $\delta^{34}S$ values in metamorphosed sedimentary ore deposits have genetic significance.

OBJECTIVES AND SCOPE OF STUDY

The present study focuses on the petrography and sulfur isotope geochemistry of the Grum deposit. Grum has been drilled extensively enough to provide a sound structural framework for interpretation of

stable isotope data. Specific objectives of the sulfur isotope study are examination of sulfur isotopic compositions for evidence of the source of sulfate, the mechanism of sulfate reduction and the physiochemical conditions of ore deposition. Vertical sections through sulfide horizons are analyzed for $\delta^{34}S$ variation to better define or explain the lithofacies variations. Laterally equivalent intersections through two sulfide horizons are analyzed to see if lateral variations in $\delta^{34}S$ can provide evidence for basin geometry or ore fluid influx. Intersections from different sulfide horizons are analyzed for variations which might enable correlation of horizons in badly deformed and faulted sections of the ore deposit.

GEOLOGIC SETTING

REGIONAL TECTONIC SETTING: THE CANADIAN CORDILLERA

The Canadian Cordillera can be subdivided into five geological and physiographic provinces (Fig. 6). The Rocky Mountain Belt, which includes the Selwyn Basin, consists of a northeasterly tapering wedge of Mid-Proterozoic to Upper Jurassic miogeoclinal and platformal carbonates and craton-derived clastics overlain by horizontally compressed and displaced Mesozoic and Cenozoic sedimentary rocks. The Omineca Crystalline Belt contains local Precambrian basement, Mid-Proterozoic to Mid-Paleozoic miogeoclinal lithologies, Paleozoic and Mesozoic volcanogenic and pelitic rocks, and Jurassic and Cretaceous plutonic rocks. Upper Paleozoic to Late Tertiary marine and non-marine volcanic and sedimentary rocks comprise the Intermontane Belt along with local

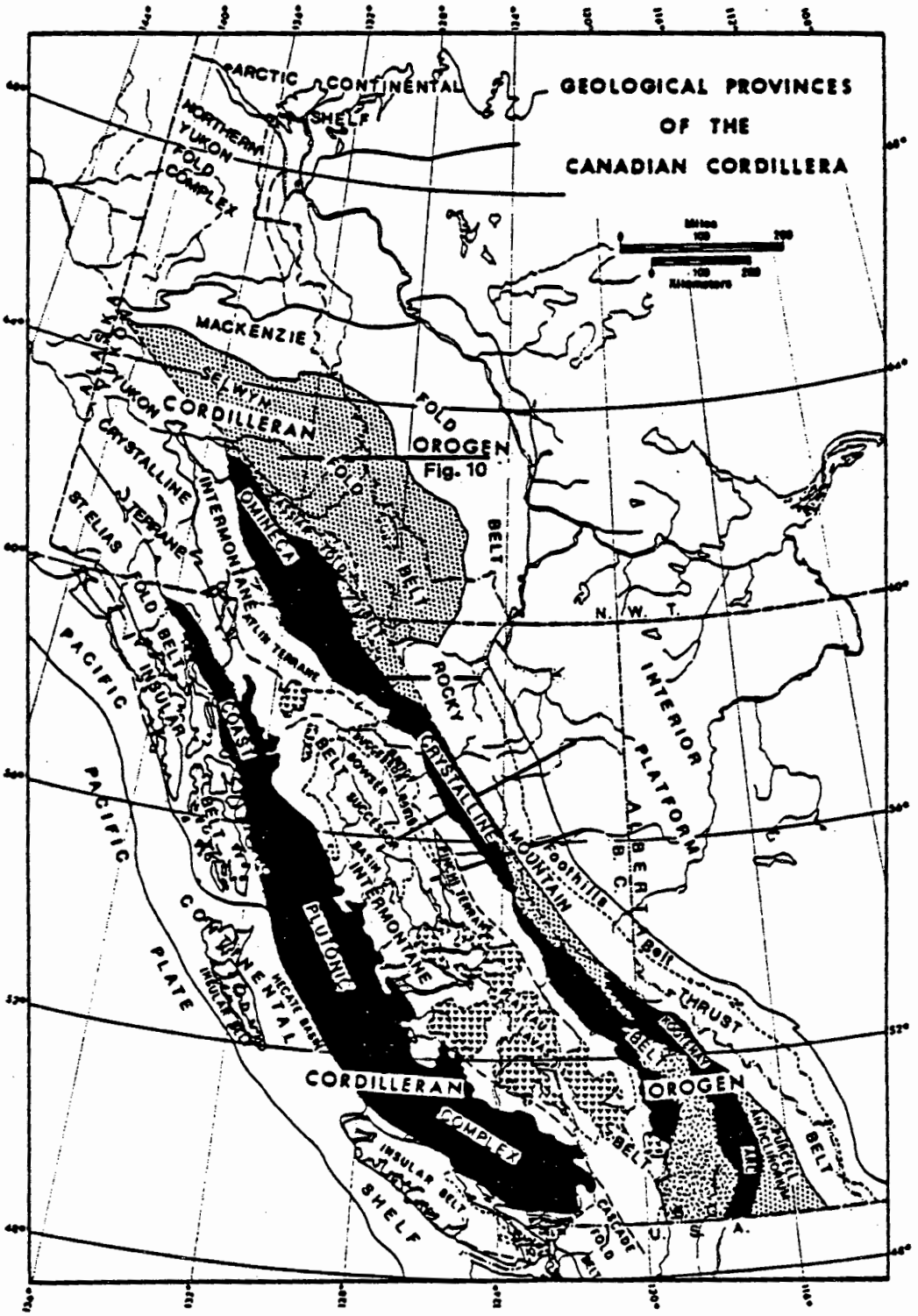

Fig. 6. Geological provinces of the Canadian Cordillera (modified after Gabrielse, 1976).

ultramafic rocks and granitic plutons. Cretaceous and Tertiary granitic plutons dominate the Paleozoic to Tertiary sedimentary and volcanic strata of the Coast Plutonic Complex. The Insular Belt consists of variably deformed, Phanerozoic volcanic and sedimentary strata (Wheeler et al., 1972; Douglas et al., 1980; Monger et al., 1982).

Precambrian crystalline basement, which extends westward from the Canadian shield to the eastern edge of the Omineca Crystalline Belt coincides with an ancient continental margin established by Helikian opening of a proto-Pacific Ocean (Coney et al., 1980; Monger and Price, 1979). A Precambrian rifting event in the Canadian Cordillera is inferred from the progressive out-building of Late Proterozoic and Early Paleozoic miogeoclinal sediments (Coney et al., 1980; Monger and Price, 1979).

Thick prisms of Late Proterozoic sediments, which prograded westward off a stable trailing margin into an Atlantic-style expanding ocean, consist of the Helikian Purcell strata and the Hadrynian Windermere Grit Unit (Wheeler et al., 1972). Helikian sediments of the Purcell sequence thicken from 3 km in the east to 12 km in the west (Monger et al., 1972; Monger and Price, 1979). Deposition spanned a 600 million year period from 1450 to 850 my (Gabrielse, 1972). Lithologies are primarily argillites, siltstones, fine-grained sandstones and carbonates. Local occurrences of conglomerates, coarse sandstones, redbeds and bedded gypsum as well as basalt flows, sills and dikes, in the Purcell sequence, reflect the Helikian rift environment (Gabrielse, 1972). Shallow water and intertidal sedimentary structures such as mudcracks, dessication breccias, and stromatolites characterize the

eastern rocks. Western strata grade from early, deep water, quartz-sand turbidite sequences to younger tidal flat, flood plain, and carbonate bank sediments (Gabrielse, 1972; Monger and Price, 1979). A comparison with sedimentation in the Gulf of Mexico implies deposition of Purcell sediments on tidal flats and flood plains as part of a prograding deltaic complex (Thompson and Panteleyev, 1976).

The Racklan orogeny interrupted the miogeoclinal depositional regime causing unconformity between Helikian and overlying Hadrynian strata. Northeasterly folding, tilting, block faulting and uplift created spectacular angular unconformities between the deformed Purcell rocks and the overlying Windermere Grit Unit (Douglas et al., 1970; Gabrielse, 1972). Minor basic volcanism is spatially related to the faults (Monger et al., 1972). It is uncertain if this orogeny resulted from short-lived subduction (Monger et al., 1972) or perhaps from renewed rifting.

Unlike the poorly exposed Purcell strata, Hadrynian Windermere rocks, 800-600 my, outcrop continuously in the Omineca Crystalline and Rocky Mountain Belts (Monger et al., 1972). Thicknesses vary up to a maximum of 4500 meters. In general, the unit thickens westward and the site of maximum thickness lies west of that for Purcell strata (Monger et al., 1972). The upper contact is a regional unconformity in the east but is conformable to overlying Cambrian strata in the west (Gabrielse, 1972). Thicknesses, lithologies, facies changes, westerly fining grain sizes, and sedimentary structures which indicate a westerly direction of transport, all imply a cratonic source for the material (Gabrielse, 1972). Lithologies of the lower part of the Winder-

mere include poorly sorted, immature, locally graded, quartzo-feldspathic grit, sandstone and shale, with thick sequences of basic and andesitic volcanics, minor cherty jasper-hematite iron formations, and basal conglomerates or conglomeratic mudstones (Wheeler et al., 1972). The lithologies of the upper part of the Windermere Grit Unit include thick limestone and dolomite sequences, argillaceous limestones and calcareous phyllites (Gabrielse, 1972). Windermere sediments represent a continental margin wedge prograded west of the Purcell rocks. Sediment immaturity suggests an eastern source area of high relief created by the Racklan uplift (Gabrielse, 1972). A depositional environment envisaged for the Windermere Grit Unit is one of relatively deep water with periodic introduction of coarse material by turbidity currents (Monger et al., 1972). The basal conglomerates are variously interpreted as glacial tillites, subaqueous mudflows, or coarse stream deposits slumped into coastal basins (Wheeler et al., 1972; Eisbacher, 1980; Gabrielse, 1972). The upper carbonates represent shallow deposition resulting from infilling of the basin (Monger et al., 1972).

Early to Mid-Paleozoic strata in the eastern Canadian Cordillera represent the continuation of trailing margin deposition. Lithologies include shales and carbonates displaying distinct linear facies relations of continental shelf, rise and slope deposits (Monger et al., 1972; Monger and Price, 1979). The location of the shale-carbonate facies transition remained between the Alberta, McDonald and Mackenzie arches and platforms, and the adjacent Alberta, Kechika and Selwyn troughs and basins until Late Devonian time (Wheeler et al., 1972;

Fig. 7). Cambrian strata include trilobite-bearing shales, shallow water carbonates with archaeocyathids, and minor mafic volcanics (Wheeler et al., 1972). Ordovician through Mid-Devonian lithologies consist of carbonate reefs on the platform and up to 4000 meters of argillaceous and limey clastics west of the platform. Occasional Ordovician to Mid-Devonian mafic pillowed flows and pyroclastic deposits occur in the outer shale facies and near the carbonate-shale facies transition (Wheeler et al., 1972).

The southeastern part of the Canadian Cordillera maintained its miogeoclinal character in Late Devonian to Early Mississippian time, accumulating thin incomplete sequences of carbonate, quartz-sand, phosphate and chert (Gabrielse, 1972; Wheeler et al., 1972). However, Mid-Devonian carbonates of the Selwyn Basin and Mackenzie Platform are overlain by chert pebble conglomerates and chert arenites (Gabrielse, 1976). Identification of the source of the chert-bearing clastic sediments has become a problem. Monger and Price (1979) suggest that widespread subsidence of the miogeoclinal terrain in Late Devonian time, occurring in a marginal basin behind a west facing volcanic arc could have led to the deposition of arc-derived sediments.

Rocks which lie west of the Rocky Mountain Belt are beyond the edge of thick Precambrian crystalline basement and must have accreted onto the North American craton. Several allocthonous (or suspect) terranes have been identified, and attempts to understand the nature and timing of collisional suturing of these terranes to the craton has occupied recent investigations of the Canadian Cordillera (Monger et al., 1982; Coney et al., 1980; Monger and Price, 1979).

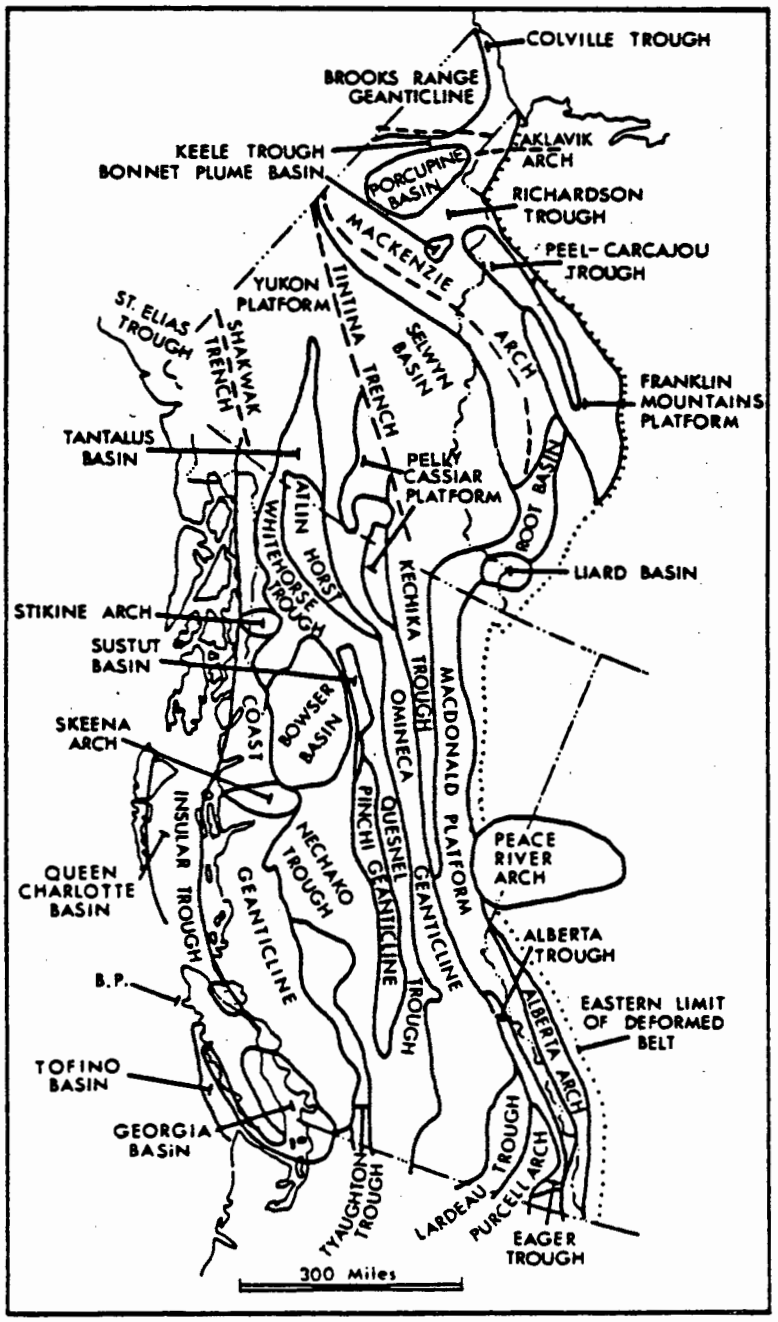

Fig. 7. Tectonic elements of the Canadian Cordillera (from Wheeler et al., 1972).

Suspect terranes identified within the Canadian Cordillera include the Eastern Assemblage in the Omineca Crystalline Belt, the Cache Creek and Stikine terranes in the Intermontane Belt and the Wrangellia and Alexander terranes in the Coast Plutonic and Insular Belts (Fig. 8). The Eastern Assemblage is a composite terrane containing fragments of Paleozoic metamorphic rocks of possible continental affinity as well as basalts, ultramafics, cherts, volcaniclastics and carbonates. Cache Creek terrane contains Late Paleozoic to Early Mesozoic oceanic crustal fragments: ultrabasics, gabbros, pillow lavas, radiolarian cherts, and shallow water fusulinid bearing carbonates (Coney et al., 1980; Wheeler et al., 1972). Stikinia contains fragments of oceanic arcs: Late Paleozoic volcaniclastics, volcanics and carbonates deformed and intruded in middle to Late Triassic time (Coney et al., 1980; Monger et al., 1982). Wrangellia and Alexander, which are thought to have amalgamated prior to collisional suturing onto the craton, contain abundant late Triassic basalts possibly indicative of rifting events or intraplate volcanism (Coney et al., 1980).

Allocthonous terranes became accreted onto the craton coincident with westward migration of the North American plate and it is possible that east dipping subduction zones repeatedly "stepped outboard" through successive accretions (Coney et al., 1980). During convergence, imbricate thrusting of miogeoclinal rocks in the Rocky Mountain Belt and obduction of terranes unto the craton occurred, as did subduction-related intrusion of granitic plutons. The collisional suture developed into dextral transcurrent faults possibly by Mid-Cretaceous time resulting in large displacements such as 450 kilometers

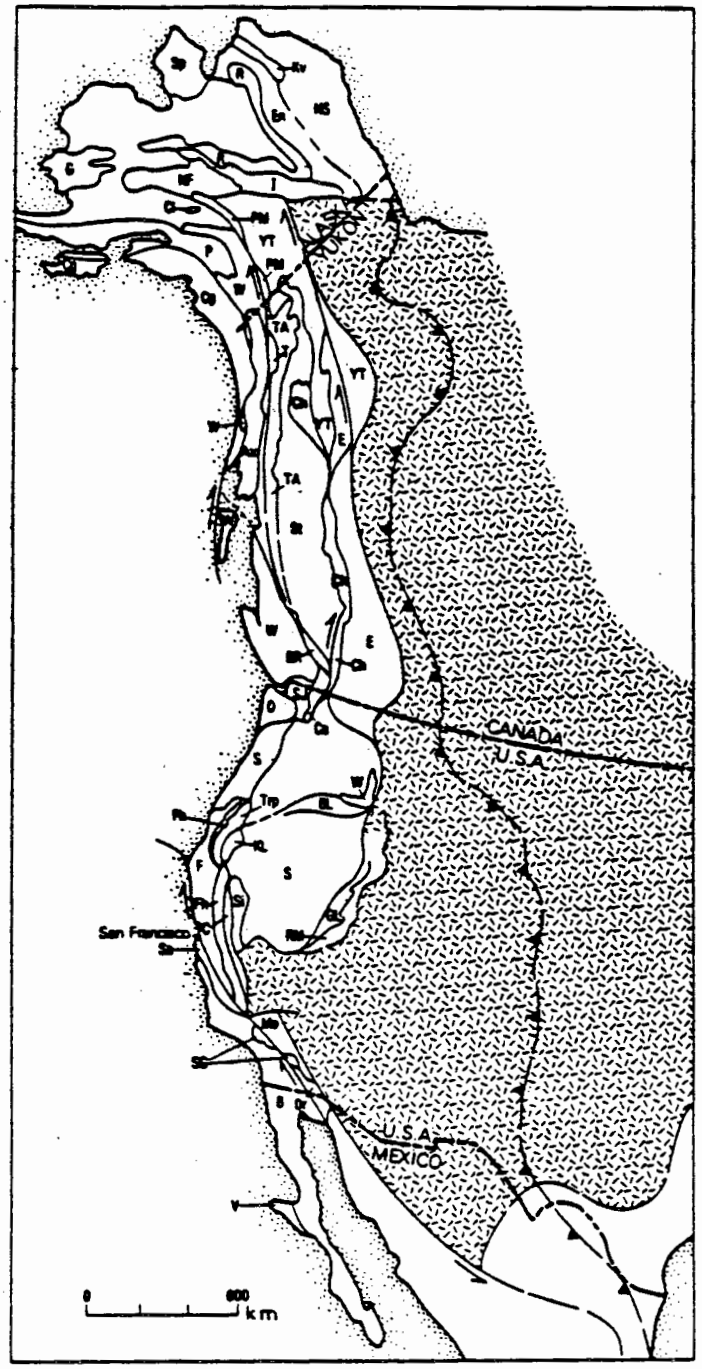

Fig. 8. Suspect terranes of the Cordillera. Terranes in the Canadian Cordillera are W, Wrangellia, Ax, Alexander, St, Stikine terrane, E, Eastern assemblage, YT, Yukon Tanana, T, Taku, TA, Tracy Arm, and BR, Bridge River terrane (from Coney et al., 1980).

along the Tintina Fault. Extensional tectonics (as evidenced by northerly trending normal fault blocks and widespread volcanism) and transcurrent faulting have controlled movements in the Canadian Cordillera since Late Cretaceous (Wheeler et al., 1972).

EVOLUTION OF THE SELWYN BASIN

The Selwyn Basin is a Lower Paleozoic, northwesterly elongate, epicontinental trough, situated east of the Tintina Trench in central and southeastern Yukon, northeastern British Columbia, and western Northwest Territories (Fig. 1). Bounded on the northeast by the Mackenzie Platform and on the southwest by the Pelly-Cassiar Platform, the Selwyn Basin evolved as a starved trough between two gradually subsiding platforms (Carne and Cathro, 1980). Selwyn Basin was originally defined by Gabrielse (1967) as a major Paleozoic tectonostratigraphic feature consisting of Cambrian through Mississippian pelites and minor limestones, but Devono-Mississippian sediments were actually deposited in a later, more widespread basin (Carne and Cathro, 1980).

The northeastern edge of the Selwyn Basin was the location of the carbonate-shale facies transition throughout Late Proterozoic and Early Paleozoic trailing margin deposition. Original uplift of the Mackenzie Platform could have occurred during the Racklan Orogeny (Brock, 1976). Restriction of the basin to the southwest was effected by development of the Pelly Cassiar Platform, an event of uncertain age. Templemen-Kluit and Blusson (1977) propose initiation of the platform as a major positive feature by build-up of an extensive, Late Cambrian andesitic volcanic pile. However, existence of middle Ordovician or Lower Silur-

ian graptolites in siltstones below extensive mafic volcanics in western Selwyn Basin imply that the basin developed prior to build-up of the volcanic pile (Jennings et al., 1980). It is possible that the Pelly Cassiar Platform developed by rapid carbonate build-up on an Early Cambrian rift-related basement horst (Mortensen, 1982). This would imply that the Selwyn Basin was a secondary rift basin. Understanding of the Pelly Cassiar Platform is hindered by overlapped allocthonous terranes and by Mesozoic deformation (Carne and Cathro, 1980).

Basement in the Selwyn Basin consists of Helikian Purcell strata overlain by Hadrynian to Lower Cambrian strata including the Grit Unit and overlying pelites (Fig. 9). Cambrian Sekwi and Backbone Formations near the Mackenzie Platform thicken and change facies westward into the Rabbitkettle "wavy banded" limestones and phyllites (Brock, 1976). The Ordovician to Mid-Devonian Road River Formation overlies the Rabbitkettle and consists of calcareous shales, black shales, mudstones, siltstones, cherts, and minor limestones. Chert and variegated shale comprise a central deep water facies. This is flanked by shallow carbonaceous shale, shaley limestone and calcarenite facies which grade into platform carbonates at the basin edge (Dawson, 1977). Mid-Devonian uplift and block faulting within the basin resulted in erosion of Road River sediments and deposition of widespread coarse clastic rocks which not only filled the Selwyn Basin but covered both platforms. Upper Devono-Mississippian clastic sediments are variously called the Canol, Imperial, Iron Creek, Yara Peak, Gunsteel, and Warneford Formations, the Earn and Besa River Groups or, collectively, the "Black Clastic Group" (Carne and Cathro, 1980). Black clastic lithologies include

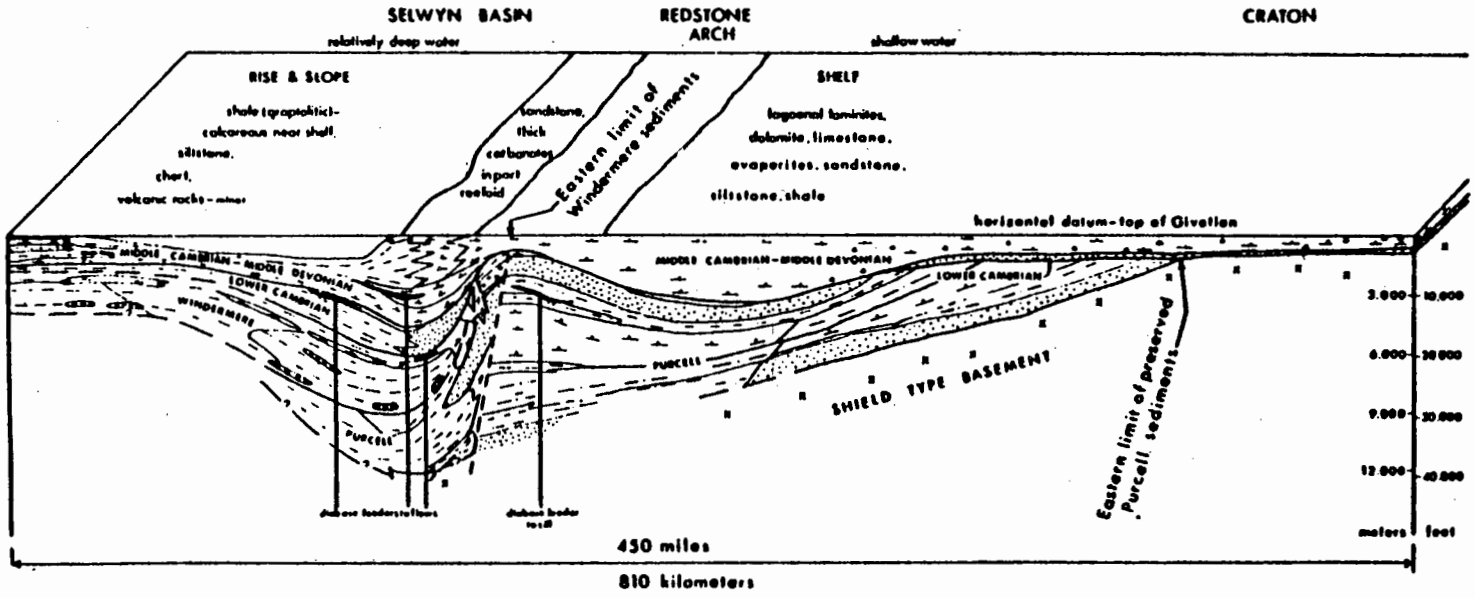

Fig. 9. Restored section of pre-mid-Devonian miogeoclinal rocks from the craton to Selwyn Basin. Location of section is shown in Figure 6 (from Gabrielse, 1976).

siliceous black shales and siltstones, tuffaceous shales, greywackes, sandstones, and chert pebble conglomerates which formed as turbidite fans and submarine density flows (Carne and Cathro, 1980; Dawson, 1977). These clastic sediments mark the end of the Selwyn Basin and initiation of a more widespread, unnamed basin.

The western Selwyn Basin was deformed into the Selwyn Fold Belt during Late Triassic-Early Jurassic collisional suturing, imbricate foreland thrusting, overriding of the craton by allocthonous terranes and Cretaceous magmatism. Displacement along the Tintina Trench offset a segment of the basin and of the Pelly Cassiar Platform (Templeman-Kluit, 1977).

ANVIL RANGE GEOLOGY

INTRODUCTION

The Anvil Range in southcentral Yukon Territory is located slightly northeast of the Tintina Trench near the western margin of Selwyn Basin. The Tintina Fault separates the Selwyn Fold Belt from rocks of the Yukon Crystalline Terrane (Fig. 6). Anvil Range consists of a Paleozoic metasedimentary and metavolcanic pile intruded by a Cretaceous quartz monzonite to granodiorite batholith. Intrusion of the Anvil Batholith warped the predominant foliation into a broad "Anvil Arch", the major structural feature in the range. The following information regarding the stratigraphy, structure and mineralization of the Anvil district is from Jennings et al. (1980), informal talks given by D.S. Jennings and G.A. Jilson in Faro, July of 1980, and personal communication with these and other Cyprus Anvil geologists during 1980-

1982.

LITHOLOGY

The Anvil Range metasediments and metavolcanics are divided into two packages: an older Lower Paleozoic sequence containing noncalcareous and calcareous pelites, mafic metavolcanics, and graphitic phyllites, and an upper package of graphitic phyllites, cherts and chert conglomerates, and metabasalt flows.

The Lower Paleozoic sequence consists of three conformable formations: the Mt. Mye, Vangorda, and Menzie Creek (Fig. 10). The Hadrynian to Lower Cambrian Mt. Mye Formation is a pelitic unit with a minimum thickness of perhaps two kilimeters. Lower parts of the Mt. Mye Formation consist of monotonous noncalcareous phyllites whereas noncalcareous phyllites of the upper part are interbedded with minor metabasites, calc-silicate phyllites, phyllitic marbles, graphitic phyllites and phyllitic quartzites. The metabasite units could contain either flows or sills or both. Contact metamorphism near the Anvil Batholith has converted Mt. Mye phyllites to schists and gneisses. The contact between the Mt. Mye Formation and the overlying Vangorda Formation is a gradational transition zone which varies in thickness from tens to hundreds of meters.

The Lower Cambrian to Lower Ordovician Vangorda Formation consists primarily of silty calcareous phyllites with appreciable amounts of interlayered noncalcareous phyllite, phyllitic marble, graphitic phyllite, metabasite and green tuffaceous phyllite. Higher grade metamorphic equivalents of calcareous Vangorda pelites are calc-silicate phyllites

Fig. 10. Lower Paleozoic stratigraphy of the Anvil Range. Sulfide deposits occur near the Mt. Mye - Vangorda transition and are associated with lenses of graphitic phyllite. The volcanic component within the Vangorda Formation increases upward. The Menzie Creek Formation intertongues with the Vangorda Formation and with graphitic metapelites equivalent to the Road River Formation (after Cyprus Anvil Mining Corp. stratigraphy).

Fig. 11. Geologic map of the Anvil area. Sulfide deposits occur in a northwesterly trend along the Mt. Mye - Vangorda contact and are associated with lenses of graphitic phyllite (generalized after Cyprus Anvil Mining Corp. map).

LOWER PALEOZOIC STRATIGRAPHY OF THE ANVIL RANGE

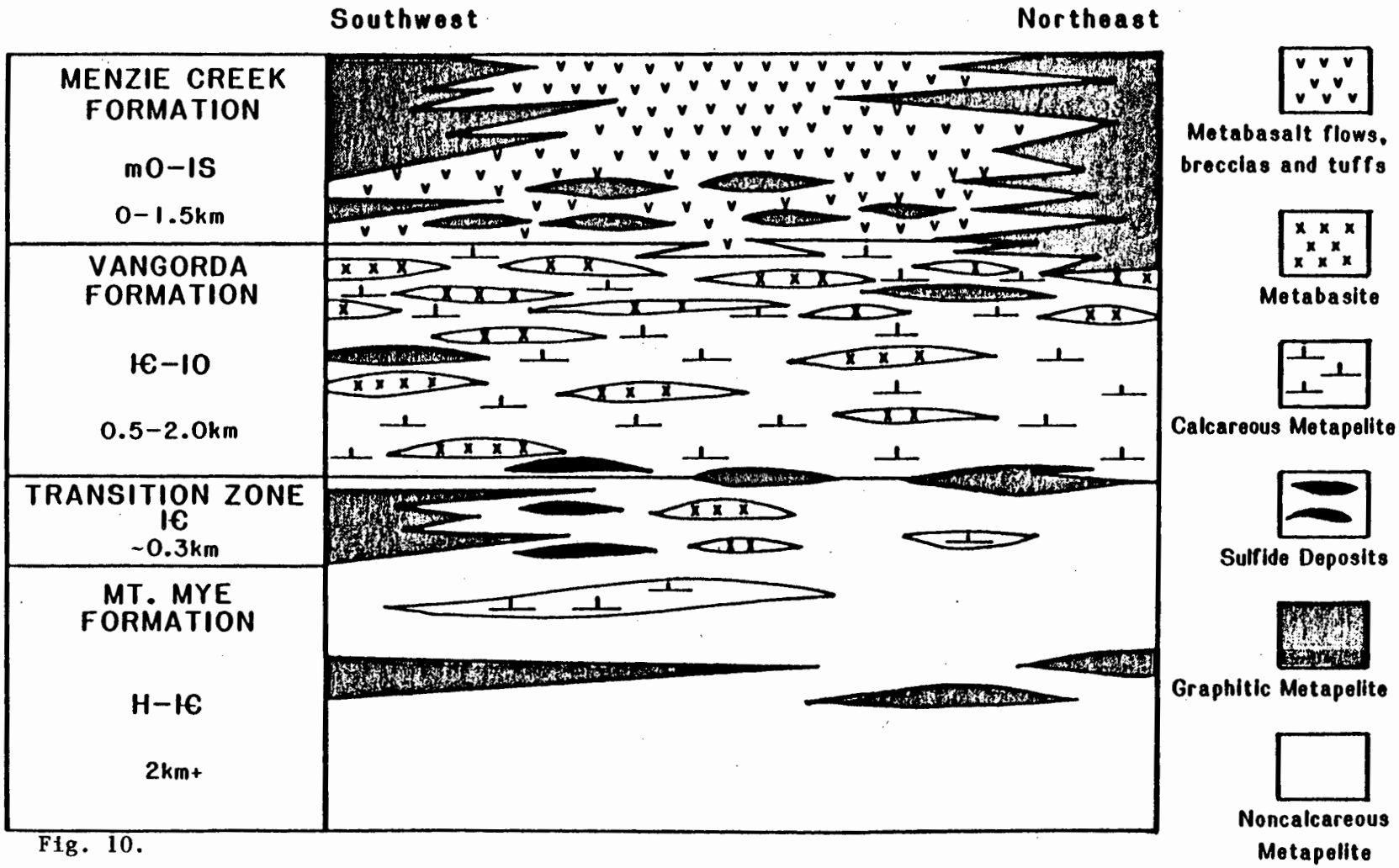

Fig. 10.

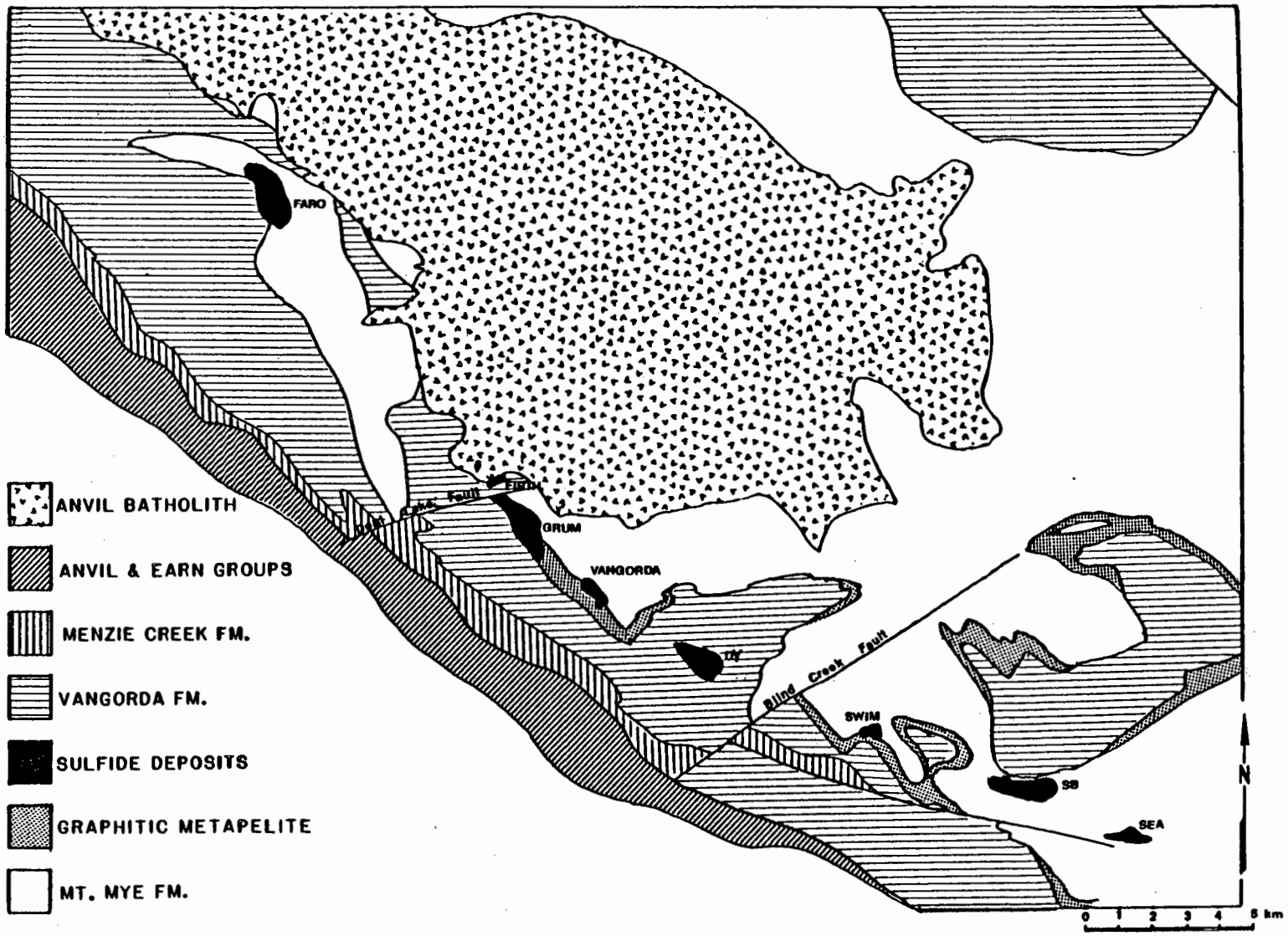
ANVIL BATHOLITH
ANVIL & EARN GROUPS
MENZIE CREEK FM.
VANGORDA FM.
SULFIDE DEPOSITS
GRAPHITIC METAPELITE
MT. MYE FM.
FARO
GRUM
VANGORDA
Blind Creek Fault
SWIM
SEA
N
0 1 2 3 4 5 km

Fig. 11.

or schists. Metabasites of the Vangorda Formation are medium to dark green, equigranular to porphyritic, fine to medium grained, massive metamorphosed basalts. Metabasites occur as lenses, one to one hundred meters thick and one to ten kilometers long. Despite a lack of pillows and amygdules, the lenses are thought to be flows rather than sills, an interpretation based largely on a common spatial association of metabasite lenses with aprons of laminarly banded, green tuffaceous phyllites. Volcanic material comprises ten to thirty percent of the section in the Vangorda Formation and increases volumetrically upsection. The Vangorda Formation varies from one half to two kilometers in thickness. Upper Vangorda rocks conformably intertongue with overlying Menzie Creek metavolcanics.

The Middle Ordovician to Lower Silurian Menzie Creek Formation consists of metabasaltic rocks up to 1.5 kilimeters thick and extends at least 200 kilometers along strike and 30 kilometers across strike. Similar to metabasites of the Vangorda Formation in composition, Menzie Creek volcanics differ by displaying abundant, clearly volcanic textures and structures. Pillowed flows, massive flows, amygdaloidal basalts, monolithic breccias and thin-bedded tuffs constitute the dominant lithologies. A volcanic center in the northeastern Anvil Range consists of thick, coarse, volcanic breccias topped by massive flows with very large amygdules which are in turn overlain by conglomerates and dolomitic sandstones consisting of volcanic grains. This assemblage could be interpreted as an upward shoaling volcanic cone that eventually became emergent. Black slates and siltstones intertongue with the distal facies of Menzie Creek flows and tuffs and contain

Middle Ordovician or Lower Silurian graptolites.

Cyprus Anvil geologists have compiled an alkali-silica plot of metabasite and metavolcanic compositions from the Mt. Mye, Vangorda, and Menzie Creek Formations. The analyses collectively straddle the alkaline-subalkaline field. A crude stratigraphy in the chemistry is apparent: Mt. Mye volcanics are primarily subalkaline while Menzie Creek volcanics plot in the alkaline field. A Ti-Zr-Y plot for Lower Paleozoic volcanics in the Anvil Range shows that the majority of the analyses plot in a "within plate" field. Company geologists interpret this as not inconsistent with a theory of basalts erupted during tensional episodes on a trailing continental margin.

Cyprus Anvil geologists have correlated Lower Paleozoic Anvil Range stratigraphy with other Selwyn Basin lithologies (Table 3). The Mt. Mye Formation correlates with the uppermost Grit Unit, Vangorda Formation with the Rabbitkettle Formation and Lower Kechika Group and Menzie Creek with the Road River Formation and Upper Kechika Group.

The upper package on the north flank of the Anvil Range is correlative with the Earn Group. On the south flank, the upper package consists of five lithologic units which comprise one or two imbricate thrust sheets. A Middle Devonian unit of black phyllite with minor crinoidal limestones is overlain by grey-beige phyllitic chert and chert conglomerates, and a stratiform barite unit. These three units, which are correlative with the Upper Devonian-Mississippian Earn Group, are overlain by the Upper Triassic Anvil Group which contains red and beige-green cherts beneath massive basalt flows (Table 3).

The Anvil Batholith, which has been dated by Rb/Sr and K-Ar at ap-

AGE	UNIT	LITHOLOGY	EQUIVALENT
Upper Triassic	Anvil Group	basalt flows chert	
Upper Devonian- Mississippian		stratiform barite phyllitic chert and chert conglomerate	Earn Group
Middle Devonian		black phyllite and minor crinoidal limestone	Earn Group
Middle Ordovician- Lower Silurian	Menzie Creek Fm.	mafic metavolcanics	Road River Fm. Upper Kechika Group
Lower Cambrian- Lower Ordovician	Vangorda Fm.	calcareous phyllites	Rabbitkettle Fm. Lower Kechika Group
Hadrynian- Lower Cambrian	Mt. Mye Fm.	non-calcareous phyllites	Upper Grit Unit

TABLE 3. Anvil Range stratigraphy. Predominant lithologies and correlative equivalents within the Selwyn Basin are given (after Jennings et al., 1980).

proximately 95 my, consists of an eastern muscovite-biotite granodiorite phase and a western quartz monzonite phase. Varieties of the batholith include foliated gneissose phases, equigranular phases and phases with K-feldspar phenocrysts. Dikes and plugs of varied compositions are related to late phases of the Anvil Batholith and occur throughout southern Anvil Range, intruding the metasediments which flank the batholith. These include quartz monzonite, hornblende-biotite-quartz diorite, smokey quartz-feldspar porphyry and pyroxenite. The northwest end of the Faro deposit abuts against a heavily altered medium grained quartz monzonite and the southeastern end is intruded by smokey quartz-feldspar porphyry and hornblende biotite diorite dikes.

STRUCTURE

Two thermal events and five phases of deformation have been recognized in the Anvil Range. The predominant fabric is a penetrative second phase foliation surface, S_2 (Plate 1). Metamorphic micas defining S_1, which are crenulated by S_2, are axial planar to primarily northeasterly vergent F_1 folds. Bedding, S_0, is commonly transposed parallel to S_1. Existence of first phase folds in Anvil Group rocks indicates that deformation event D_1 was, at the earliest, Upper Triassic to Lower Jurassic in age. Deformation event D_2 has been dated by the Anvil Batholith as Lower Upper Cretaceous because early phases of the batholith are cut and foliated by S_2 whereas later phases crosscut S_2. Third, fourth and fifth phase brittle deformation events resulted from relaxation following D_2 and are represented by flexural slip folding and nonpenetrative foliation surfaces. Fourth phase folding is

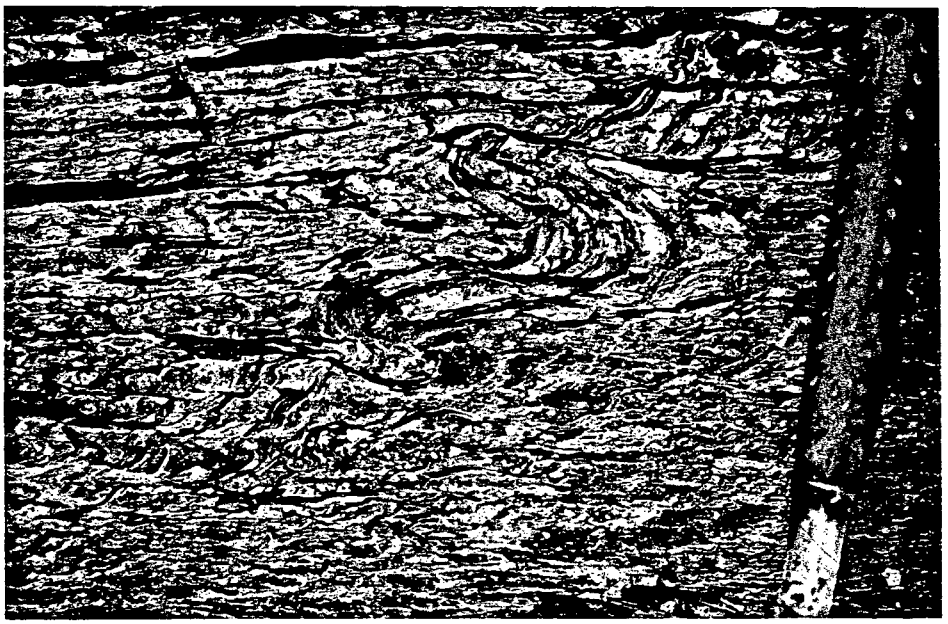

Plate 1. Predominant shallow S_2 foliation in outcrop of Vangorda Formation calcareous muscovite-chlorite phyllite. The attitude of S_1 is steeper than S_2 and dips to the left in this photograph. Outcrop is located near the DY deposit.

especially important in the Faro deposit and also in the northeastern Anvil Range where a D_4 gravity slide off the batholith resulted in crustal shortening taken up by D_4 folds. Post D_2 events in the Vangorda Plateau deposits seem limited to a broad warping of S_2.

ORE DEPOSITS OF THE ANVIL DISTRICT

The eight stratiform massive sulfide deposits (Faro, Firth, Grum, Vangorda, DY, Swim, SB, and Sea) follow a 35 kilometer arcuate northwesterly trend in the southern Anvil Range (Fig. 11) and contain an aggregate tonnage of about 250 Mt, half of which averages 10% combined lead and zinc. The sulfide deposits are hosted by discontinuous lenses of graphitic phyllite which concentrate near the transition zone between the Mt. Mye and Vangorda Formations (Fig. 10). Lenses of metabasite and tuffs can occur near the ore horizons but are more abundant stratigraphically higher in the section.

Five major lithofacies have been recognized by Cyprus Anvil geologists in all of the Anvil deposits. Ribbon-banded ore, which displays a characteristic texture of interlayered graphite, quartz and sulfides, is usually basal or marginal on the scale of a sulfide horizon. Pyritic quartzitic ores contain 30-70% total sulfides, in bands alternating with milky quartz. Massive pyrite sulfides contain more than 80% total sulfides and seem to lie stratigraphically above the quartzitic ores. Baritic ore, which contains anywhere from 10-60% barite intimately mixed with sulfides, tends to lie toward the stratigraphic top of a sulfide horizon. A sericitic alteration facies inconsistently surrounds the ore horizons and is sometimes best developed in the footwall

The tendency for these lithofacies to occur in a stratigraphic sequence has been called the "Anvil Cycle" by Cyprus Anvil geologists (Fig. 12). Complete, incomplete and multiple cycles can be identified within single sulfide horizons.

Logging of diamond drill core from the Anvil deposits has been facilitated by the use of a combined numerical and alphabetical lithologic code (Appendix I). The first digit in the code denotes the formation: 3 is the Mt. Mye Formation, 4 is ore and 5 is the Vangorda Formation. A letter designates the lithofacies within the formation and can be further modified by numerals which represent adjectives such as calcareous, chloritic, base-metal bearing, siliceous and so forth. This lithologic code is computerized to be combined with structural data, assay data and down-hole surveys for plotting on cross sections through the deposits. The plotted data can be correlated to provide a structural interpretation of the deposits.

METHODS

SAMPLE COLLECTION

Approximately 10,000 meters of Grum drill core were logged during the 1980 and 1981 field seasons. During 1980, representative core samples for petrographic examination of ore facies and host rock lithologies were selected from drill holes on cross sections 80 West, 74 West, and 66 West through the Grum deposit (Fig. 13). In addition, an effort was made to sample each ore facies within several sulfide intersections for the purpose of sulfur isotope analyses.

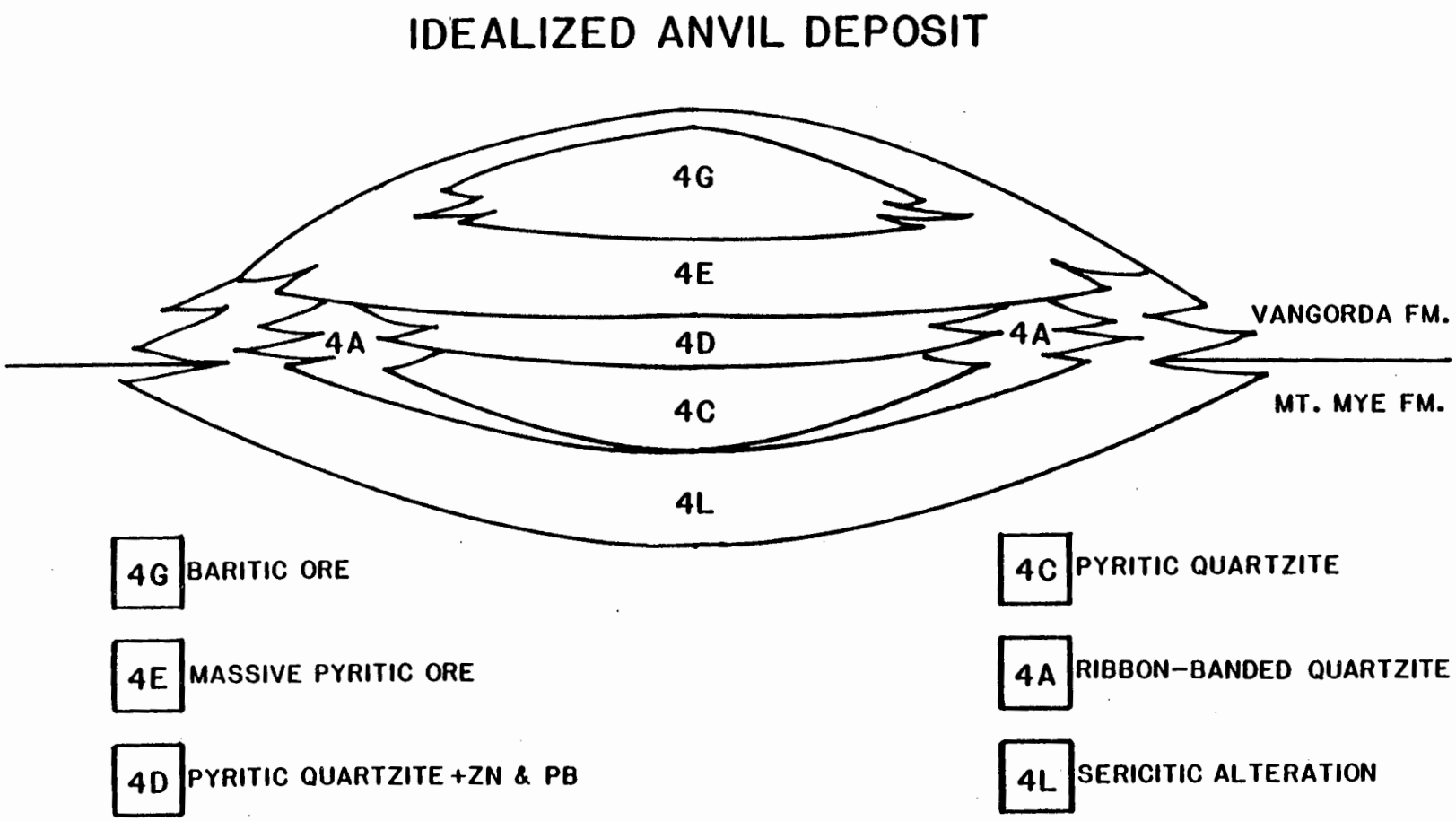

Fig. 12. Idealized Anvil Cycle (after Cyprus Anvil Mining Corp.). Numerical and alphabetical lithologic code is summarized in Appendix I. Ore facies are described in the text.

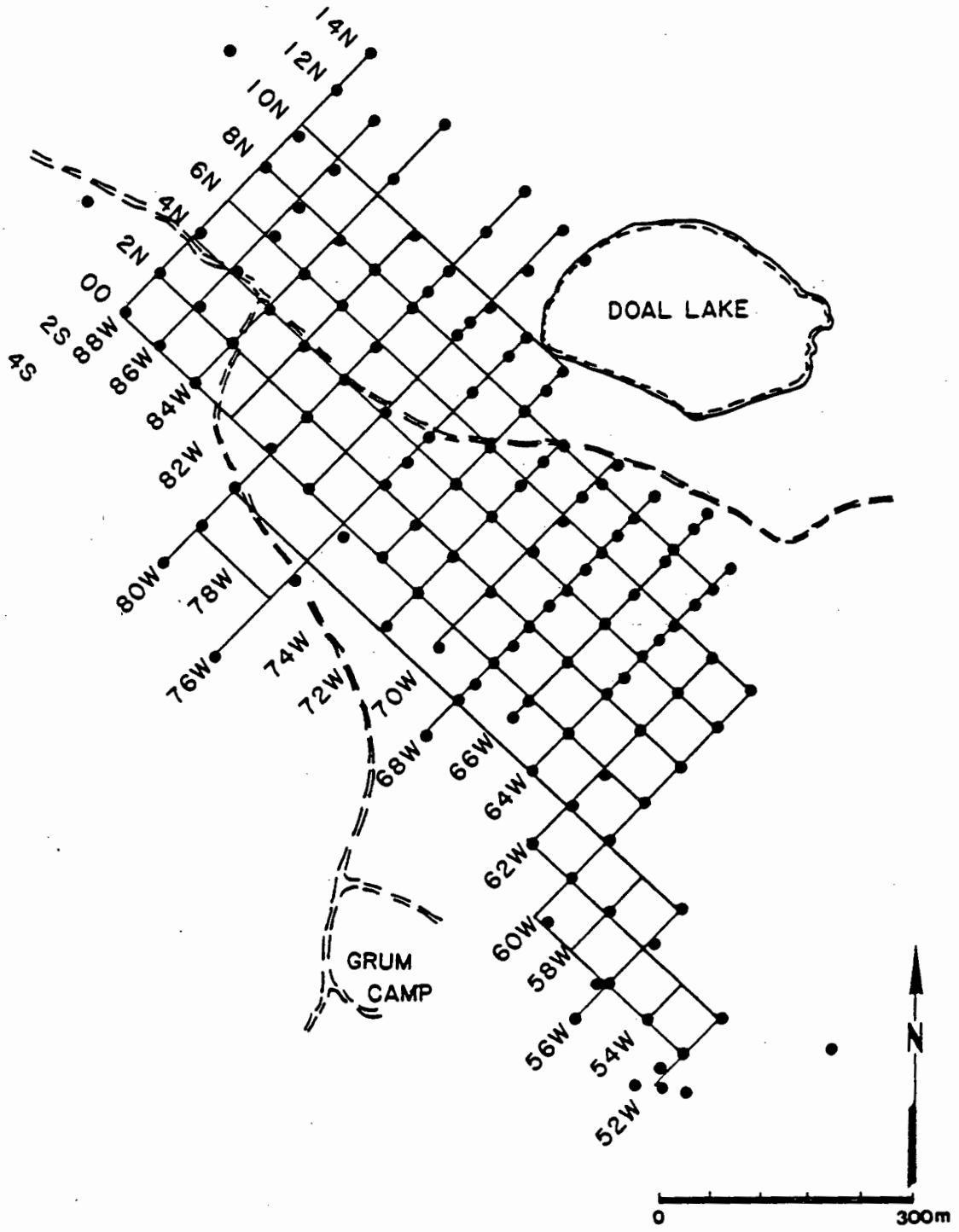

Fig. 13. Grum deposit drilling grid. Samples from cross sections 80 West, 74 West and 66 West were used in this study.

PETROGRAPHY

Fifty-eight polished thin-sections and 32 thin sections were prepared and examined under transmitted and reflected light for mineralogical and textural features in ore facies and in various host rock lithologies. In addition, X-ray diffraction techniques were used for further mineral identification and qualitative chemical analyses of individual minerals were made on a scanning electron microscope using energy dispersive X-ray techniques.

SULFUR ISOTOPES

131 sulfur isotope ratios, 65 of mineral separates (24 pyrite, 23 sphalerite, 10 barite, 7 galena and 1 sphalerite plus galena), and 66 of bulk sulfide sulfur, were determined.

PREPARATION OF Ag_2S

Core samples were crushed to 100-200 mesh for sulfur isotope analyses of sphalerite and galena separates. Sphalerite grains were then separated from other sulfides and gangue using a Frantz (Model L-1) magnetic separator. Quality of separates was checked by binocular microscope examination and SEM analysis. The galena-bearing remainder of these samples was finely ground and converted to Ag_2S by reaction with 3N HCl at 25°C in a nitrogen atmosphere for 2-5 hours. The H_2S gas evolved from this reaction was passed into a test tube containing a 10% $AgNO_3$ solution where Ag_2S precipitated. Sphalerite separates were also finely ground and similarly converted to Ag_2S by reaction with 6N HCl at 60°C for 3-6 hours. Pyrite separates were obtained

chemically by crushing samples finer than 200 mesh and reacting with 6N HCl at 60°C to remove all non-pyrite sulfides. Pyrite was then oxidized by reaction with a boiling aqua-regia and bromine solution for 1.5-3 hours. Barium sulfate was precipitated, after filtering out mineral residues, by addition of $BaCl_2$. Bulk sulfide sulfur was also converted to $BaSO_4$ by reaction with aqua-regia and bromine and addition of $BaCl_2$. Primary barite residues were saved from this reaction. Barium sulfate, both precipitated $BaSO_4$ and primary barite, was reduced to BaS by combustion with graphite for ten minutes at 1150°C in a nitrogen atmosphere. The BaS was dissociated in deoxygenated and deionized water and the resulting sulfide solution was converted to Ag_2S by filtration into a 10% $AgNO_3$ solution. In all cases, residues from the chemical extractions were examined under the binocular microscope to determine completeness of reaction, and where possible, yields were calculated as a further check.

PREPARATION OF SO_2 GAS

Silver sulfide, produced by chemical treatment of the ore samples, was filtered, dried in a dessicator and weighed to determine completeness of reaction. SO_2 gas, for mass spectrometer analysis, was prepared from the Ag_2S by reaction with Cu_2O at 1050°C. Vacuum distillation was used to remove water and CO_2 from the SO_2 gas. The volume of purified SO_2 was measured in a mercury manometer to verify yield. Conversion yields averaged 95% and most exceeded 90%.

MASS SPECTROMETRIC ANALYSIS

Mass spectrometric analyses of $^{34}S/^{32}S$ ratios were made on SO_2 gas

using a Nuclide 6-60 RMS Mass Spectrometer in the laboratory of W.C. Shanks III, University of Wisconsin. Samples were analyzed using a tank SO_2 working standard and three of the McMaster sulfur isotope reference series (Rees, 1978). Sulfur isotope ratios are expressed in per mil as $\delta^{34}S$ relative to the Canon Diablo Troilite sulfur standard. Instrument precision averaged about $\pm$ 0.06 $^{o}/_{oo}$ and was always better than $\pm$ 0.1 $^{o}/_{oo}$ at the 1.5 standard deviation level.

RESULTS

PETROGRAPHIC STUDIES

MT. MYE FORMATION

Mt. Mye Formation lithologies intersected in the Grum deposit are primarily monotonous noncalcareous grey phyllites. Minor noncalcareous graphitic phyllites also occur, as do higher metamorphic grade equivalents of the noncalcareous phyllites: fine-grained biotite staurolite schists (Plate 2).

The mineral assemblage in the noncalcareous phyllites consists of quartz, feldspar, white mica, minor chlorite and graphite, accessory pyrite, tourmaline, apatite and allanite (Plates 3 and 4). The mineral assemblage in the schists consists of quartz, feldspar, white mica, biotite and staurolite with trace zircon, zoned detrital tourmaline, ilmenite altering to leucoxene, and pyrite (Plate 5).

VANGORDA FORMATION

The most common Vangorda Formation lithology at Grum is a calcar-

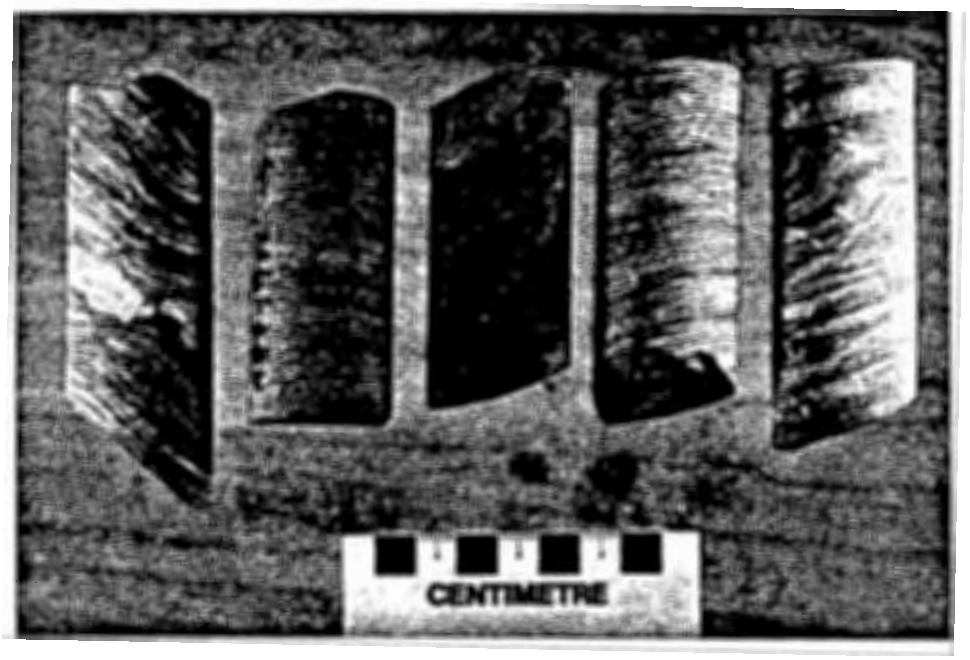

Plate 2. Some of the common host rock lithologies from the Grum deposit. From left to right: slightly carbonaceous, non-calcareous muscovite-chlorite phyllite of the Mt. Mye Formation (Sample U142-61.4); biotite-staurolite schist of the Mt. Mye Formation (Sample A77-972); graphitic metapelite of the Vangorda Formation (Sample A109-59.0); calcareous muscovite-chlorite phyllite of the Vangorda Formation (Sample U150-70.3); strongly calcareous chloritic phyllite of the Vangorda Formation (Sample A27-269).

Plate 3. Folds in noncalcareous muscovite phyllite of the Mt. Mye Formation. The folded foliation surface is S_1; S_2 is not well developed as a penetrative surface in this sample. Crossed nicols in transmitted light. Field of view is 5.4mm. (Sample A38-642).

Plate 4. Slightly carbonaceous, noncalcareous quartz-muscovite phyllite of the Mt. Mye Formation. Shallow S_2 foliation cuts and crenulates S_1 micas. Plane transmitted light. Field of view is 5.4mm. (Sample A117-204.6).

Plate 5. Biotite-staurolite schist, a localized high grade equivalent of the noncalcareous muscovite-chlorite phyllite of the Mt. Mye formation. Biotite and staurolite coexist with quartz, feldspar and muscovite. Crossed nicols in transmitted light. Field of view is 13.5mm. (Sample A77-995).

eous phyllite. Other Vangorda Formation lithologies include a variably calcareous graphitic phyllite, minor phyllitic marbles, and varying types of greenstones.

Minerals present in the common calcareous phyllites are quartz and feldspar, white mica, calcite, dolomite or ankerite, minor chlorite and graphite, accessory pyrite, pyrrhotite, tourmaline, apatite and allanite (Plate 6). The mineral assemblage in the graphitic phyllite consists of quartz, feldspar, white mica, graphite and carbonate with trace amounts of pyrite, ilmenite and tourmaline (Plate 7). Graphite content is variable. Minerals present in the phyllitic marbles are calcite and dolomite, white mica, minor chlorite and accessory pyrite, tourmaline and apatite.

The greenstone lithologies contain quartz and feldspar, calcite, dolomite and ankerite, chlorite, serpentine and muscovite, with minor pyrite, and ilmenite altering to leucoxene. These carbonated greenstones are problem rocks at Grum. District mapping of the Vangorda Formation by company geologists has revealed lenses of metabasites which are surrounded by aprons of laminated chloritic phyllites. These occurrences are interpreted as mafic flows surrounded by tuffs or tuffaceous sediments. In some localities, an intermediate rock with chlorite mottles, possibly an amygdaloidal flow top, occurs at the contact between the metabasites and the laminated tuffs. In thin section the metabasites are highly altered; the tuffs consist primarily of chlorite and feldspar. In Grum drill core, occurrence of metabasite as seen in the field is negligible. There are, however, many intersections through sericitized, carbonated, chlorite mottled rocks and

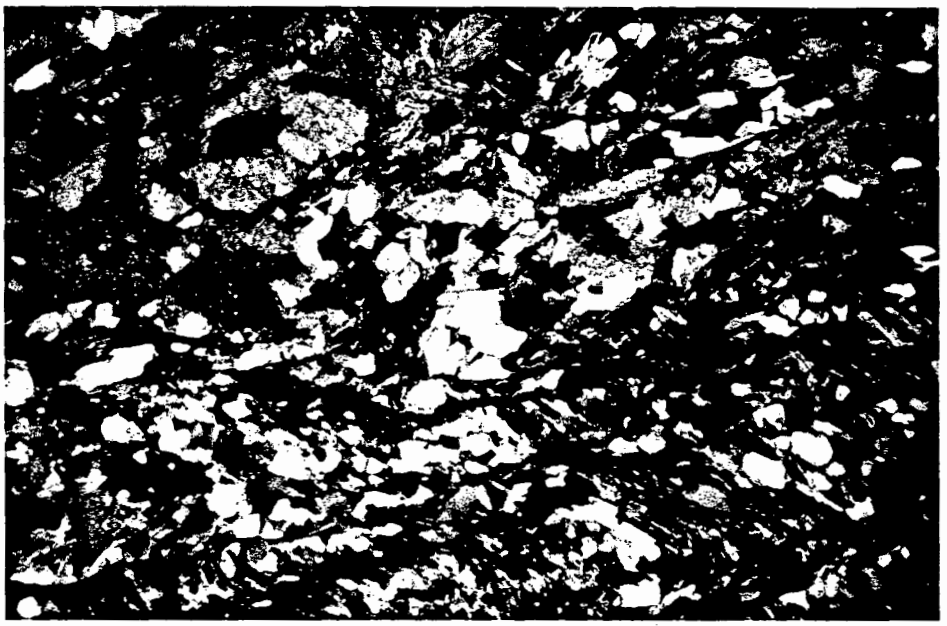

Plate 6. Typical calcareous muscovite-chlorite phyllite of the Vangorda Formation. Assemblage is quartz-feldspar-calcite-muscovite-chlorite. Crossed nicols in transmitted light. Field of view is 5.4mm. (Sample A19-250).

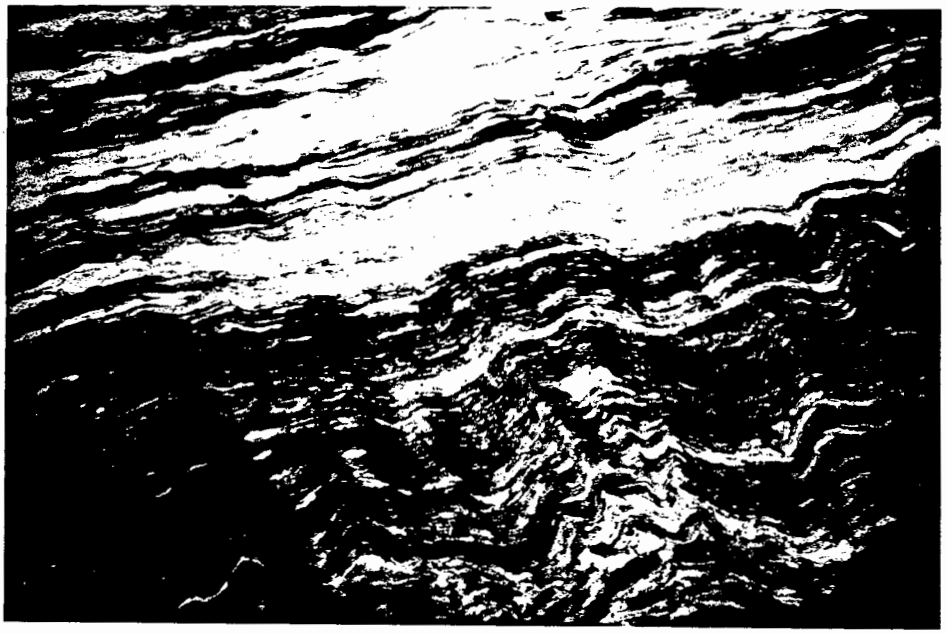

Plate 7. Typical graphitic phyllite of the Vangorda Formation, host to the sulfide deposits. Graphite, quartz, muscovite and carbonate content is variable in the graphitic metapelites. Plane transmitted light. Field of view is 13.5mm. (Sample U156-71.7).

through chloritic phyllites with a variety of banded, laminated and massive fabrics. These lithologies are variably calcareous, dolomitic, ankeritic and siliceous. In contact with the ore horizons, all of these lithologies become more sericitized and commonly contain, in place of chlorite, blebs, streaks or mottles of a mineral thought to be fuchsite, a chromium muscovite. X-ray diffraction analysis of five samples of this mineral indicated that rather than fuchsite, it is either kaolinite or serpentine. Qualitative scanning electron microscope analyses of 3 samples showed that the mineral contains aluminum, silica, magnesium, iron and chromium, indicating that at least some of it is serpentine, although there may be kaolinite as well. Petrographic features of 2 samples are consistent with those of serpentine (samples U146-38.8 and A11-217). If the serpentine is an alteration of chlorite there has been a loss of aluminum which could have been taken up by hydrothermally or metasomatically formed sericite and addition of magnesium probably brought by the ore fluids. The presence of chromium is not inconsistent with interpretations of these lithologies as metamorphosed mafic flows and/or tuffs. These greenstone lithologies occur abundantly and in close proximity to the ores in cross section 74 West, near the center of the deposit, but are less abundant in other cross sections through the deposit (Plate 8).

ORE PETROGRAPHY

Mineralogy

The opaque mineralogy of Grum consists predominantly of pyrite with variable amounts of sphalerite and galena (Plates 9, 10 and 11).

Plate 8. Close association of chlorite-ankerite mottled or banded rock of possible volcanic origin with sulfides in DDH U39, cross section 74 West. Close association of metabasites and tuffs with the ore is not common. Width of drill core is 3.5 cm.

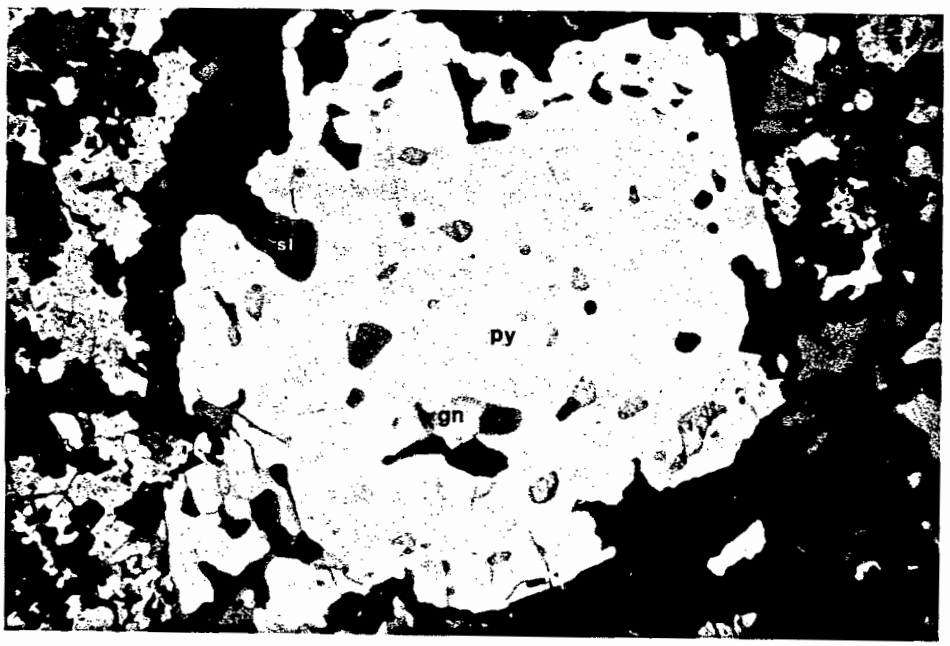

Plate 9. Seive texture of subhedral pyrite grain (py) containing rounded inclusions of sphalerite (sl) and galena (gn). This is more poikilitic than most pyrite grains in the Grum deposit. Reflected light. Field of view is 2.25 mm. (Sample A99-140.5).

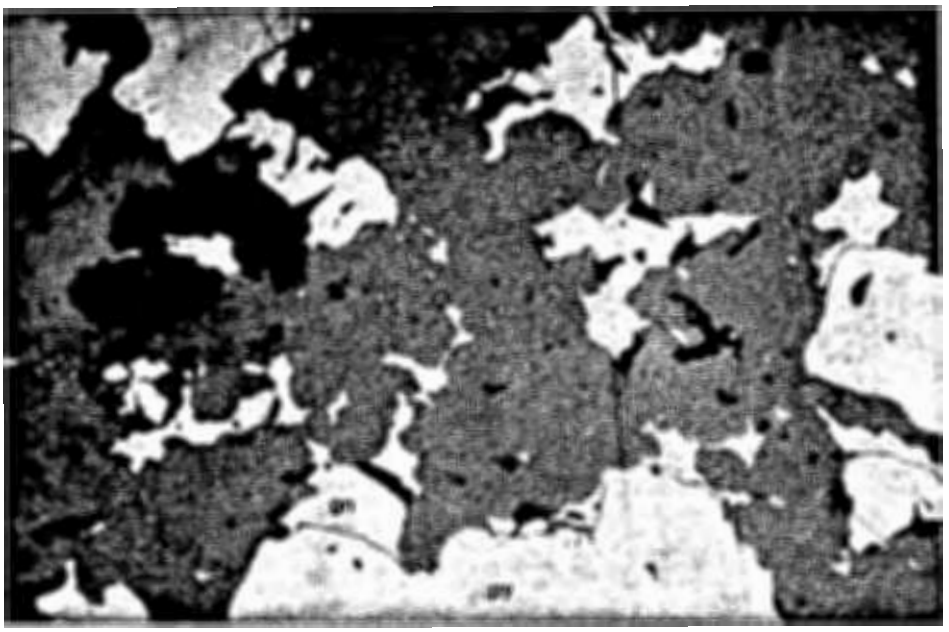

Plate 10. Typical sphalerite (sl) -- galena (gn) relationship in high grade section of massive pyritic (py) ore. Oil immersion in reflected light. Field of view is 0.57mm. (Sample A24-338.6).

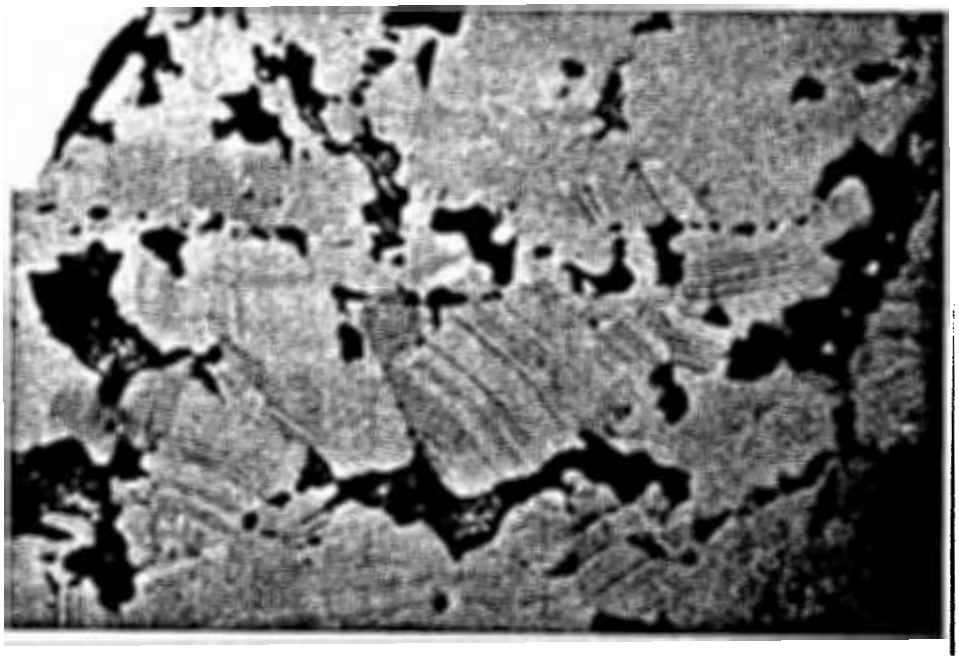

Plate 11. Lamellar twinning and grain boundaries revealed by etching of sphalerite with 1:1 HNO_3. Twinning could be deformational in origin. Oil immersion in reflected light. Field of view is 0.57mm. (Sample A24-343.5).

Arsenopyrite and chalcopyrite are widespread minor minerals (Plates 12 and 13), whereas magnetite (Plate 14), pyrrhotite (Plate 15), and graphite, which can be present in large amounts, occur only locally within the deposit. Tennantite-tetrahedrite occurs in trace to minor amounts (Plate 13) and is probably the most important silver-bearing mineral at Grum. Electron microprobe determination of the composition of the solid solution was not made. One sample contained boulangerite crystals enclosed by galena (sample U151-13.9). Marcasite occurs only as fine-grained alteration rims on pyrrhotite. Carson (1977) reported two occurrences of native gold blebs in Grum ores, though no gold was detected in this study. Occurrence of opaque minerals is summarized in Table 4.

Non-opaque minerals are quartz, barite, and carbonate minerals (ankerite, siderite, calcite, and dolomite) with minor amounts of muscovite, chert, chlorite and a single trace occurrence of chloritoid and garnet.

Lithofacies recognized in other Anvil deposits are common in the Grum deposit. The average sulfide grain size at Grum is roughly 0.15 mm and the ores are well-banded. Pyritic and base-metal bearing quartzitic ores usually show a banded segregation of siliceous versus sulfide rich layers ranging from 2.0 to 20.0 mm wide. Massive sulfides (and sometimes the sulfide bands within quartzitic ores) frequently show a banding of predominantly pyrite layers alternating with predominantly base-metal sulfide layers.

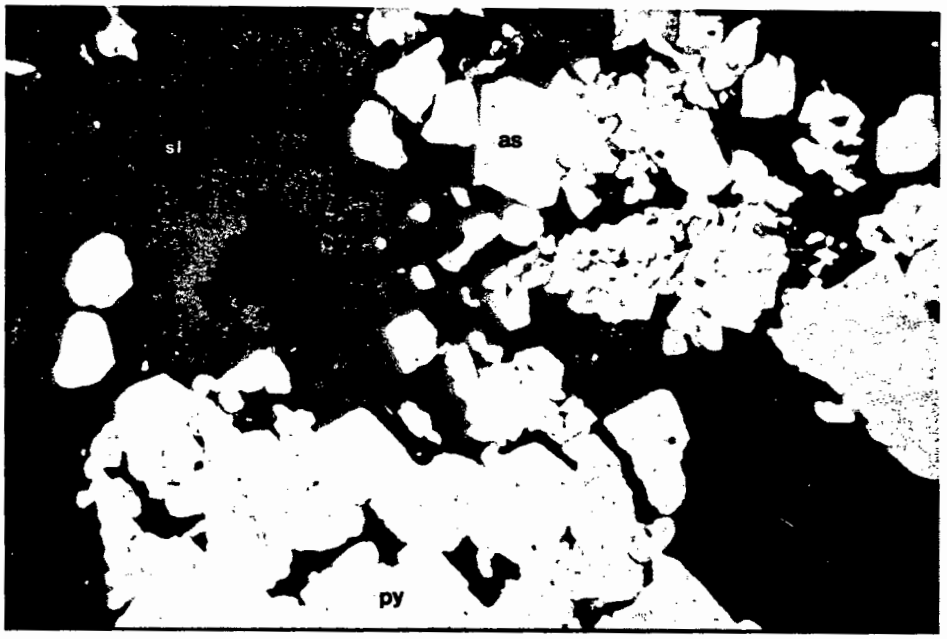

Plate 12. Pyrite (py) and arsenopyrite (as) within sphalerite (sl). Arsenopyrite in the Grum deposit is frequently twinned and can show concentric overgrowth rims. Oil immersion in reflected light. Field of view is 0.57 mm. (Sample U151-13.9).

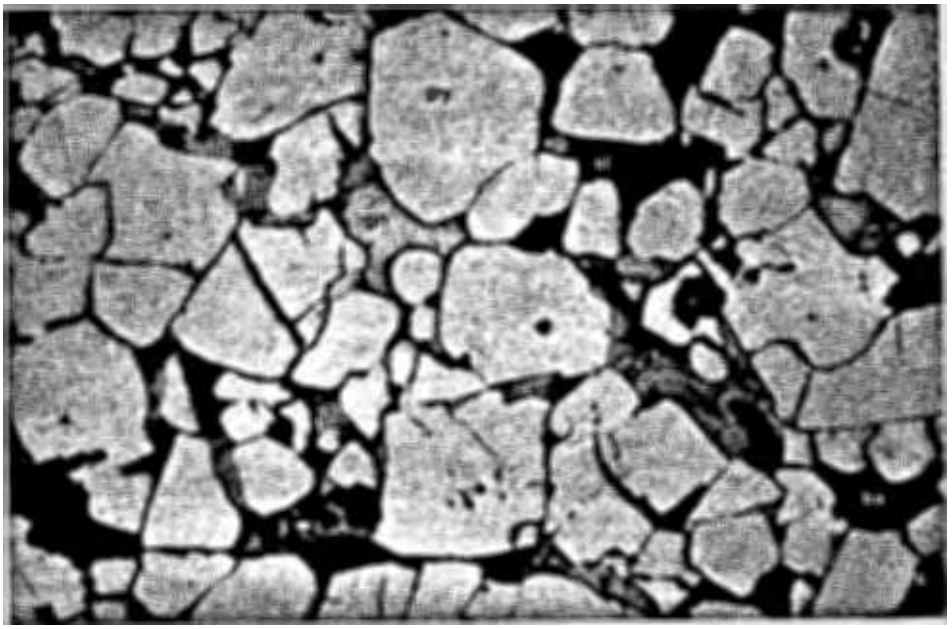

Plate 13. Galena (gn), sphalerite (sl), chalcopyrite (cpy), and tennantite-tetrahedrite (te) interstitial to subhedral and rounded pyrite (py) in baritic (ba) ore facies. Reflected light. Field of view is 1.44mm. (Sample U153-40.6).

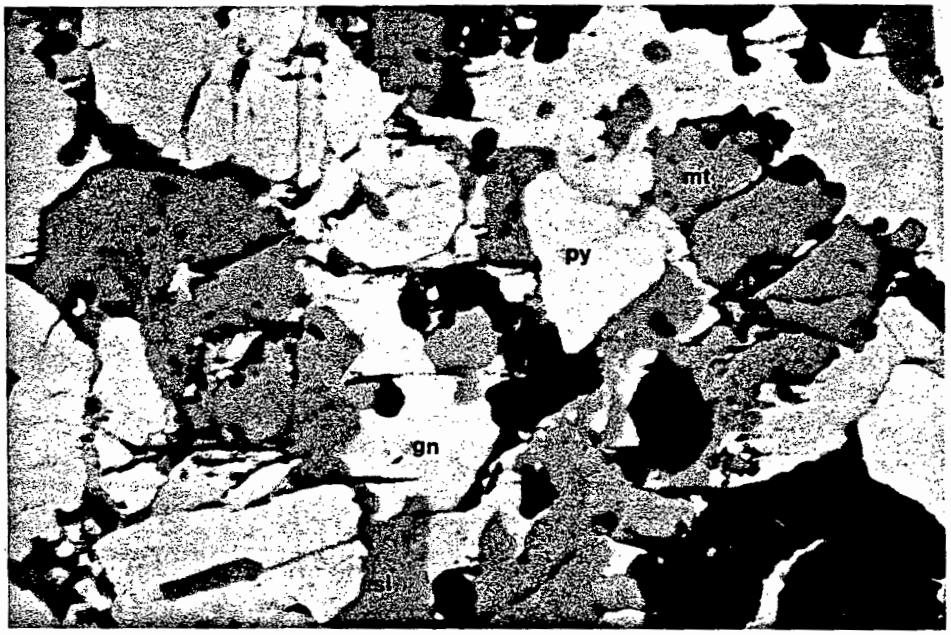

Plate 14. Typical cracked, subhedral magnetite (mt) grains invaded by galena and associated with pyrite (py) and sphalerite (sl). Reflected light. Field of view is 2.25 mm. (Sample U15-24.7).

Plate 15. Localized concentration of pyrrhotite (po) in high grade massive pyritic ore. Pyrite (py) magnetite (mt) galena (gn) sphalerite (sl) chalcopyrite (cpy). Reflected light. Field of view is 1.44 mm. (Sample U151-60.6).

TABLE 4. Opaque mineralogy of the Grum deposit. Occurrence indicates the number of thin sections in which a mineral was observed (out of 53 total sections). Abundance ranges are reported in approximate volume percent.

Mineral	Occurrence	%	Remarks
pyrite (py)	53	5-85	euhedral to subhedral or rounded; embayed, poikilitic, cracked; foliation rare; framboidal textures absent.
sphalerite (sl)	52	Tr-50	pale yellow, honey-colored, orange, red-orange, or deep red; interstitial to py and gangue; as rounded inclusions in poikilitic py grains; convex toward gn; granular aggregates and unoriented lamellar twinning revealed by etching.
galena (gn)	50	Tr-25	interstitial to py and gangue; concave toward sl; as inclusions in py; invading cracks in py and as; coarser grained in high grade samples and near second phase fold closures.
arsenopyrite (as)	39	Tr-5	euhedral rhombic and prismatic; cracked and invaded by softer sulfides; twinning common; zoning shown by concentric inclusions or rims of different crystallographic orientation.
chalcopyrite (cpy)	31	Tr-2	anhedral masses interstitial to py; filling cracks in py; as remobilized veinlets; in association with sl, gn, te, po and mt; most common in 4E, 4C and 4G ore facies.
tennantite-tetrahedrite (te)	15	Tr	interstitial to py; commonly associated with cpy, gn, sl, and as; occasionally as rounded inclusions in py and gn.
pyrrhotite (po)	14	Tr-6	interstitial to py; associated with cpy, sl, gn; occasionally as minute rounded inclusions in py; as elongate masses rimmed by fine-grained ma.

TABLE 4 (continued)

magnetite (mt)	11	Tr-10	cracked and corroded; can concentrate in lenses of carbonate or barite surrounded by massive sulfides; evidence of replacement relationship with py.
graphite (g)	10	2-5	discrete blebs and streaks; invariably associated with muscovite and quartz.
marcasite (ma)	8	Tr	as fine grained rims along po grain boundaries.
boulangerite (b)	1	Tr	associated with gn, cpy and te.

Ore Facies

Ribbon-banded ore (4A): The ribbon-banded graphitic pyritic quartzite contains 40-80% quartz, 2-50% pyrite, 2-40% graphite, 0-25% muscovite, 0-25% sphalerite and 0-15% galena. The most common, or "normal" ribbon-banded ore at Grum consists approximately of 55% quartz, 25% muscovite plus graphite, and 20% total sulfides (Plate 16). Ribbon-banded ore in the Faro deposit is somewhat more graphite-rich than that of the other deposits. There are four common variations of this facies:

1) sphalerite and galena bearing, with greater than 5% Zn+Pb
2) siliceous, containing up to 80% quartz with a corresponding decrease in graphite and muscovite
3) pyrite-rich, containing up to 60% pyrite, and
4) "phyllitic", containing very little graphite, consisting primarily of quartz, muscovite, and sulfides. This variety is usually low grade.

Polished thin section examination of 9 samples of the 4A lithofacies shows that arsenopyrite is a common trace to minor constituent, while chalcopyrite, pyrrhotite, tennantite-tetrahedrite, marcasite, and carbonate are only rarely present and only in trace amounts. Sphalerite is typically red or orange-red in the ribbon-banded ore.

This ore facies is called ribbon-banded because the graphite and micas frequently form a texturally distinctive interlamination with quartz and sulfides (Plate 17). The quartz grain size varies in different bands, decreasing with increasing mica and graphite content.

Ribbon-banded ore grades into a poorly-mineralized variably calcareous graphitic phyllite of the Vangorda Formation (5A). Furthermore, ribbon-banded ore can grade into other ore facies: 1) As the quartz and sulfide contents increase and graphite plus mica content

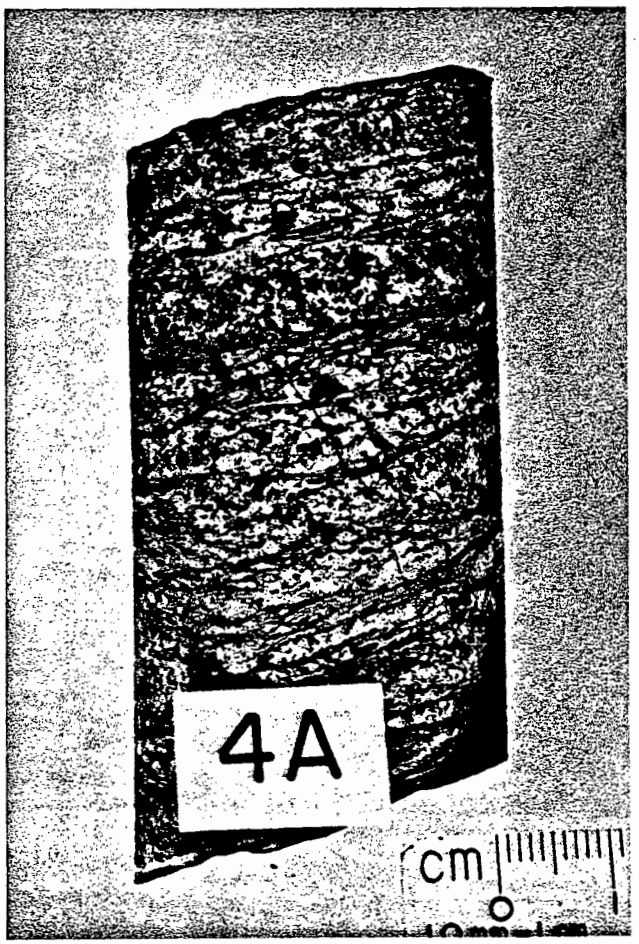

Plate 16. Ribbon banded ore (4A). Typical low grade sample of 4A containing quartz, graphite, muscovite and pyrite (Sample A121-148.5).

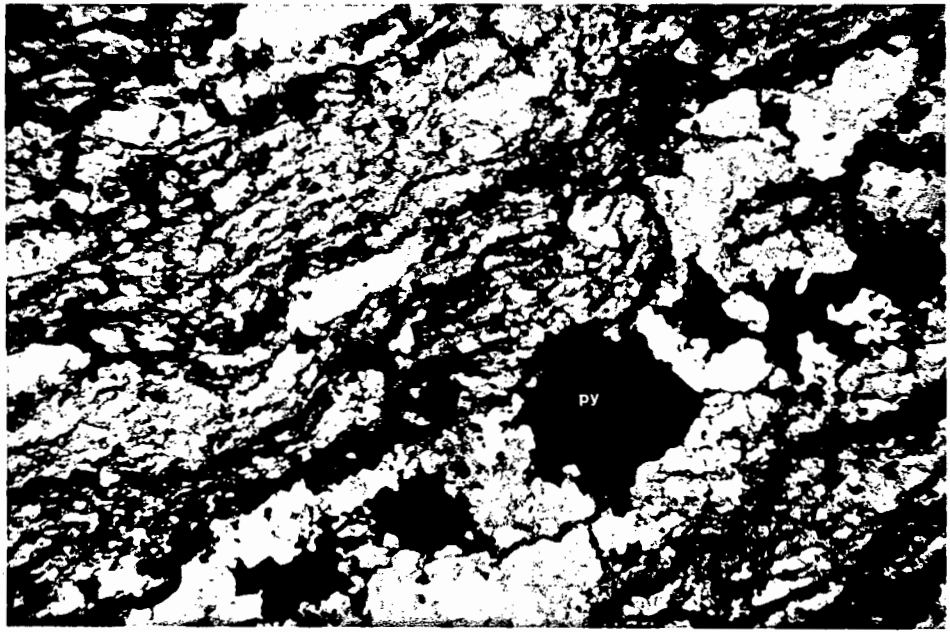

Plate 17. Ribbon banded ore. Graphite (black), quartz (white), pyrite (py) and sphalerite (red) form a distinctive interlamination. Plane transmitted light. Field of view is 5.4mm. (Sample U153-8.8).

decreases, 4A grades into the pyritic quartzitic or the base-metal bearing quartzite. 2) As the total sulfide content increases at the expense of all other constituents, 4A grades into the massive sulfide ore facies. 3) As the graphite content decreases, the phyllitic variety of 4A can grade into a bleached sericitic alteration facies (4L).

Pyrite-free base-metal bearing quartzite (4B): The pyrite-free base-metal bearing quartzite is a banded ore facies consisting primarily of milky quartz with bands of base-metals (Plate 18). Pyrite is present only in trace or very minor amounts. The facies is not common at Grum. There are three varieties:

1) nearly pure quartz with minor thin (1 mm) laminae of sphalerite and galena; less than 5% combined Zn+Pb
2) banded quartz and base-metals with minor pyrite; bands are 0.5 to 2.5 cm wide and combined Zn+Pb assays exceed 5%
3) sericitic quartzite with varying amounts of base-metal sulfides usually occurring in bands

The mineralogy of the 4B ore facies, based on thin section examination of only two samples is quartz, sphalerite, galena, pyrite, arsenopyrite, chert, carbonate and muscovite in order of decreasing abundance (Plate 19). The color of the sphalerite in 4B is orange or red.

The 4B facies grades into other facies. With increasing pyrite, 4B grades into the base-metal bearing pyritic quartzite. With increasing sericite content it grades into a siliceous variety of the alteration facies. Occasionally 4B can contain minor wisps of graphite and so grades into 4A. Hypothetically, this ore facies could grade into 4J, the massive base-metal sulfide facies, though neither are common at Grum.

Plate 18. Pyrite-free, base metal-bearing quartzitic ore (4B). Thin laminae of sphalerite and galena within milky quartz (Sample A79-267).

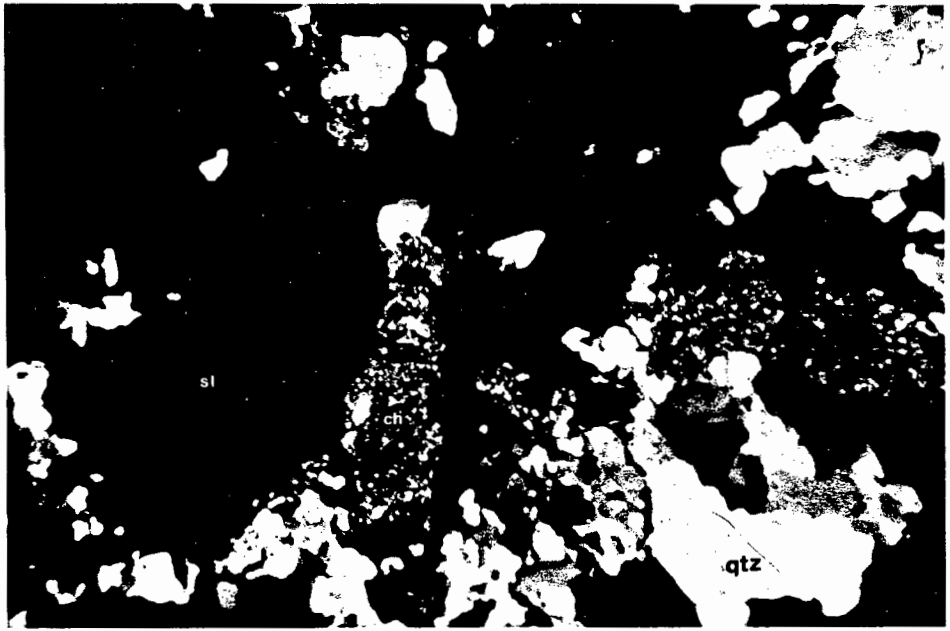

Plate 19. Chert (ch) masses in association with recrystallized quartz (qtz) and sphalerite (sl) in a sample of 4B quartzitic ore. Crossed nicols in transmitted light. Field of view is 5.0mm. (Sample A24-331.8).

Pyritic quartzite (4C): The pyritic quartzite ore facies is a banded, pyrite and milky quartz rock with less than 80% total sulfides and less than 5% combined zinc-lead (Plate 20). Commonly, 4C simply contains pyrite and quartz in a 40:60 ratio. However, carbonate, sericite, magnetite, pyrrhotite, chalcopyrite, sphalerite and galena alsc can be seen in minor amounts in hand samples. Polished thin section examination of 5 samples of 4C reveal the following range of abundances: 25-60% pyrite, 25-60% quartz, 2-15% carbonate, 0-5% each muscovite, magnetite and arsenopyrite, 0-3% sphalerite and galena, 0-2% chalcopyrite, pyrrhotite and chert, and in 1 sample, trace Mg-chlorit chloritoid and garnet (sample U143-113).

The principle varieties of 4C at Grum are:

1) sericitic, containing up to 20% white mica
2) carbonaceous, containing trace to minor wisps of graphi
3) sulfide-rich, containing 60-80% sulfides
4) variously chalcopyrite, magnetite, pyrrhotite, or carbo ate bearing

These varieties can grade into other ore facies; the sericitic v riety grades into a siliceous 4L with increasing sericite content; th carbonaceous variety grades into a siliceous and pyritic 4A; and the sulfide-rich variant grades into a siliceous variety of the massive pyritic ore.

Base-metal bearing pyritic quartzite (4D): The base-metal bear pyritic quartzite is another banded ore facies. It contains less tha 80% total sulfides and more than 5% combined zinc-lead (Plate 21). predominant mineralogy of this facies is quartz, pyrite, sphalerite, and galena. Thin section examination reveals that 4D usually contai

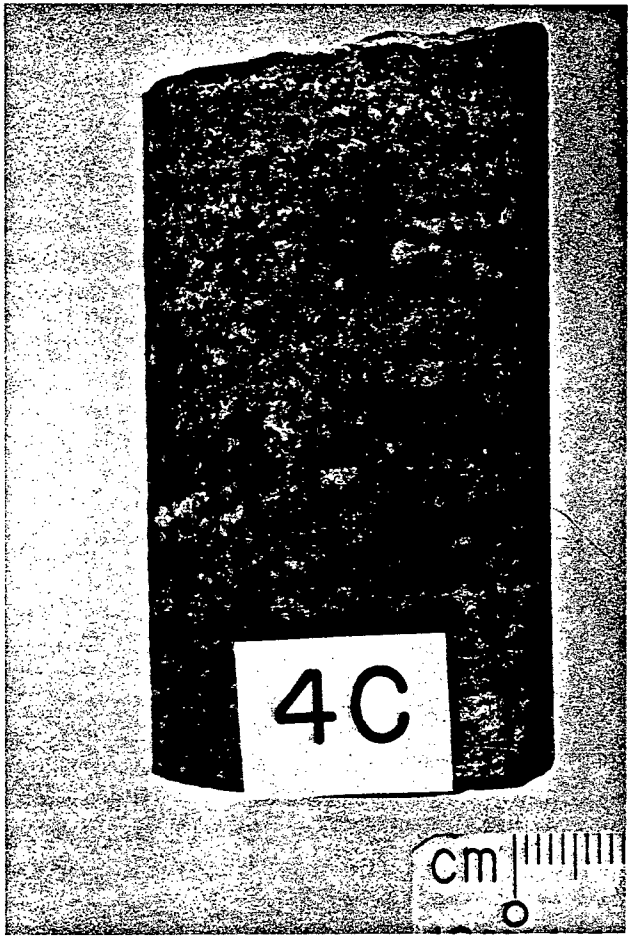

Plate 20. Pyritic quartzitic ore (4C). Banded ore consisting primarily of pyrite and quartz (Sample A135-157.8).

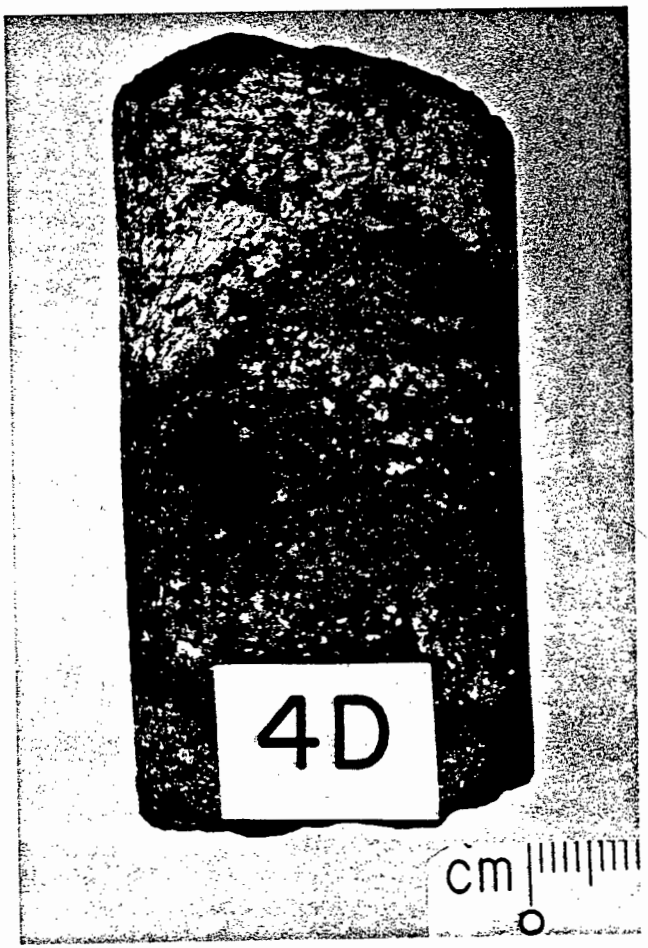

Plate 21. Base metal-bearing, pyritic quartzitic ore (4D). This sample shows some segregation of pyrite from sphalerite and galena in addition to the sulfide-quartz banding (Sample U15-114.3).

trace to minor amounts of muscovite, carbonate, chert and arsenopyrit Furthermore, 4D can locally contain trace to minor amounts of chalco- pyrite, magnetite, pyrrhotite, and graphite. Tennantite-tetrahedrite was not observed in the 4D samples studied. Barite and magnetite are not common. The sphalerite in 4D samples is usually red, though occa sionally orange and in one sample, honey-colored sphalerite was obse ved (Plate 22). The average sample of 4D at Grum contains approxima ly 40% total sulfides occurring in 2-20 mm bands alternating with mi quartz. The sulfides consist of pyrite, sphalerite, and galena and assay values range between 5 and 10% combined zinc-lead. There are several variations of this average 4D which are also common at Grum:

1) sphalerite and galena bearing 4D contains greater than 10% combined Zn+Pb
2) carbonaceous 4D contains minor wisps or laminae of gra- phite
3) sericitic 4D contains up to approximately 15 to 20% mu covite
4) chalcopyrite, pyrrhotite, magnetite or carbonate beari 4D varieties contain these constituents in variable bu minor amounts
5) "patchy" 4D is a textural variant in which a massive s fide matrix with or without abundant quartz gangue, su rounds irregular 10-20 mm patches of quartz
6) sulfide rich 4D contains 60-80% total sulfides in a fa ric which is more massive than banded

The carbonaceous variety grades into a sulfide-rich, siliceous the sericitic variety grades into a siliceous sulfide-bearing variet of the alteration facies, and the sulfide-rich variety grades into a base-metal bearing, siliceous pyritic massive sulfide.

The banding in 4D usually consists of alternating milky quartz sulfide bands of pyrite, sphalerite and galena. Occasionally, 4D ha shown segregation into quartz bands, pyrite bands, and sphalerite pl

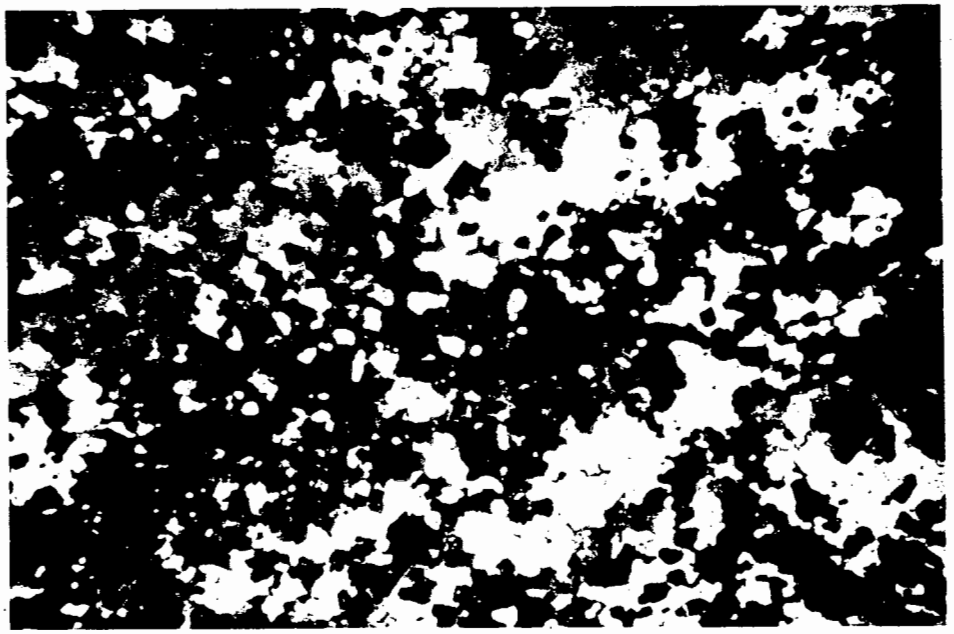

Plate 22. Banded texture of base metal-bearing, pyritic quartzitic ore (4D). Light orange sphalerite is not common in the 4D ore facies which usually contains orange-red or red sphalerite. Sphalerite (yellow-orange), pyrite (black), quartz (white). Plane transmitted light. Field of view is 13.5mm. (Sample U150-138.9).

galena bands.

Massive pyritic sulfides (4E): The massive pyritic sulfide ore facies consists of greater than 80% total sulfides with pyrite as the predominant iron sulfide (Plate 23). The mineralogy is primarily pyrite with occasional minor sphalerite, galena, magnetite, pyrrhotite, carbonate, barite and quartz (Plate 24). Furthermore, polished thin section studies of 17 samples of 4E reveal arsenopyrite, chalcopyrite, tennantite-tetrahedrite, marcasite, mica, chert, chlorite, and graphite all occasionally present in trace to minor quantities. Sphalerite color is usually orange to red.

A number of variations of 4E are common:

1) siliceous, massive pyritic sulfides contain 20-25% quartz usually as 1-2 mm quartz "eyes" evenly dispersed through a sulfide matrix or as occasional irregular patches of quartz about 15 mm in diameter
2) base-metal bearing massive pyritic sulfides contain greater than 5% combined Zn+Pb
3) carbonate bearing massive pyritic sulfides contain up to 20% carbonate minerals commonly ankerite, either interstitial gangue or as irregular coarse patches of buff colored ankerite
4) barite bearing massive pyritic sulfides contain up to 10% barite
5) magnetite bearing massive pyritic sulfides contain the magnetite in streaks or laminae and commonly contain carbonate or barite gangue as well
6) pyrrhotite bearing massive pyritic sulfides usually contain abundant sphalerite and galena as well

There can be and usually are combinations of these variants such as magnetite, base-metal, and carbonate bearing massive pyritic sulfide. Also, the varieties are seen to grade into other ore facies. For example, extremely siliceous varieties of 4E are similar to sulfide rich 4D, barite bearing 4E grades into the barite facies with in-

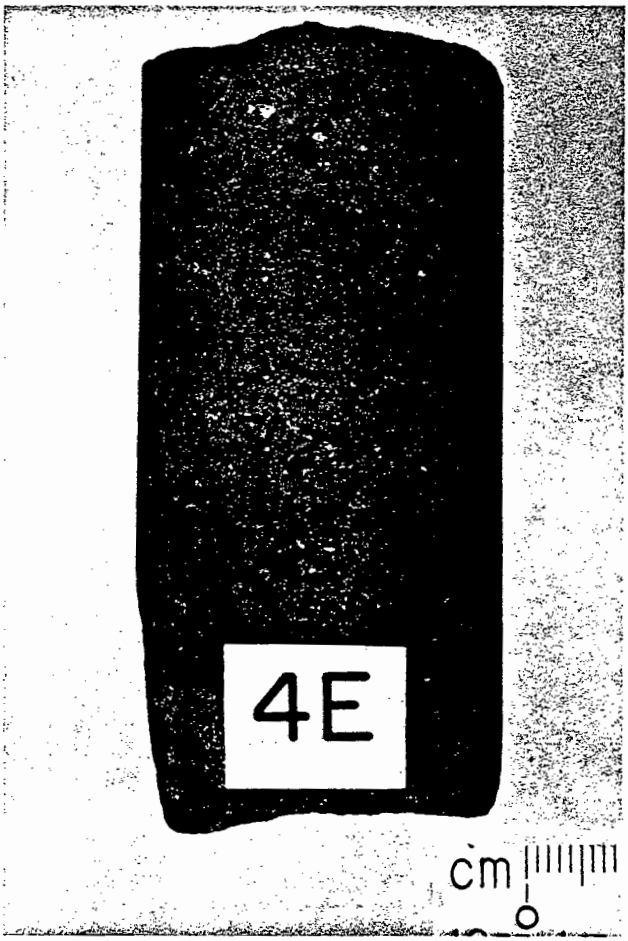

Plate 23. Massive pyritic sulfide(4E). Sample U151-3.7.

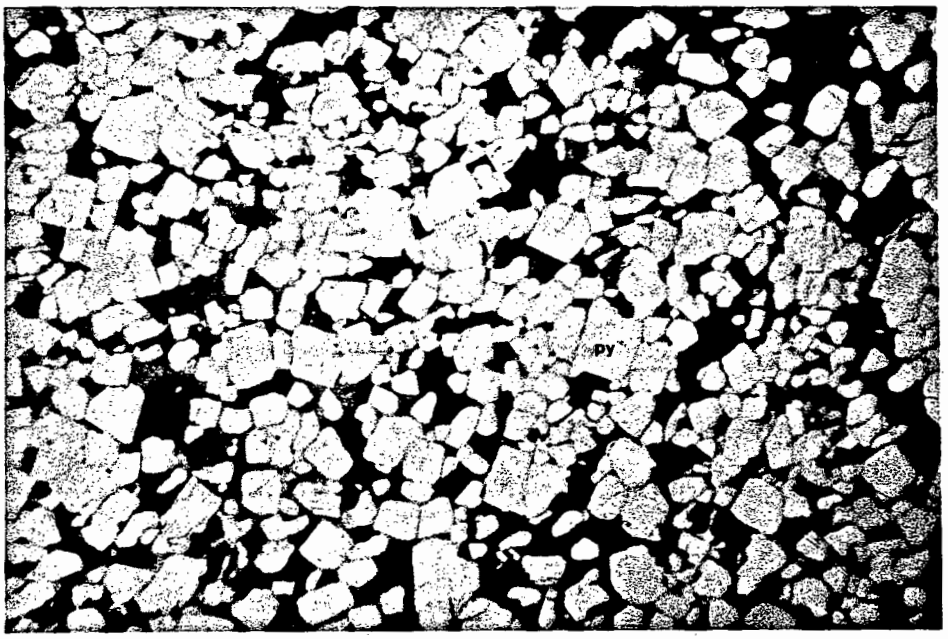

Plate 24. Typical texture of massive pyrite (py) from a massive pyritic sulfide band within a sample of baritic ore. Reflected light. Field of view is 5.4mm. (Sample A99-142.1).

creased barite content, carbonaceous and siliceous massive pyritic sulfides can grade into a sulfide rich 4A, with increased base-metal content 4E can grade into a base-metal massive sulfide, the patchy ankerite bearing 4E grades into 4K with increased carbonate content, and the pyrrhotite bearing variety grades into the pyrrhotitic massive sulfide 4H, as pyrrhotite becomes the predominant iron sulfide. Samples of massive pyrite with negligible base-metal sulfides can show local evidence of foliation and annealing of pyrite grains (Plate 25).

Baritic ore (4G): The baritic facies is a massive sulfide ore facies containing greater than 10% white barite intimately mixed with sulfide minerals (Plate 26). At Grum, the average 4G has approximately 25% barite and 5-10% combined zinc-lead, though the barite content can range up to 60% and the grade can vary (Plate 27). In the Faro deposit 10-15% barite is maximum. This facies is usually well-laminated with thin 1-2 mm thick bands of varying barite content.

The mineralogy of the 4G ore facies consists primarily of pyrite, barite, sphalerite and galena. Carbonate, arsenopyrite, chalcopyrite, and tennantite-tetrahedrite are nearly ubiquitous trace to minor constituents in the 12 thin sections studied. Magnetite is occasionally present in minor amounts. Quartz, muscovite, chert, chlorite, and pyrrhotite with associated marcasite only rarely occur and then only as trace constituents. Graphite is totally absent from this facies.

Sphalerite in the baritic ore is usually honey colored or even pale yellow (Plate 28). Only very rarely is baritic ore seen with red or orange sphalerite. To a certain extent, this pale sphalerite is

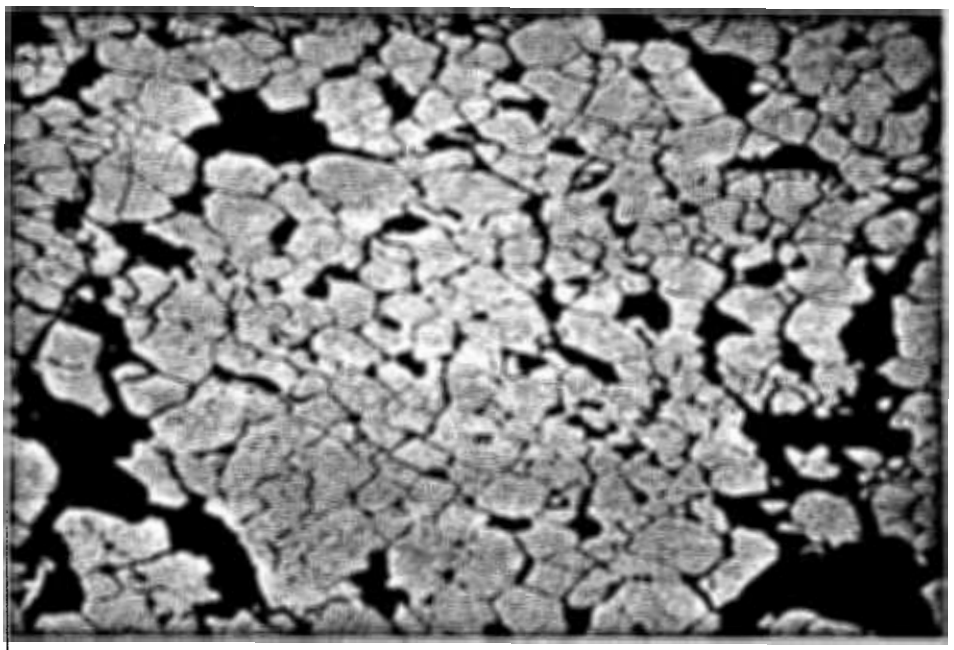

Plate 25. Foliation and annealing of pyrite (py) in a massive pyritic band within pyritic quartzite (4C). Such foliation is rare in the Grum deposit. Reflected light. Field of view is 5.0 mm. (Sample U15-115.3).

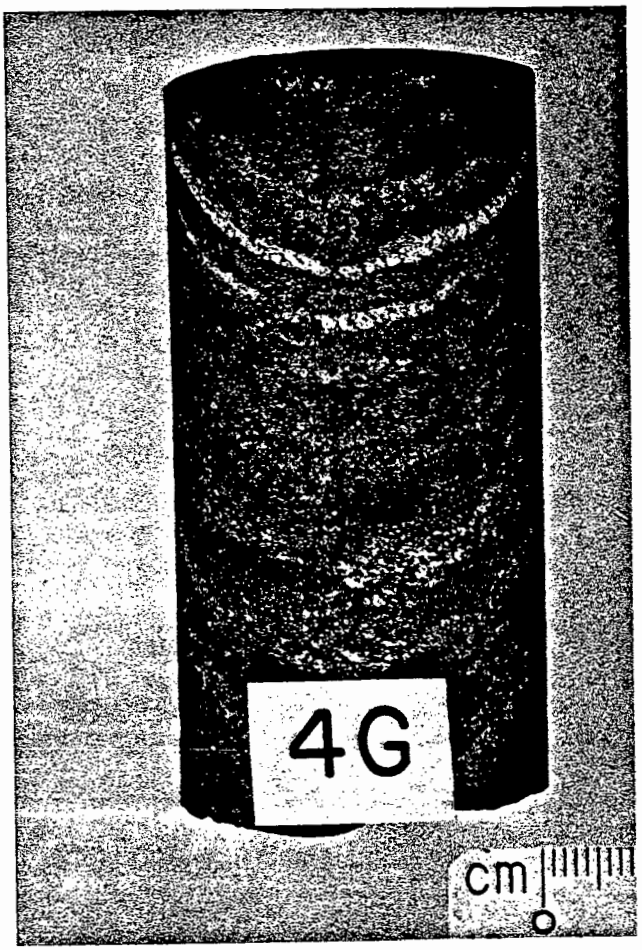

Plate 26. Massive sulfide and barite ore -- the baritic facies (4G). This well-laminated sample contains minor magnetite (Sample A38-1156.5).

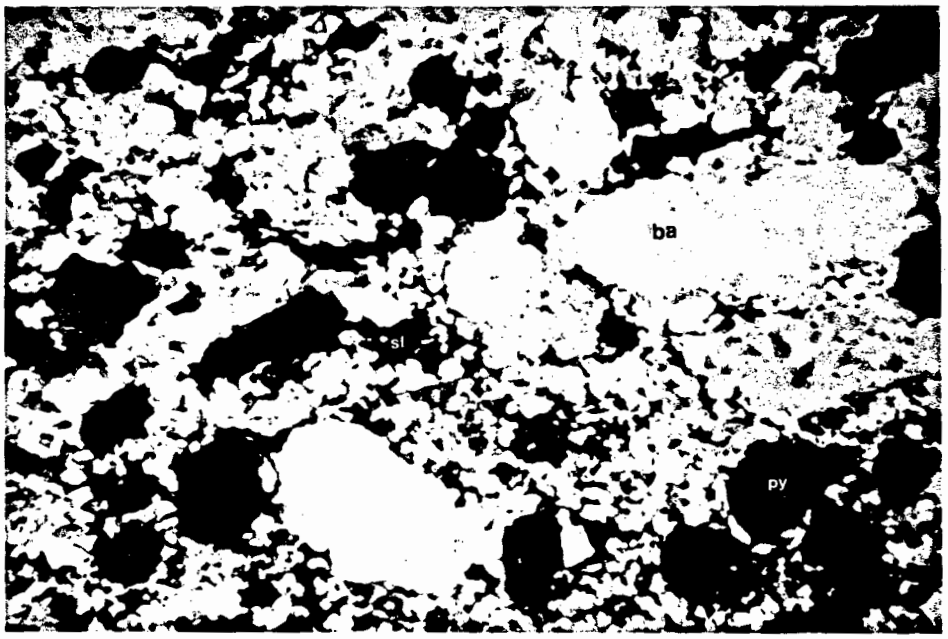

Plate 27. Texture of a barite-rich sample showing grain size changes including large recrystallized elongate grains of barite (ba). Minor pale sphalerite (sl) and pyrite (py). Plane transmitted light. Field of view is 5.4mm. (Sample A99-142.1).

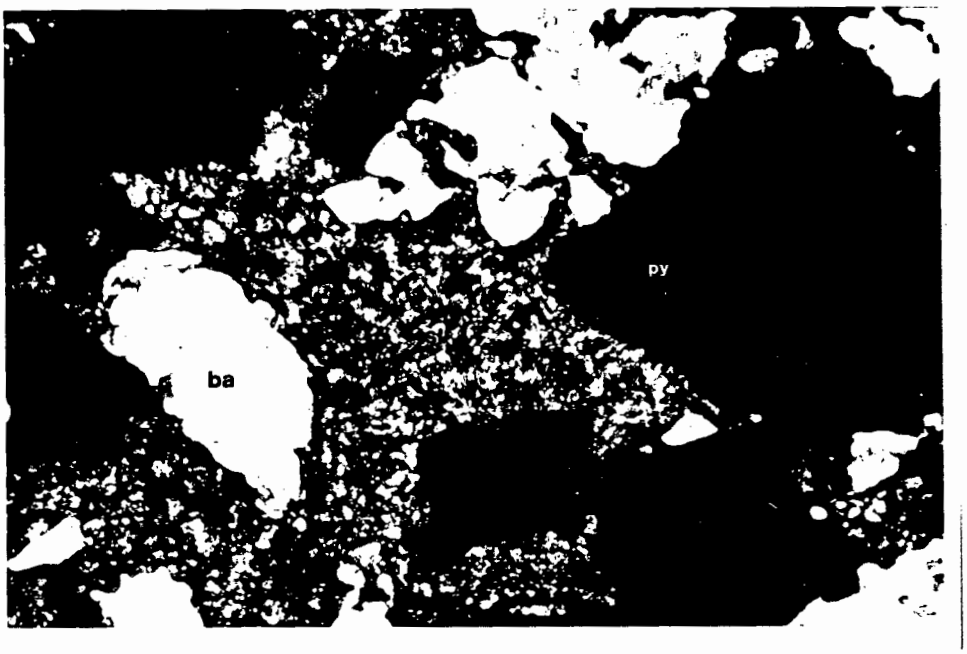

Plate 28. Pale sphalerite (sl) in baritic (ba) ore. Rounded inclusion of orange-red sphalerite within pyrite (py) grain. Pyrite grains often contain rounded inclusions of sphalerite that are a different color from the surrounding sphalerite. Plane transmitted light. Field of view is 1.44mm. (Sample U15-27.4).

exclusive to the baritic ore.

A common variety of 4G is carbonate bearing. Carbonate minerals can be of the same habit as barite and intermingled with the barite, or the two gangue minerals can alternate in bands or the carbonate gangue can dominate to the exclusion of the barite over an interval of up to a meter or so. Barite deficient zones seem to be intimately associated with the barite facies and are not very common. The carbonate mineral is calcite, dolomite or ankerite by X-ray diffraction, though Tetsuro Urabe has identified barytocalcite in some of the DY ore (D.S. Jennings, personal communication).

A related variety of the baritic ore is the porous variety in which zones or perhaps laminae of carbonate gangue have been leached leaving a porous sulfide rock.

Other ore facies: The 4K or ankerite bearing ore facies is the most common minor facies at Grum. It consists of a massive sulfide matrix surrounding at least 35% coarse, buff colored, ankerite patches. The coarse and patchy nature of the ankerite gives the facies a brecciated textural appearance. Commonly, 4K has a massive pyrite matrix with 50% coarse (1-1.5 cm) ankerite patches associated with patches and discordant veinlets of remobilized sphalerite and galena and occasionally chalcopyrite. However, the sulfide matrix can have massive pyrrhotitic or massive base-metal sulfide affinities, and quartz can be associated with the ankerite (Plate 29).

The pyrrhotitic massive sulfide facies, 4H, contains more than 80% total sulfides and less than approximately 25% of the sulfides are iron

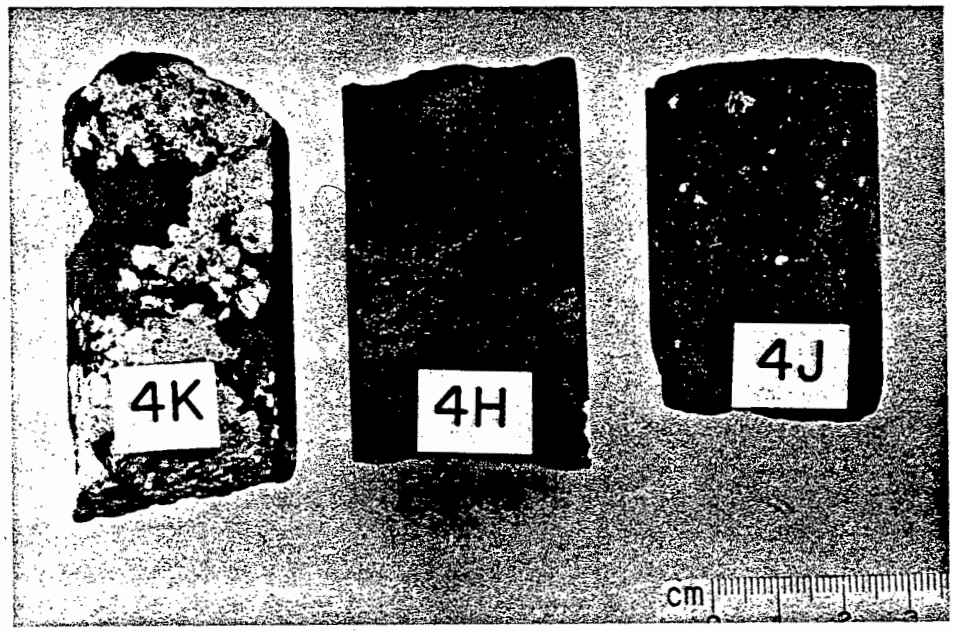

Plate 29. Less common ore facies in the Grum deposit. 4K is an ankerite-bearing facies which commonly displays a "brecciated" texture of large ankerite clasts in a sulfide matrix (Sample U156-57.7). 4H is the massive pyrrhotitic sulfide facies (Sample A135-137.1). 4J is the massive base-metal sulfide facies (Sample U39-82.5).

sulfides (Plate 29). Though not common at Grum it can occur as localized 10-30 cm intervals within a massive pyritic sulfide unit or as 2-3 cm bands within a unit of the alteration facies.

The massive base metal sulfide facies, 4J, contains more than 80% total sulfides and less than approximately 25% of the sulfides are iron sulfides (Plate 29). This is a rare, high grade ore facies at Grum. When it does occur, it is associated with high grade sections of massive pyritic sulfides. The mineralogy is predominantly sphalerite, galena and minor pyrite though it can contain up to 20% quartz "eyes" and fine pyrite porphyroblasts.

Buckshot ore, 4F, is a high grade massive ore with coarse porphyroblastic pyrite found at Faro due to a higher degree of metamorphic recrystallization there. Buckshots are approximately 1-2 mm in diameter. This facies is not seen at Grum. The only correlative would be the fine-grained buckshots (0.5-1.0 mm) seen in the 4J ore facies and occasional, isolated porphyroblasts.

ALTERATION

Sericitized and variably mineralized rocks irregularly surround the Anvil Range ore deposits and are sometimes best developed in the footwall. Cyprus Anvil geologists suggest that this alteration could be related to ore fluid influx. This is evidenced in some Anvil deposits by footwall alteration closely associated with stringers of mineralization discordant to bedding ($S_0//S_1$).

Altered phyllites around the Grum deposit are bleached (sericitized) and variably silicified and mineralized (Plate 30). They can

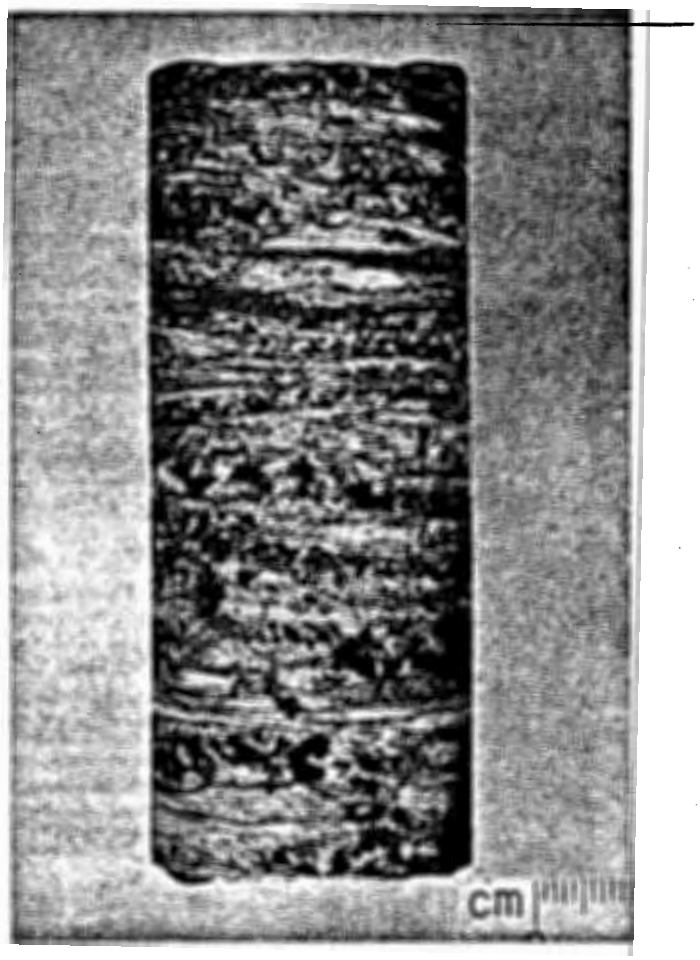

Plate 30. Sample of 4L, the sericitic alteration which inconsistently surrounds the ore horizons. This sample (U39-32.7) is siliceous and pyritic.

be classified as siliceous, pyritic, pyrrhotitic, chalcopyrite-bearing, sphalerite and galena-bearing and occasionally carbonate or talc-bearing. Sometimes bleached, unmineralized phyllites occur at some distance from the ore horizons. Siliceous, sericitized, mineralized phyllites can also occur within the orebodies and are seen to grade into more siliceous, less sericitic quartzitic ore and into graphite-poor, phyllitic, ribbon-banded ores.

Thin section examination of 6 samples of 4L lithologies provided no further clues to the origin of the alteration. Minerals observed were muscovite (confirmed by X-ray diffraction), quartz, sericitized feldspar, pyrite, pyrrhotite, minor sphalerite, galena, chalcopyrite, marcasite, garnet, carbonate, and trace ilmenite, zircon, allanite and tourmaline. Pyrrhotite is perhaps more common in 4L samples at Grum than in the ore facies.

STRUCTURE

The structure of the Grum deposit is being interpreted in detail by Cyprus Anvil geologists. The predominant foliation surface in the Grum deposit is S_2. Although this surface generally dips gently to the southwest in the area of the deposit, Kerr Addison geologists also mapped horizontal and gentle northeasterly dipping S_2 surfaces in the underground workings. The S_1 foliation, which is folded by S_2, is preserved as crenulated microlithons of metamorphic micas (Plate 4). Occasionally, S_3 and/or S_4 are seen as non-penetrative foliation surfaces steeper than the earlier S_2, or as kink folds which fold S_2.

By assuming that the dip direction of S_2 is a constant 230°, sec-

ond phase symmetry data could be obtained from drill core. If, in a given core, S_1 dips in the same direction as S_2 but at a steeper angle, the symmetry (looking northwest) is S-symmetry. If S_1 dips more gently than S_2 or in the opposite direction, the symmetry is Z-symmetry. In areas of pervasive $S_2(S_0//S_1//S_2)$, horizontal S_2, or where S_1 dips at right angles to S_2, symmetry cannot be determined. Wherever possible, symmetry observations were recorded and compiled so that microlithon symmetry could be extrapolated to the symmetry of major D_2 folds as an aid in interpretation of cross sections (Plate 31).

The overall deposit structure is that of a refolded first phase fold very similar in fold style to that of an outcropping fold in green, laminarly-banded tuffaceous phyllite of the Vangorda Formation (Plate 32). The second phase fold which affects the Grum deposit plunges to the northwest bringing the deposit near to the surface in the southeast but extending it to depths of 350 meters in the northwest. The deposit consists of four separate sulfide horizons. Figure 14 is a generalized cross section through the 4 sulfide horizons of the Grum deposit showing the fold structure. Horizons 1 and 2 are in Mt. Mye Formation; horizons 3 and 4 are in Vangorda Formation.

Horizon 2 is the major sulfide horizon and contains all of the ore facies. It usually consists of ribbon-banded and quartzitic ore capped by massive and baritic ore at the stratigraphic hangingwall and displays well developed footwall alteration. The host unit is Mt. Mye noncalcareous phyllite. Graphitic or calcareous muscovite-chlorite phyllites of the Vangorda Formation overlie the second horizon. Horizon 2 defines the refolded fold and is about 1250 meters in unfolded length across the

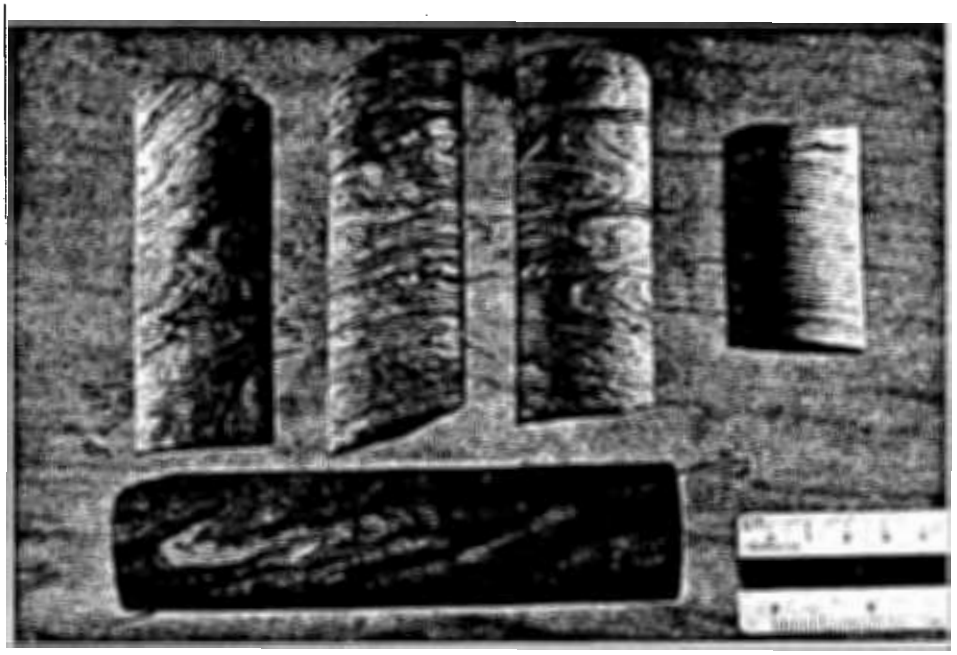

Plate 31. Second phase symmetry seen in drill core can be extrapolated to the symmetry of major second phase folds in cross section interpretation. From left to right, symmetry looking northwest is: S symmetry (Sample A11-113.3); Z symmetry (Sample A32-920); symmetry indeterminate because S_2 is horizontal (Sample U150-107.9); indeterminate because S_2 is pervasive (Sample A79-974.3). Lower sample is Z symmetry (Sample U153-53.4).

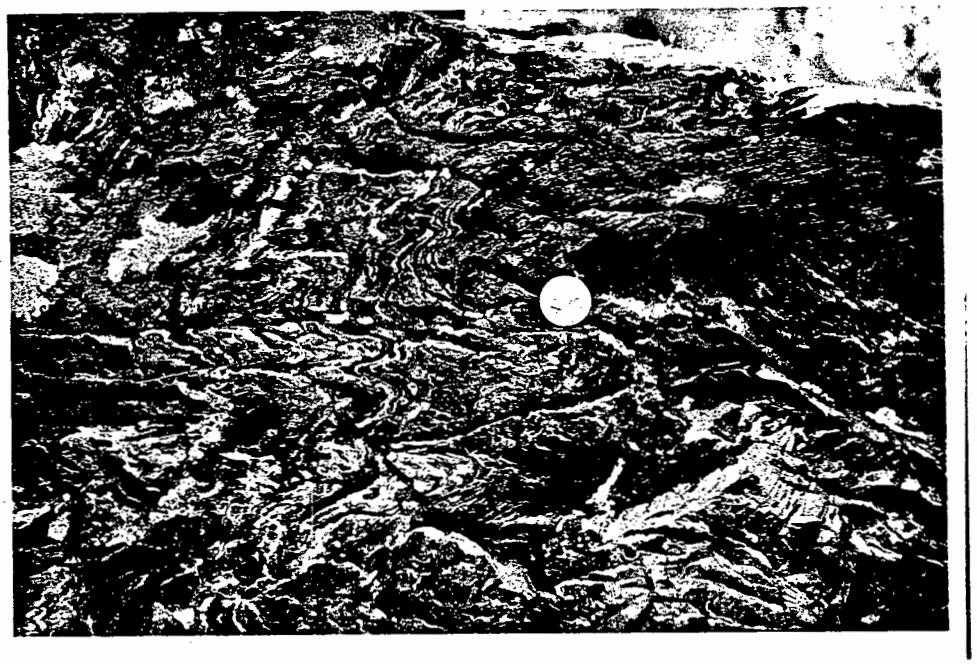

Plate 32. First phase fold closure refolded by second phase deformation in an outcrop of laminarly banded tuff near the DY deposit. First phase closure can be seen clearly 2 cm at 10:00 from the coin. The interpreted fold style of the Grum deposit is very similar to the fold style in this outcrop.

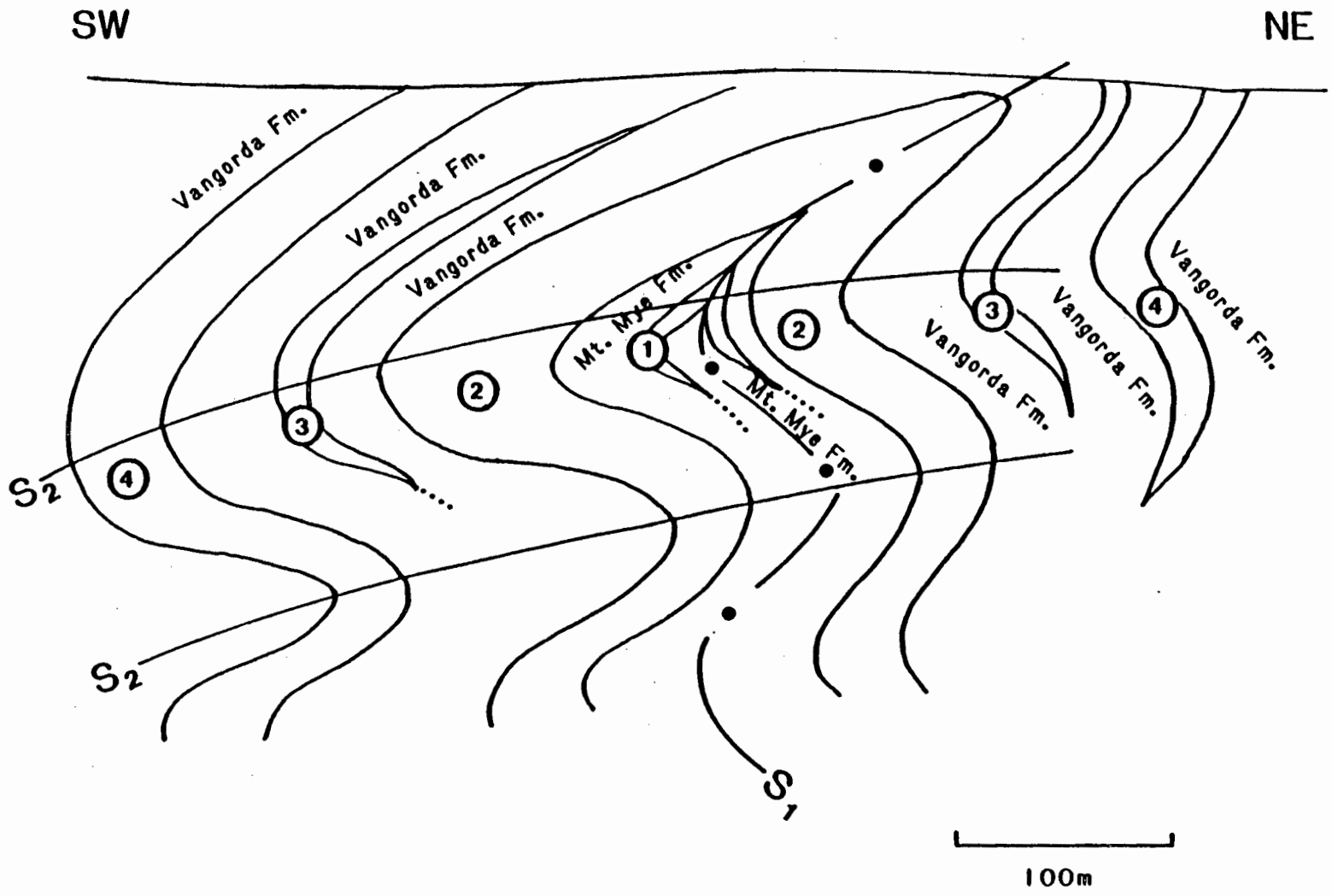

Fig. 14. Generalized cross section through the Grum deposit showing the fold structure. Sulfide horizons 1 through 4 are sequenced from lowest to highest stratigraphic position. S_1 and S_2 foliations are axial planar to F_1 and F_2 folds. Scale is approximate.

deposit, though exploration of the deeper limbs is incomplete.

Horizon 4 is smaller than horizon 2 but is a major horizon as well. Characteristically more lead-rich than horizon 2, horizon 4 contains abundant magnetite. Horizon 4 is surrounded by calcareous muscovite-chlorite or graphitic Vangorda Formation phyllites and contains all of the ore facies.

Horizons 1 and 3 are thin and discontinuous. Horizon 1 in the Mt. Mye Formation consists mostly of ribbon-banded ore and sericitic alteration. Horizon 3 in the Vangorda Formation contains baritic ore and sericitic alteration with some massive pyritic ore and some ribbon-banded ore.

Thicknesses of the horizons range from 5 meters to 60 meters and stratigraphic distance between horizons is approximately 20-50 meters. There is some tectonic thickening of the sulfide horizons in the second phase fold closures and the ore grade is somewhat increased near the hinges as well. Discontinuity of horizons 1 and 3 is possibly a result of tectonic localization of sulfides along axial planes of folds.

The Grum deposit, particularly the southeastern half of the deposit, is disrupted by a multitude of faults expressed in drill core as zones of fault gouge and brecciation. Zones of faulting often intersect sulfide horizons creating sulfide breccias which vary from well-healed massive sulfide breccias to open vuggy, ankerite-healed breccias. At least one sample of a double breccia was seen indicating two episodes of faulting locally. Movement along many of the faults has been negligible but significant displacement along other of the faults has greatly complicated an already complex structure. One of the most

significant faults is a low angle detachment fault, the Doal Lake Detachment, which occurs in cross sections south of 70 West, and below which is a thick and continuous sulfide horizon of uncertain stratigraphic origin. The lower block containing the sulfide horizon is thought to have been displaced to the northeast relative to the overlying block and the fault could be part of a step-like detachment from the batholith (D.S. Jennings, personal communication). It is thought that this horizon is correlative with horizon 2 and it may extend farther to the north than present drilling shows.

Samples from three cross sections through the Grum deposit were used in this study. Cross section 80 West is a typical section through the deposit which shows the fold structure and all four sulfide horizons (Fig. 15). Horizons 1 and 3 are not continuous; horizon 4 is of highly variable thickness and seems to pinch out rather than continue around the first phase fold closure; horizon 2 is large and continuous. Both 2 and 4 are overlain by graphitic phyllite. The Mt. Mye-Vangorda contact can be drawn along horizon 2. Second phase folding has attenuated stratigraphic thicknesses on the fold limbs and thickened the fold hinges. Movement along a steep fault in the north half of the cross section has repeated the first phase fold nose.

Cross section 74 West has been complicated by a multitude of faults but the first phase closure is still clearly shown. A preliminary sketched interpretation of 74 West is shown in Figure 16.

Cross section 66 West might contain all four sulfide horizons as shown in an interpretation in Figure 17. The first phase closure, cored by Mt. Mye phyllites, is not clearly evident but can be extrapo-

Fig. 15. Structural interpretation of cross section 80 West. Surface drill holes are labelled with "A" before the diamond drill hole (DDH) number; holes drilled from underground workings are labelled "U". Sulfide horizons are sequenced bottom to top with circled numbers. Dotted lines indicate sericitic alteration. Wavy lines represent faults. Elevation above sealevel is given in meters. Arrows mark sulfide intersections studied in detail, with arrowheads pointing to the stratigraphic hangingwall (generalized after Cyprus Anvil Mining Corp.).

Fig. 16. Preliminary sketched interpretation of cross section 74 West through the Grum deposit. Arrows show two sulfide intersections used in this study with arrowheads pointing to the interpreted stratigraphic hangingwall. Scale is approximate.

Fig. 17. Structural interpretation of cross section 66 West through the Grum deposit. Symbols are the same as for Figure 16 (generalized after Cyprus Anvil Mining Corp.).

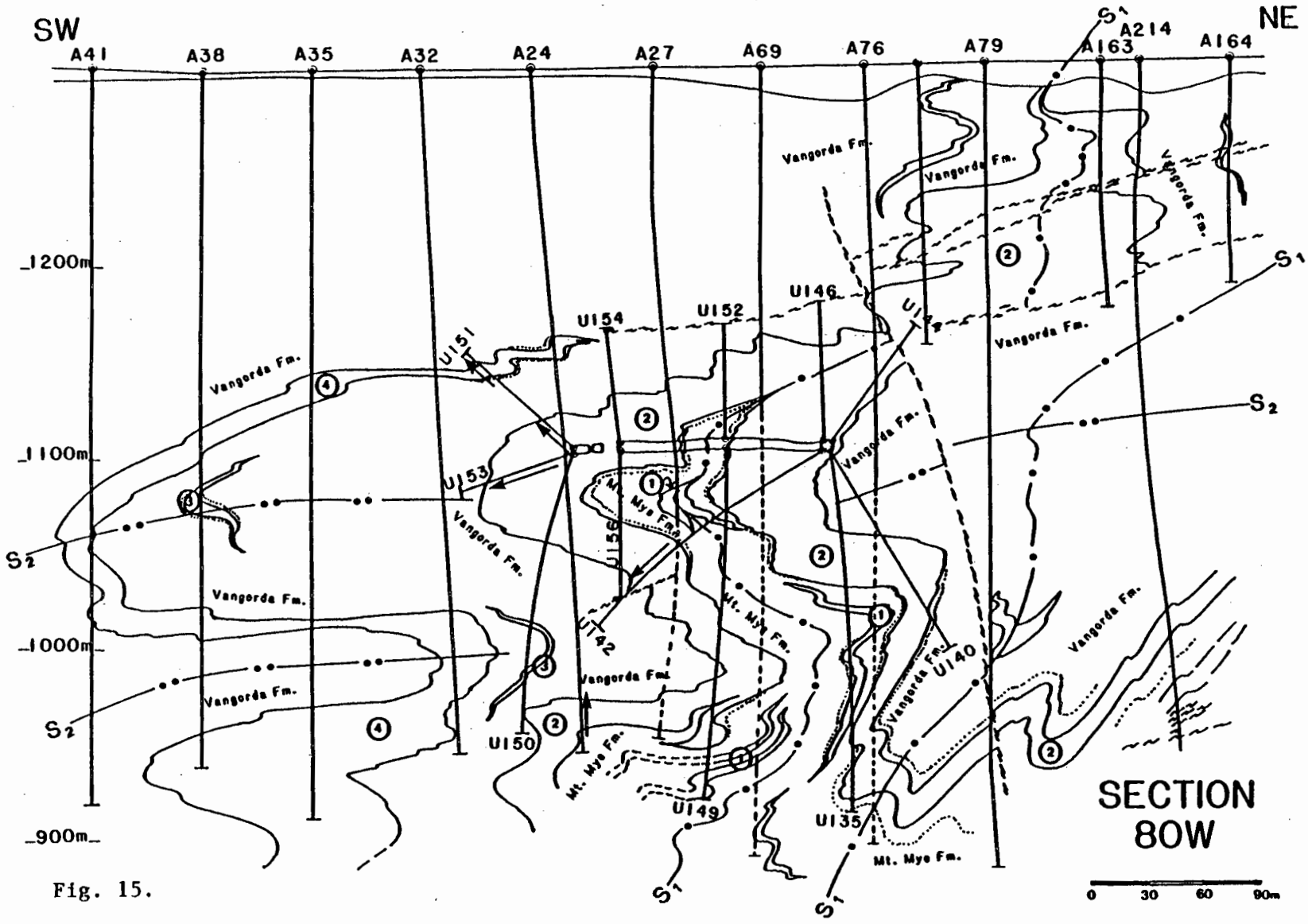
SW
NE
A41
A38
A35
A32
A24
A27
A69
A76
A79
A163
A214
A164
1200m
1100m
1000m
900m
S1
S2
U151
U154
U152
U146
U153
U156
U142
U150
U149
U135
U140
Vangorda Fm.
Mt. Mye Fm.
SECTION
80W
0
30
60
90m

Fig. 15.

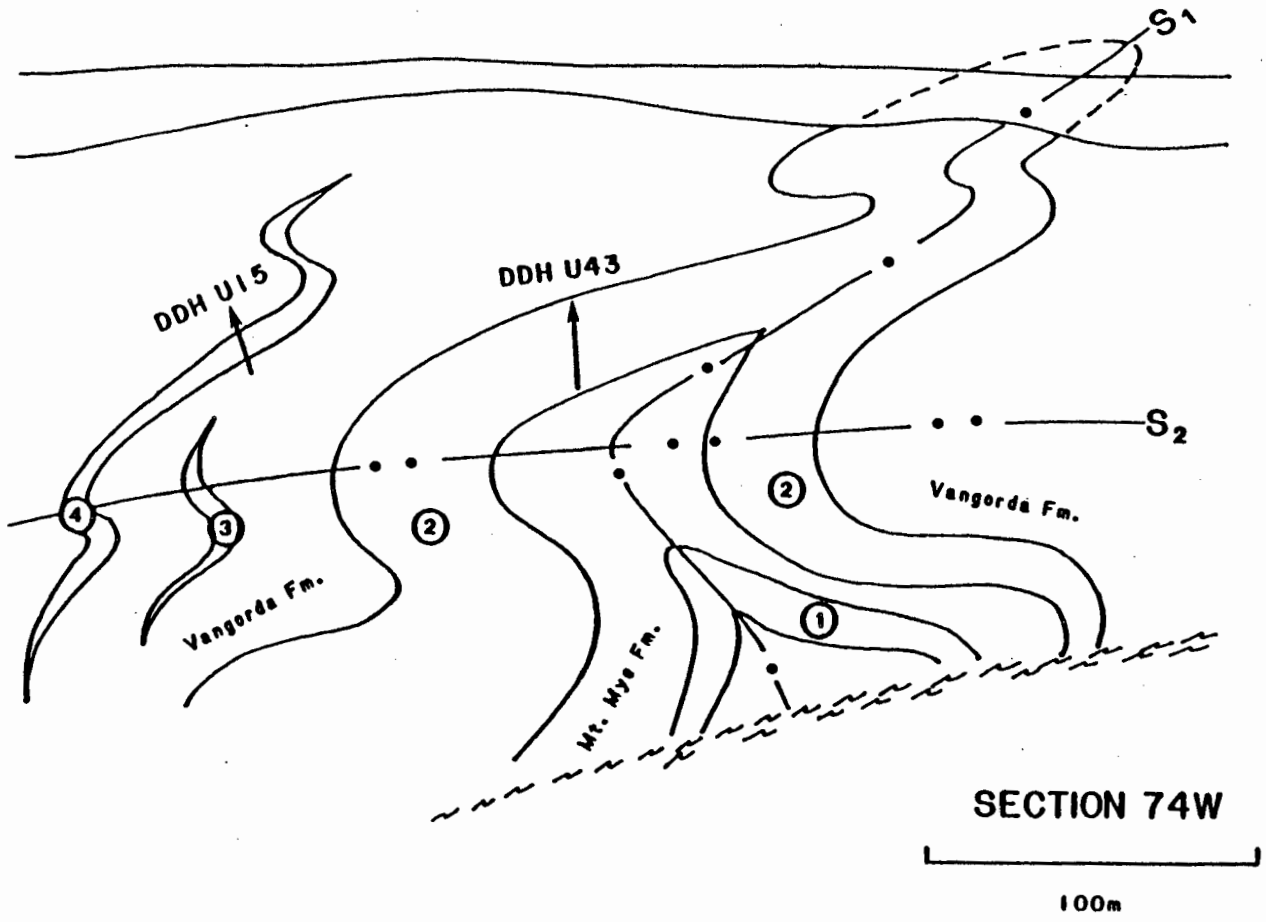
S1
DDH U15
DDH U43
S2
4
3
2
2
Vangorda Fm.
Vangorda Fm.
Mt. Mye Fm.
1
SECTION 74W
100m

Fig. 16.

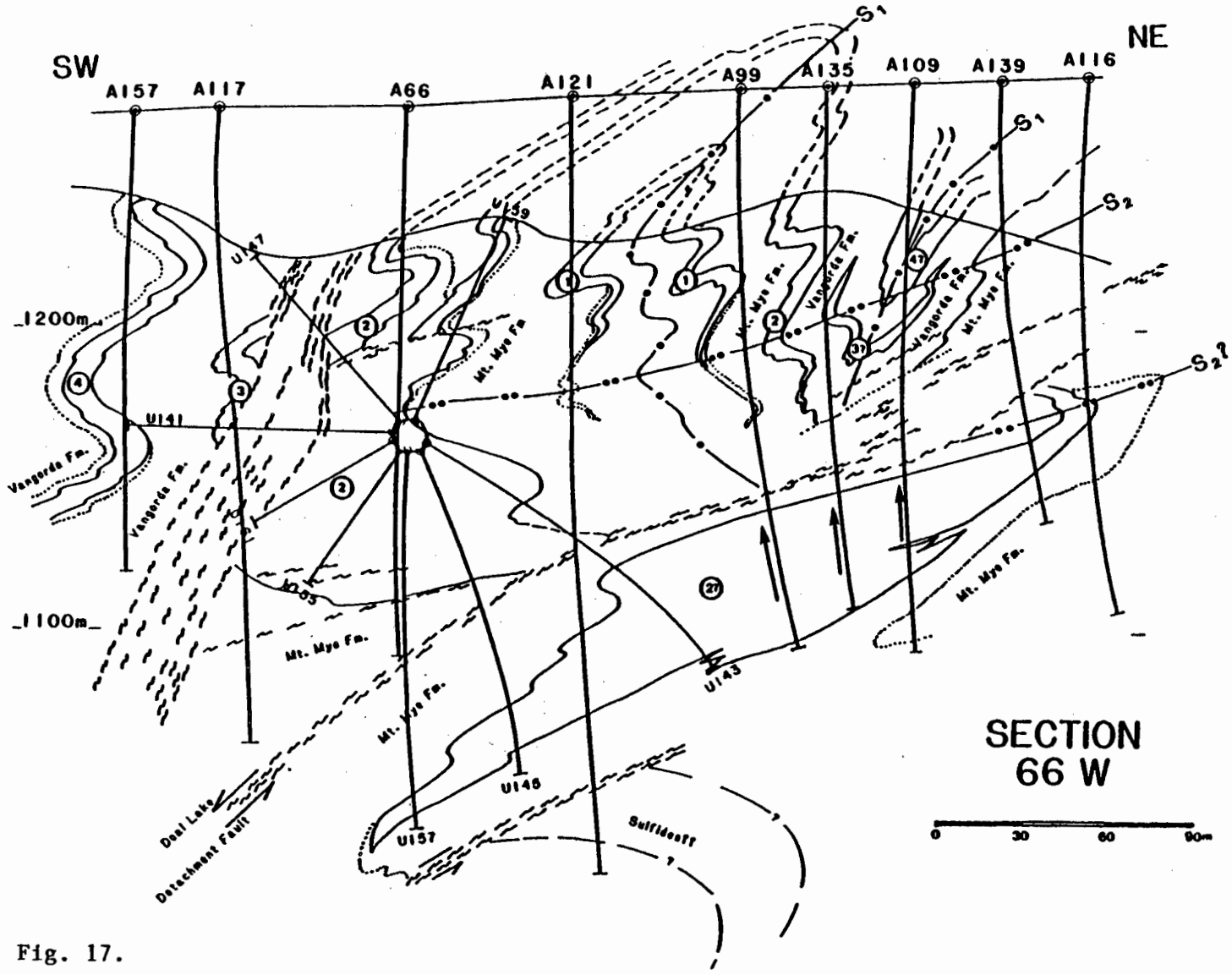
SW
NE
A157
A117
A66
A121
A99
A135
A109
A139
A116
S1
S2
S2?
U147
U139
U141
U105
U143
U145
U157
-1200m
-1100m
Vaqueros Fm.
Mt. Mye Fm.
Dual Lake Detachment Fault
Sulfidesoft
SECTION
66 W
0
30
60
90m

Fig. 17.

lated into the overburden. A major zone of disruption in the southwest block of this cross section has been interpreted as a fault zone which has truncated horizon 2 along the second phase closure and brought the southwest block with horizons 3 and 4 closer to the northeast block. The Doal Lake Detachment, mentioned previously, is present in the cross section and is underlain by a continuous sulfide horizon which has a consistent baritic cap and consistent footwall alteration.

SULFUR ISOTOPES

INTRODUCTION

131 sulfur isotope ratios were determined for mineral separates and bulk sulfide sulfur of 71 samples. Samples were selected from 10 sulfide intersections located on 3 different cross sections through the deposit (Figs. 15-17). Two of the intersections are from horizon 4, five from horizon 2, and three from a horizon of uncertain stratigraphic position, (possibly horizon 2), which lies below the Doal Lake Detachment in the southeastern part of the deposit. The five intersections through horizon 2 are widely spaced over a 420 meter unfolded lateral extent. One of these intersections is on the lower long limb of an S-symmetry second phase fold, one on the short Z-symmetry limb, and three near the fold closure. The three sulfide intersections from the horizon below the detachment are closely spaced, only 30 meters apart. Several of the intersections, especially the three closely spaced ones, show complete or partial Anvil Cycles in the vertical lithofacies variation, with the baritic facies indicating stratigraphic top. Polished thin sections of samples from seven of the chosen intersections were

examined prior to sulfur isotope analysis.

Bulk sulfide sulfur isotopic compositions of a representative sample from each ore facies in nine of the intersections were determined, and where mineral separation was possible, sphalerite, galena, pyrite and barite separates were analyzed. Total range of sulfide $\delta^{34}S$ values is 9.41 to 23.13. Average $\delta^{34}S$ of sulfur from galena is 12.85, sphalerite 15.03, pyrite 16.12, bulk sulfide sulfur 15.89 and barite 31.76. Frequency distributions for sulfur isotopic compositions of mineral separates are shown in Figure 18. Ranges and means for $\delta^{34}S$ of mineral separates and bulk sulfide sulfur are shown in Figure 19. Lower Cambrian seawater sulfate had a sulfur isotope value of approximately 30, making average sulfide sulfur about 15 per mil lighter than sulfur in this sulfate. Barite sulfur isotope values straddle the Lower Cambrian seawater sulfate value and range up to 35. Average sulfide-sulfate separation based on barite-sulfide pairs is 13.8. To a certain extent, sulfur isotope values of barite "track" coexisting sulfide mineral values (Fig. 20).

In general, baritic and massive ore contain heavier isotope values as indicated by average $\delta^{34}S$ values of bulk sulfide sulfur in the various ore facies (Fig. 21). In fact, after a decrease from the ribbon-banded ore there is a gradual stratigraphic increase in $\delta^{34}S$ values from the quartzitic ores through massive ores to the baritic ores. Average $\delta^{34}S$ of the sericitic alteration facies is 14.97, or ribbon-banded ore 15.70, quartzitic ores average 14.72, massive ore averages 16.11 and baritic ore averages 17.05. Increase in average $\delta^{34}S$ from quartzitic through massive to baritic ore is only 2.33 but increases

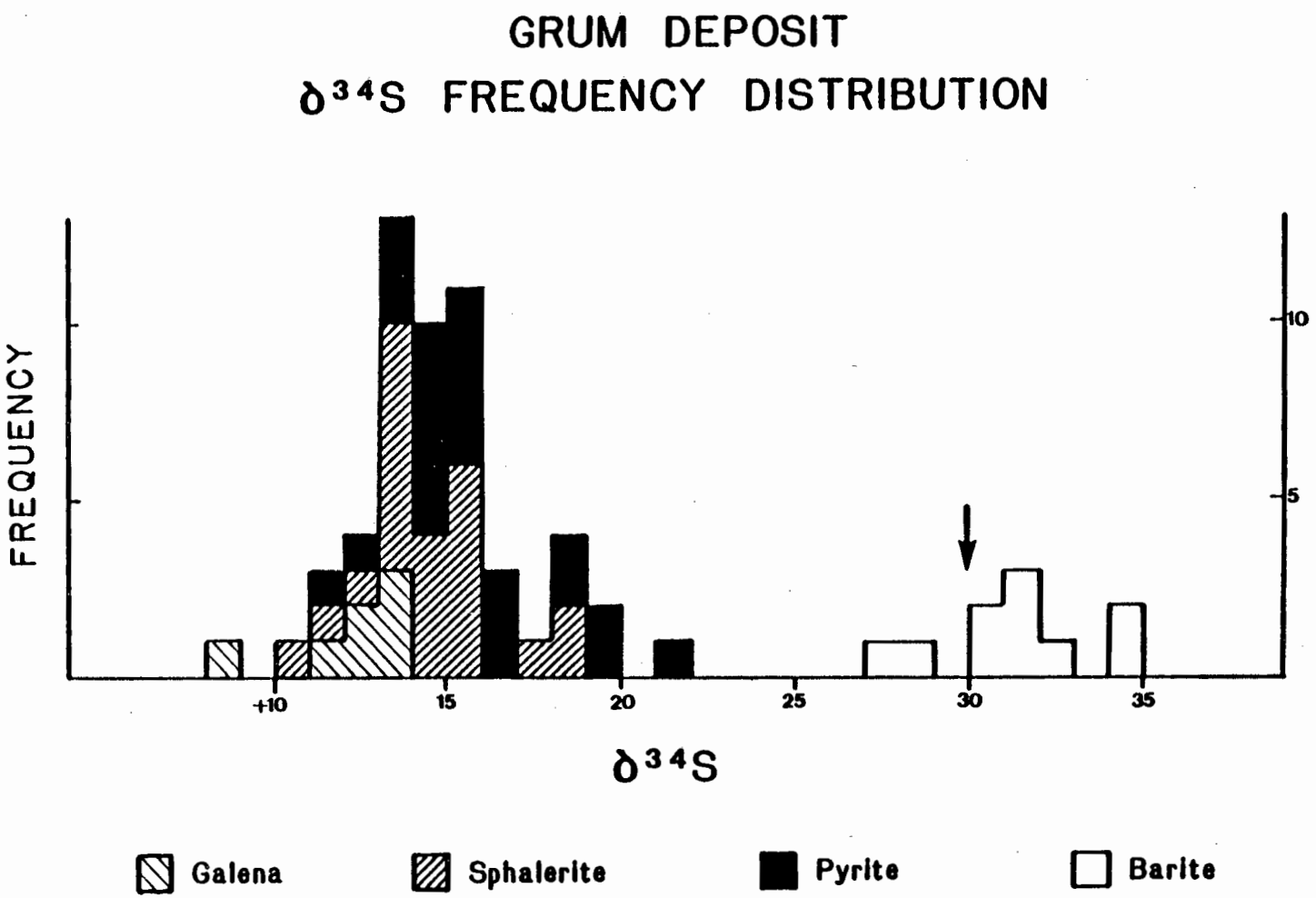

Fig. 18. Frequency distribution for $\delta^{34}S$ of mineral separates in samples from the Grum deposit. Arrow shows approximate composition of Lower Cambrian seawater sulfate.

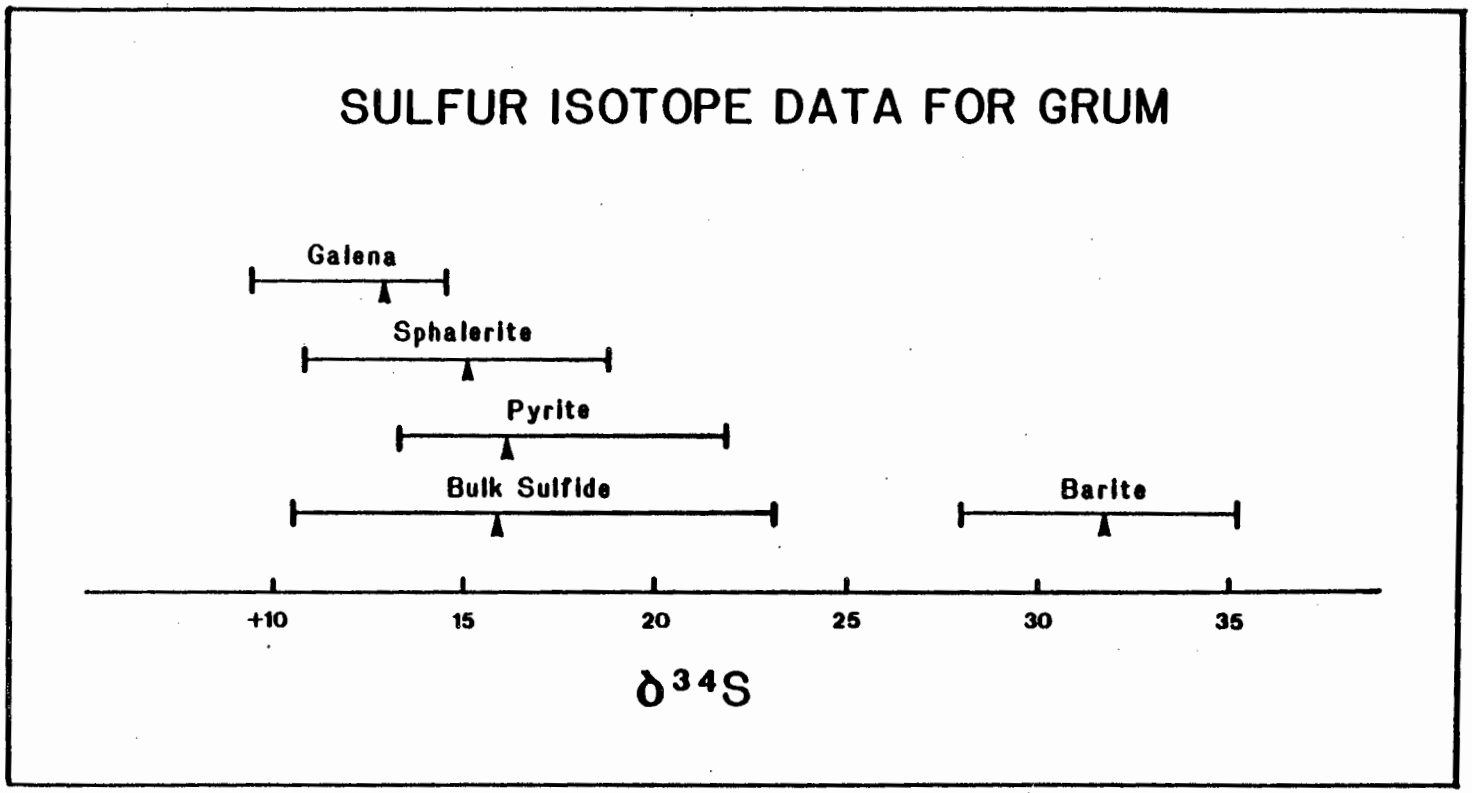

Fig. 19. Range of $\delta^{34}S$ values for galena, sphalerite, pyrite, bulk sulfide sulfur and barite in the Grum deposit. Arrowheads point to mean values.

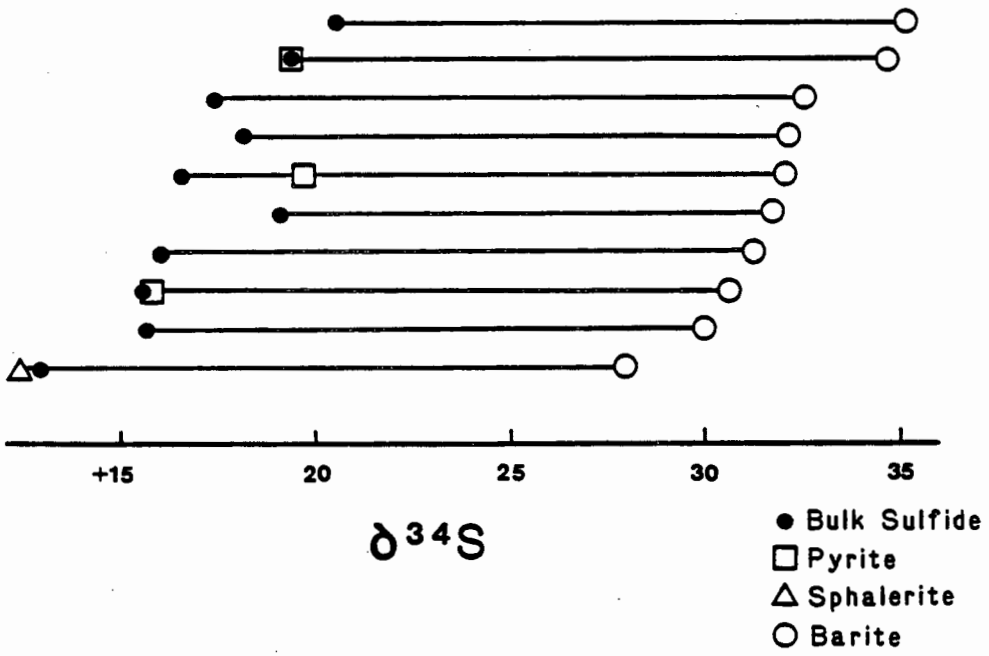

Fig. 20. Plot of $\delta^{34}S$ showing covariation for sulfide-sulfate pairs in the Grum deposit. Sample numbers from the top down are: U15-27.4; U142-122.7; U151-58.0; A109-136.1; A99-153.5; A135-139.7; A24-329.5; A99-142.1; U153-41.3; U153-37.4. Data is reported in Appendix II.

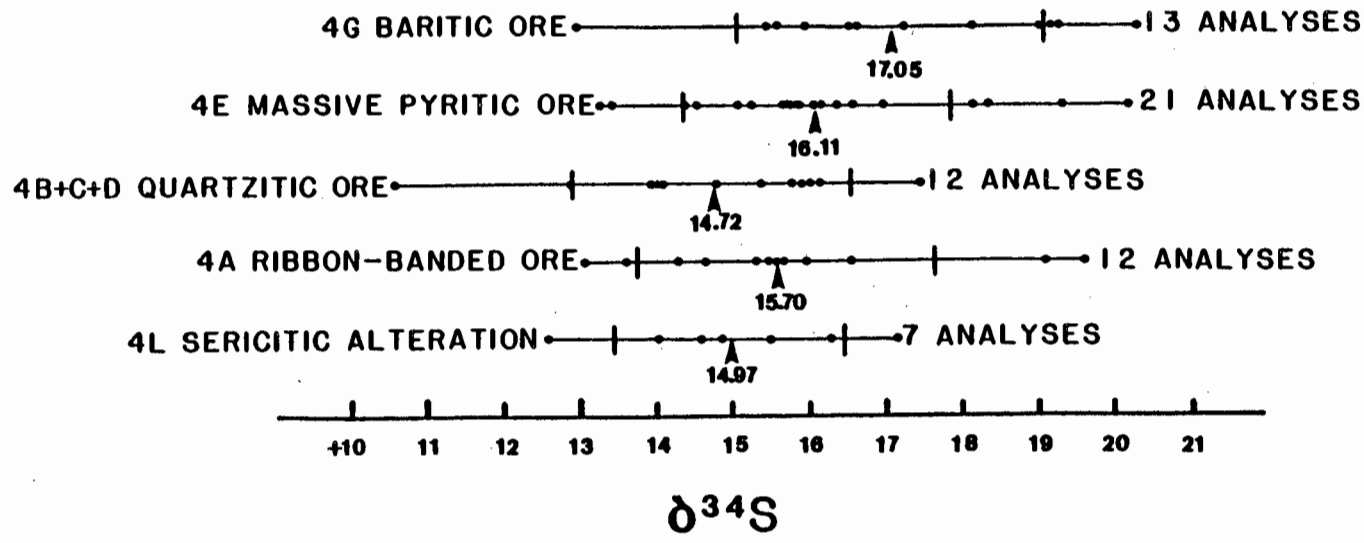

Fig. 21. Range of $\delta^{34}S$ values for bulk sulfide sulfur from various ore facies in the Grum deposit. Arrowheads point to mean values. Mean values show gradual upward increase. Error bars outline the 1.0 standard deviation level. Sample U153-17.0 is not included.

within a given sulfide intersection are as much as 7 per mil. In two intersections, samples above the baritic facies were analyzed and both show a large (7.7 and 5.5) drop in $\delta^{34}S$ relative to the underlying unit. Plots of sphalerite, galena and pyrite averages for the different ore facies follow the same trend of decreasing slightly from the ribbon-banded ore to the quartzitic ores and then increasing to the top of the cycle (Fig. 22).

DETAILED INTERSECTION DATA

The sulfur isotopes follow a similar stratigraphic trend in each of three closely spaced intersections from cross section 66 West, DDH A99, DDH A135, and DDH A109 (Figs. 23, 24 and 25). Following an initial decrease to a minimum value in quartzitic ore (and stratigraphically equivalent siliceous 4L in A109) there is a gradual increase of $\delta^{34}S$ values to the baritic ore at the top of the cycle in each intersection. Above the baritic ore in DDH A99, $\delta^{34}S$ drops off to a minimum and then increases to the top of a different partial cycle. The values of the correlated ore facies show no pronounced lateral variation. Perhaps the minimum $\delta^{34}S$ could be used as a correlation tool. Bulk sulfide values in some samples of DDH A99 are equal to pyrite values for the same sample owing to the predominance of pyrite.

Two intersections, DDH U43 and DDH U151, through horizon 2 show decreasing sulfur isotope values followed by an upward increase. DDH U43, which intersects an Anvil Cycle of sericitic ore at the base followed by ribbon-banded then massive ore, a return to quartzitic ore with minor graphite, and finally massive ore with minor barite, shows

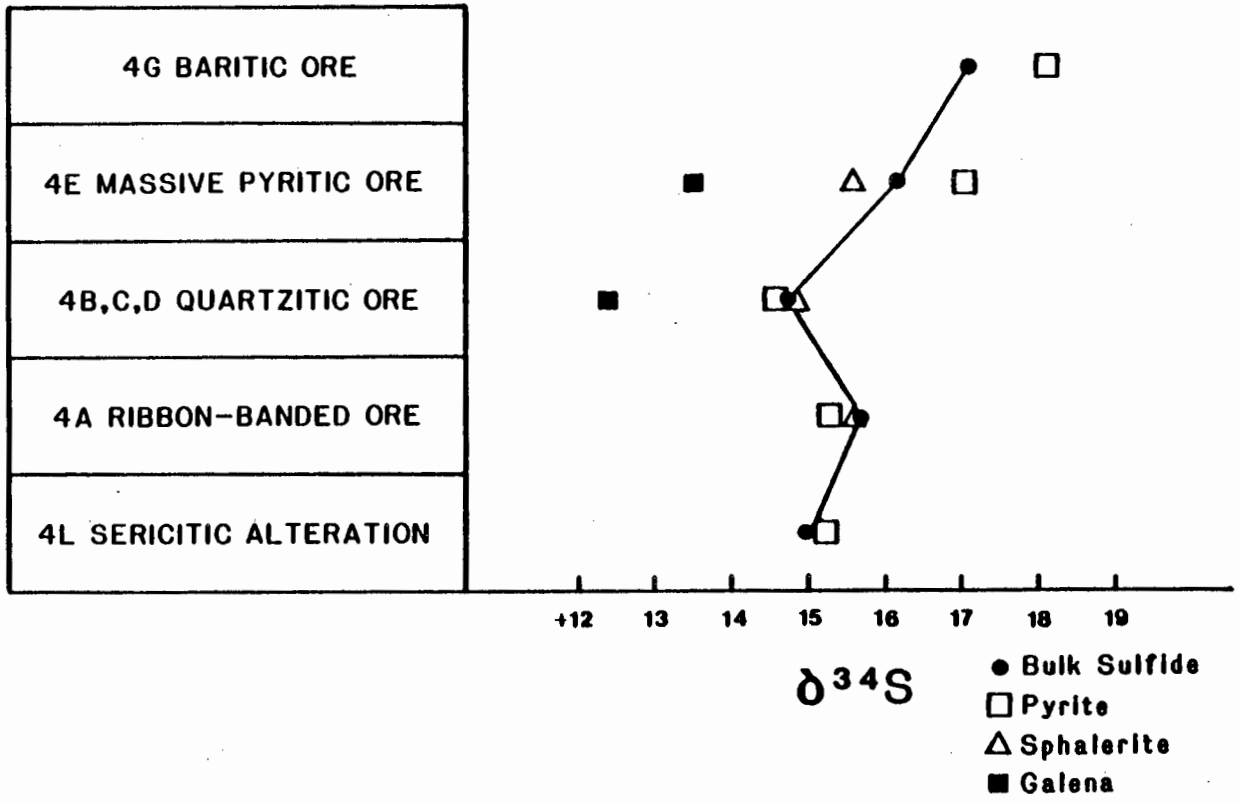

Fig. 22. Mean $\delta^{34}S$ values for pyrite, sphalerite, galena and bulk sulfide sulfur from various ore facies in the Grum deposit. Mean values show an increase in $\delta^{34}S$ from the quartzitic ore to the massive pyritic ore to the baritic ore.

Figs. 23-32. $\delta^{34}S$ values of different intersections through the Grum deposit sulfide horizons. Locations of intersections are shown by arrows in Figures 15-17. Intersections are plotted with the interpreted stratigraphic hangingwall up. The intersections are plotted at the same scale (except DDH A24). Lithologies are labelled using lithologic code presented in Appendix I. More detailed lithologies are reported in Appendix II along with assay data and sulfur content. Sample locations are indicated on lithologic columns.

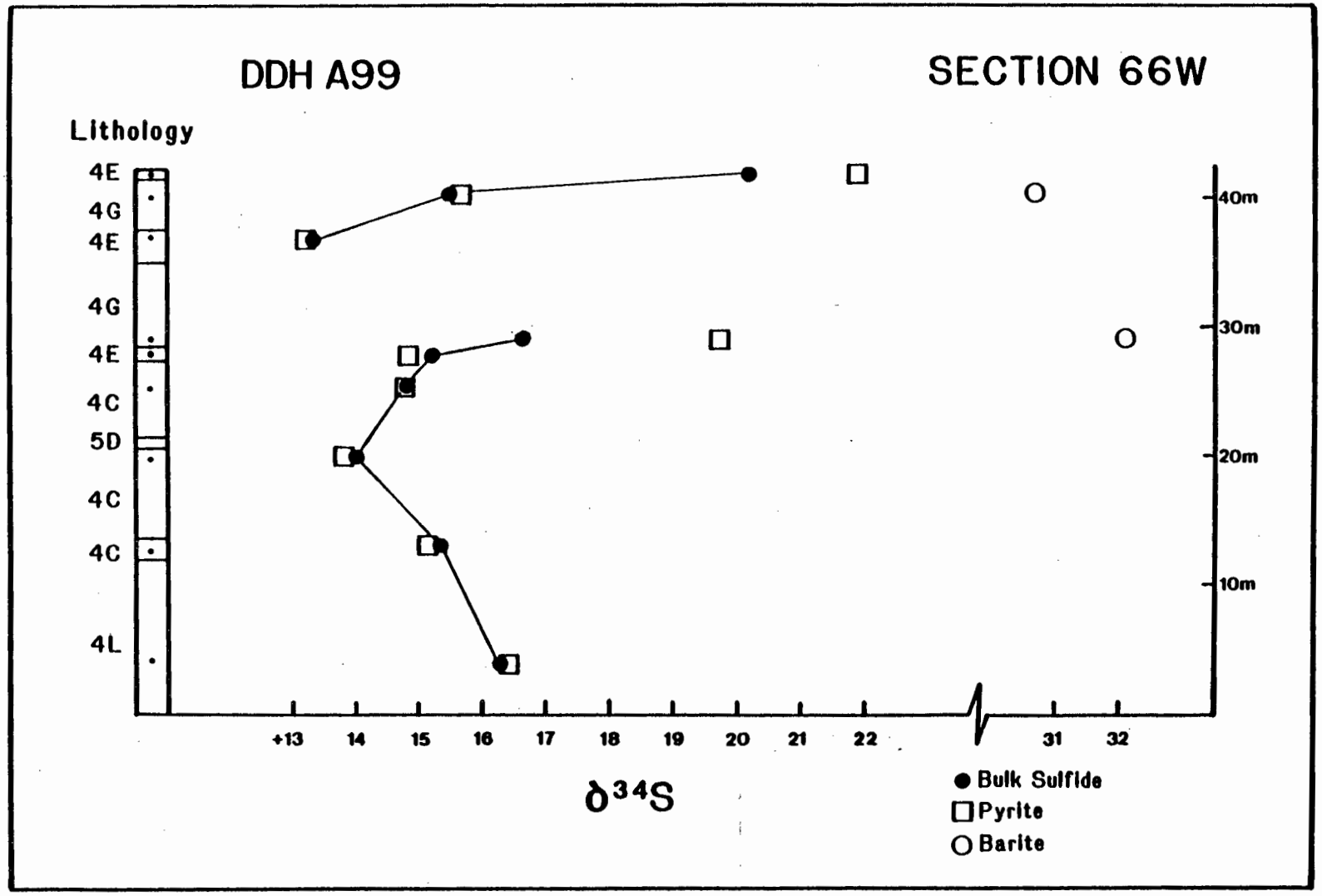
DDH A99
SECTION 66W
Lithology
4E
4G
4E
4G
4E
4C
5D
4C
4C
4L
40m
30m
20m
10m
+13
14
15
16
17
18
19
20
21
22
31
32
δ34S
Bulk Sulfide
Pyrite
Barite

Fig. 23.

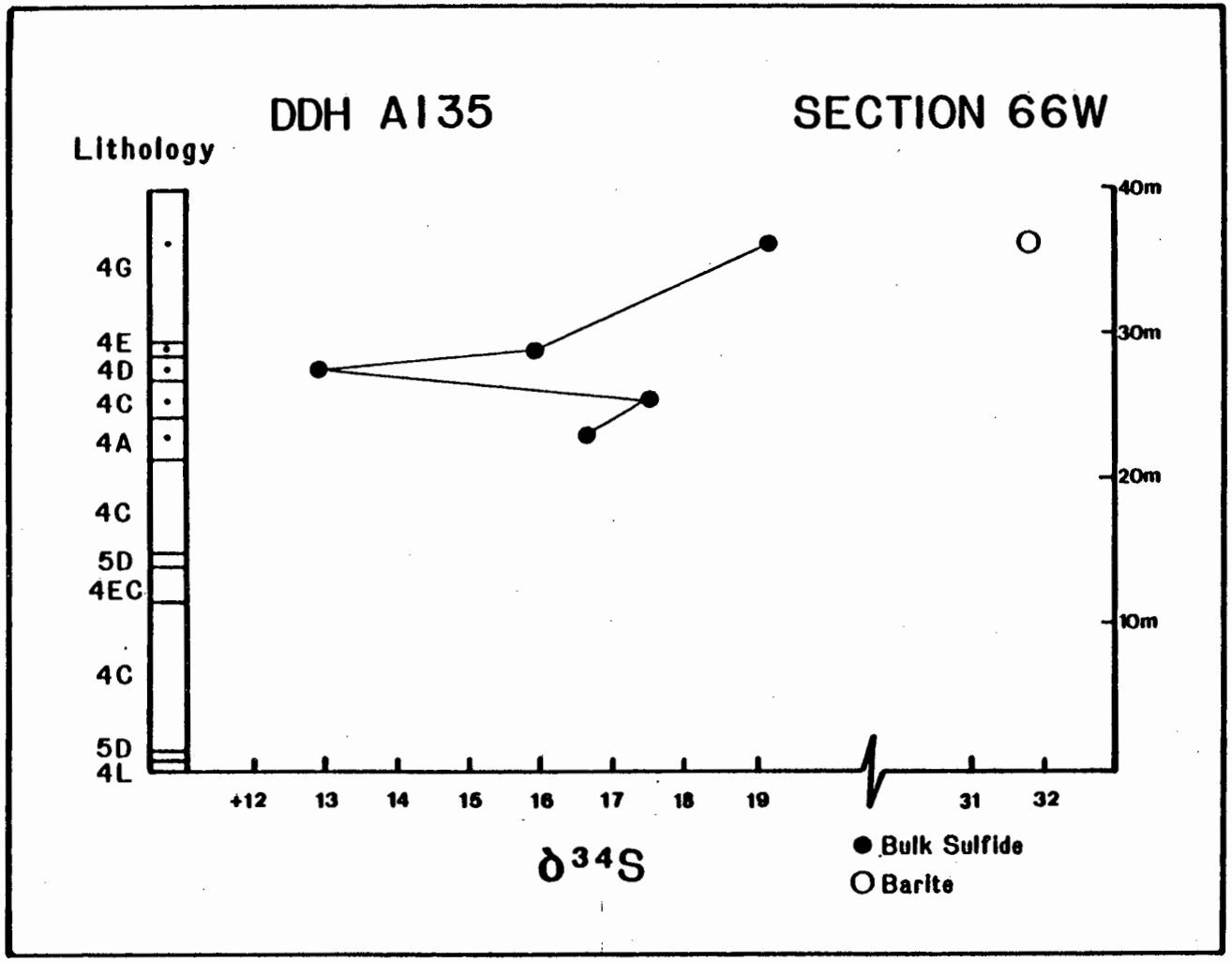
DDH A135
SECTION 66W
Lithology
4G
4E
4D
4C
4A
4C
5D
4EC
4C
5D
4L
40m
30m
20m
10m
+12
13
14
15
16
17
18
19
31
32
δ34S
Bulk Sulfide
Barite

Fig. 24.

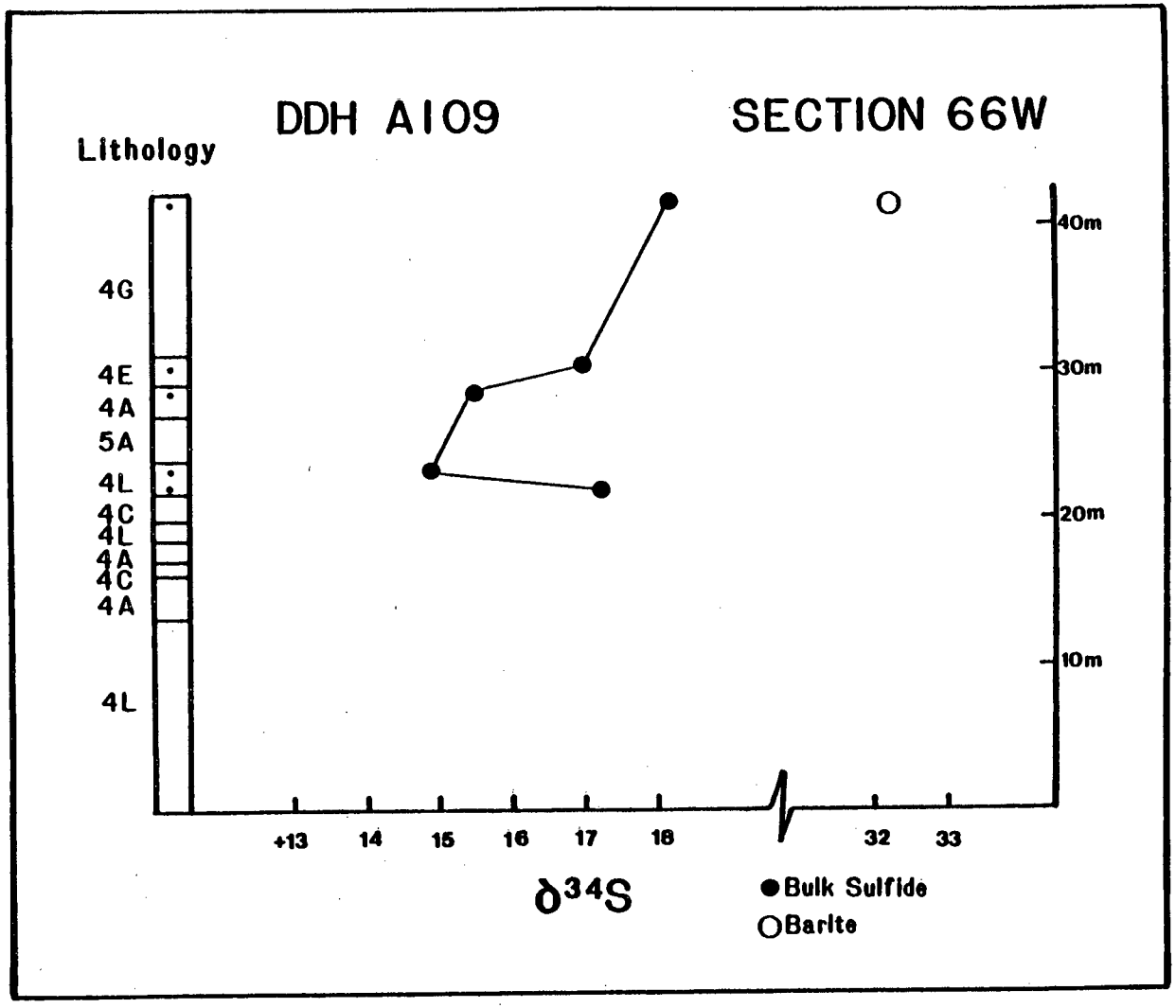
DDH A109
SECTION 66W
Lithology
4G
4E
4A
5A
4L
4C
4L
4A
4C
4A
4L
40m
30m
20m
10m
+13
14
15
16
17
18
32
33
δ34S
Bulk Sulfide
Barite

Fig. 25.

$\delta^{34}S$ values decreasing irregularly to a minimum and then increasing slightly to the top (Fig. 26). DDH U151 intersects two partial cycles. Sulfur isotope values for sphalerite mineral separates increase through the lower partial cycle. The second partial cycle, beginning with the 4B unit, shows a pattern very similar to that of DDH U43, decreasing to a minimum and then increasing only very slightly to the top which is lacking in barite (Fig. 27).

DDH U153 shows fairly constant sulfur isotope values (Fig. 28) except for anomalously light values for bulk sulfide and sphalerite from the baritic ore facies (sample U153-37.4; Appendix II) and anomalously high values for the ribbon-banded ore facies (samples U153-19 and U153-21.5; Appendix II). Perhaps the anomalously heavy interval within the thick ribbon-banded unit intersected in DDH U43, U151 and also U153 (Figs. 26-28) could be used as a correlation tool.

Intersections U142 and A24 through horizon 2 show increasing $\delta^{34}S$ upward through the Anvil Cycle without an initial decrease. DDH U142 intersects a simple cycle of sericitic, ribbon-banded, massive (with minor barite) and baritic ore (Fig. 29). Upward increase in $\delta^{34}S$ is about 5 per mil. DDH A24 (shown on an expanded scale of 1:250 instead of 1:500; Figure 30) shows an irregular 3 per mil increase to a maximum $\delta^{34}S$ value in the baritic unit and then a 5.5 drop within one half meter. Lithofacies variation through DDH A24 is not a clear-cut Anvil Cycle, but ribbon-banded ore concentrates near the base and the baritic unit is near the top. Bulk sulfide values plot close to sphalerite values in some samples of A24 because the samples are high grade, zinc rich.

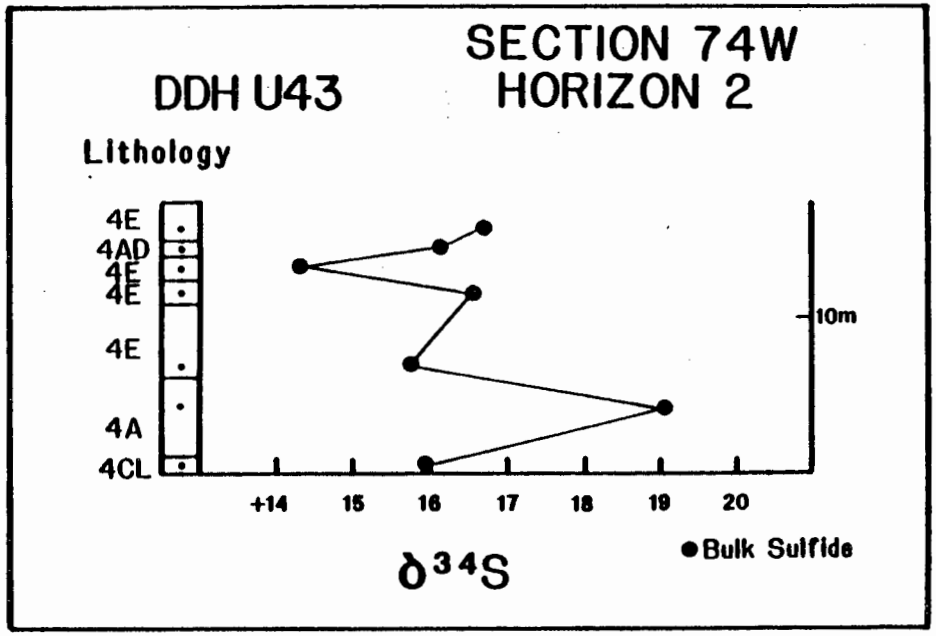
SECTION 74W
HORIZON 2
DDH U43
Lithology
4E
4AD
4E
4E
4E
4A
4CL
10m
+14
15
16
17
18
19
20
δ34S
Bulk Sulfide

Fig. 26.

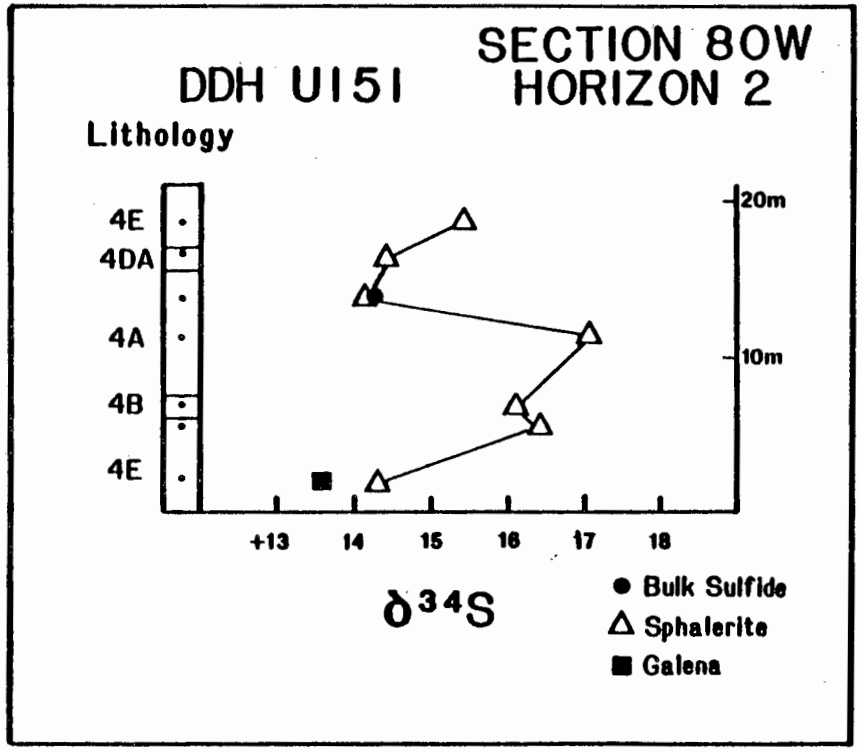
SECTION 80W
HORIZON 2
DDH U151
Lithology
4E
4DA
4A
4B
4E
20m
10m
+13
14
15
16
17
18
δ34S
Bulk Sulfide
Sphalerite
Galena

Fig. 27.

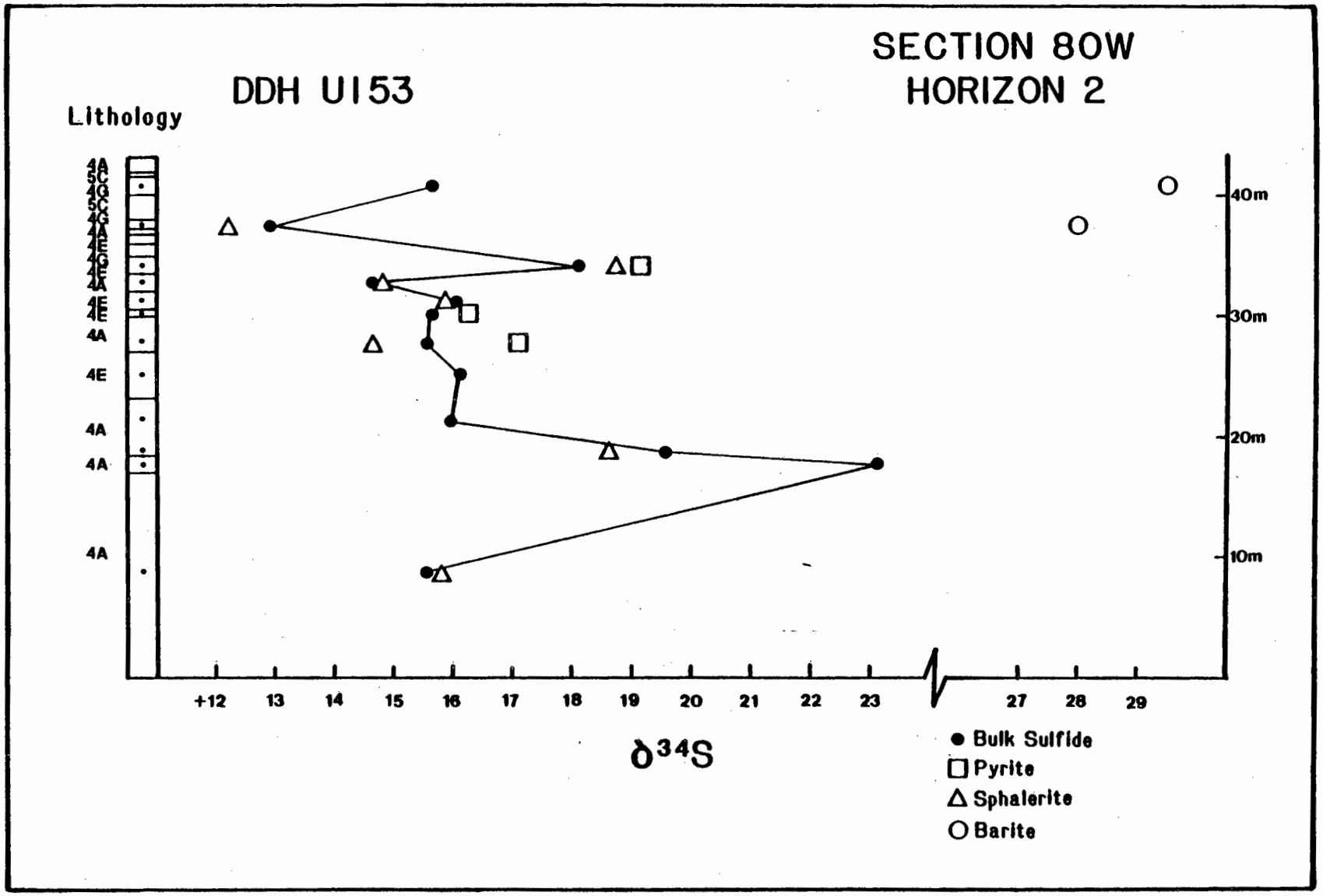
SECTION 80W
HORIZON 2
DDH U153
Lithology
4A
5C
4G
5C
4G
4A
4E
4G
4E
4A
4E
4E
4A
4E
4A
4A
4A
40m
30m
20m
10m
+12
13
14
15
16
17
18
19
20
21
22
23
27
28
29
δ34S
Bulk Sulfide
Pyrite
Sphalerite
Barite

Fig. 28.

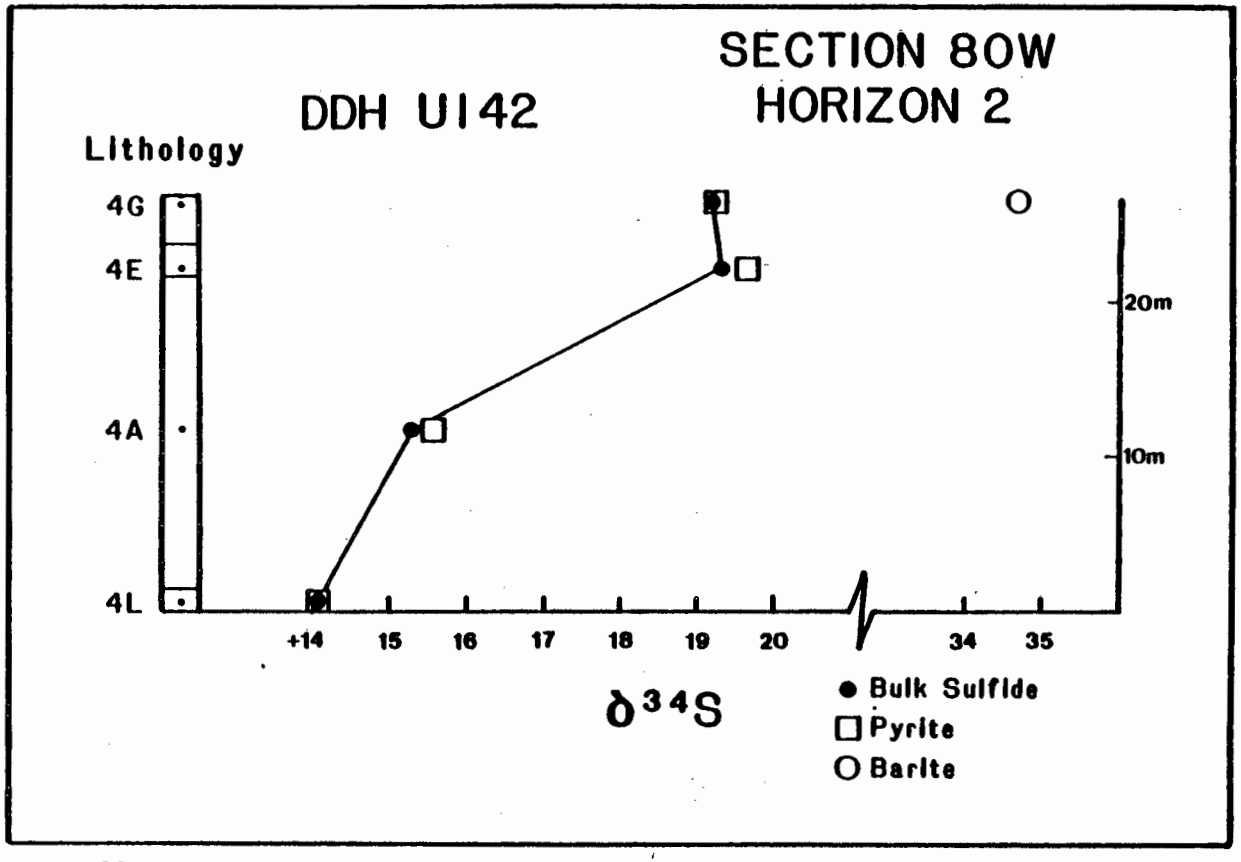
SECTION 80W
HORIZON 2
DDH U142
Lithology
4G
4E
4A
4L
20m
10m
+14
15
16
17
18
19
20
34
35
δ34S
Bulk Sulfide
Pyrite
Barite

Fig. 29.

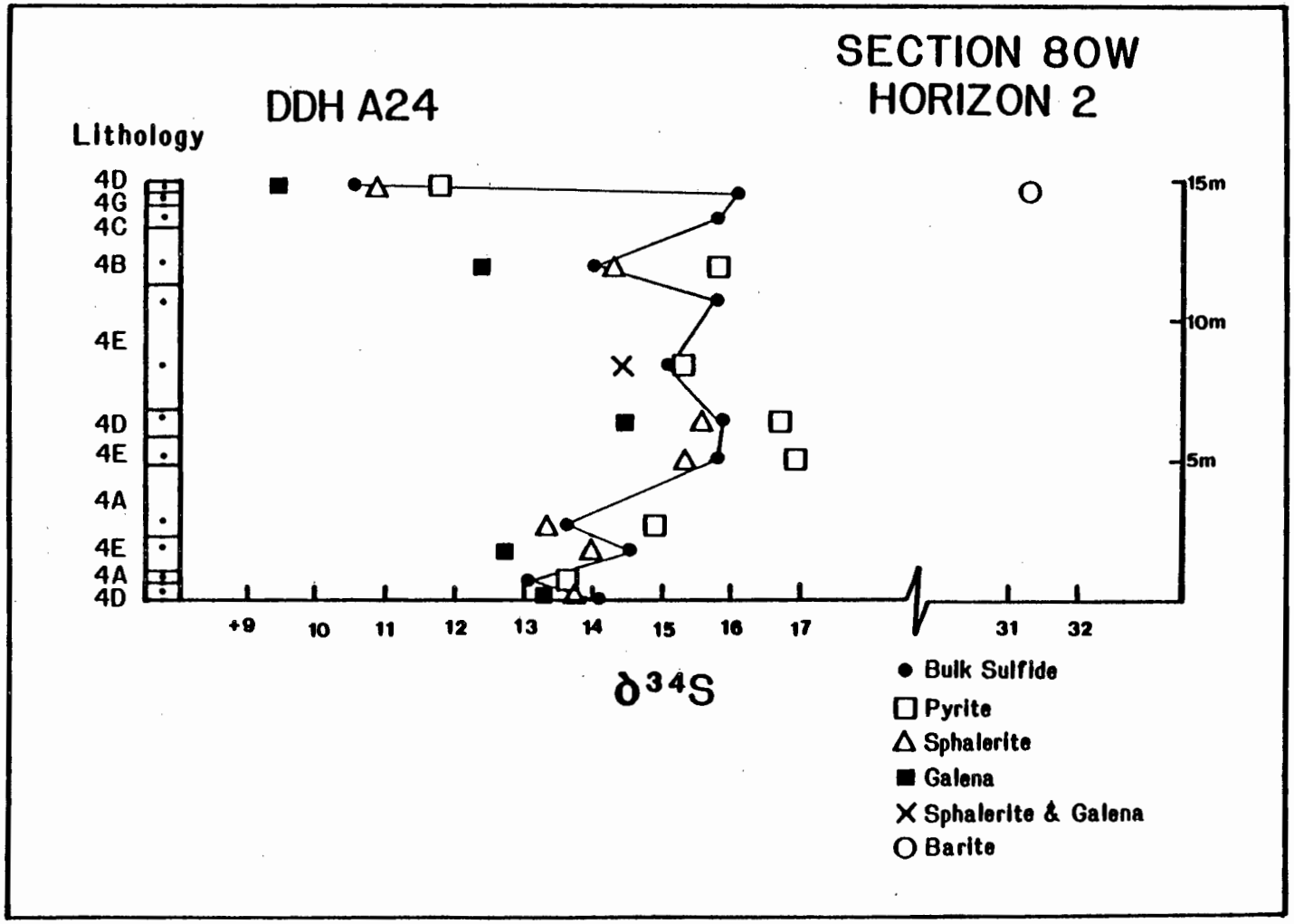
SECTION 80W
HORIZON 2
DDH A24
Lithology
4D
4G
4C
4B
4E
4D
4E
4A
4E
4A
4D
15m
10m
5m
+9
10
11
12
13
14
15
16
17
31
32
δ34S
Bulk Sulfide
Pyrite
Sphalerite
Galena
Sphalerite & Galena
Barite

Fig. 30.

Two intersections through horizon 4; U15 and U151, show no obvious deviations from sulfur isotopic composition of horizon 2 (Figs. 31 and 32). In DDH U15, although no Anvil Cycle is evident, the baritic facies values are heavy, the sericitic facies values light and the massive pyritic values are intermediate. Also, $\delta^{34}S$ decreases by 7.7 per mil in samples above the upper baritic unit. The top unit of DDH U151 is very light, and is the only sample of the ankerite facies (4K) analyzed.

MINERAL PAIRS

Sulfide-sulfate pairs are shown in Figure 20. Temperatures were calculated from sulfur isotopic analyses of 7 sphalerite-galena, 3 pyrite-sphalerite-galena and 3 barite-pyrite mineral pairs (Table 5). Three sphalerite-galena pairs giving temperatures above 900°C were samples which were very difficlt to separate. Apparently, contamination accounts for the homogenization in these three samples. Other temperatures range from 178°C to 585°C. This wide range of temperatures suggests lack of isotopic equilibration. Disequilibrium can be attributed to precipitation of minerals at different times and/or from different sulfur sources, very rapid precipitation, or destruction of equilibrium by partial isotopic exchange during metamorphism, short of re-equilibration. Because of the massive nature of much of the ore in the Grum deposit, rapid precipitation would not be inconsistent. However, it is not possible to see through metamorphism of the Grum deposit to determine the degree of original equilibrium.

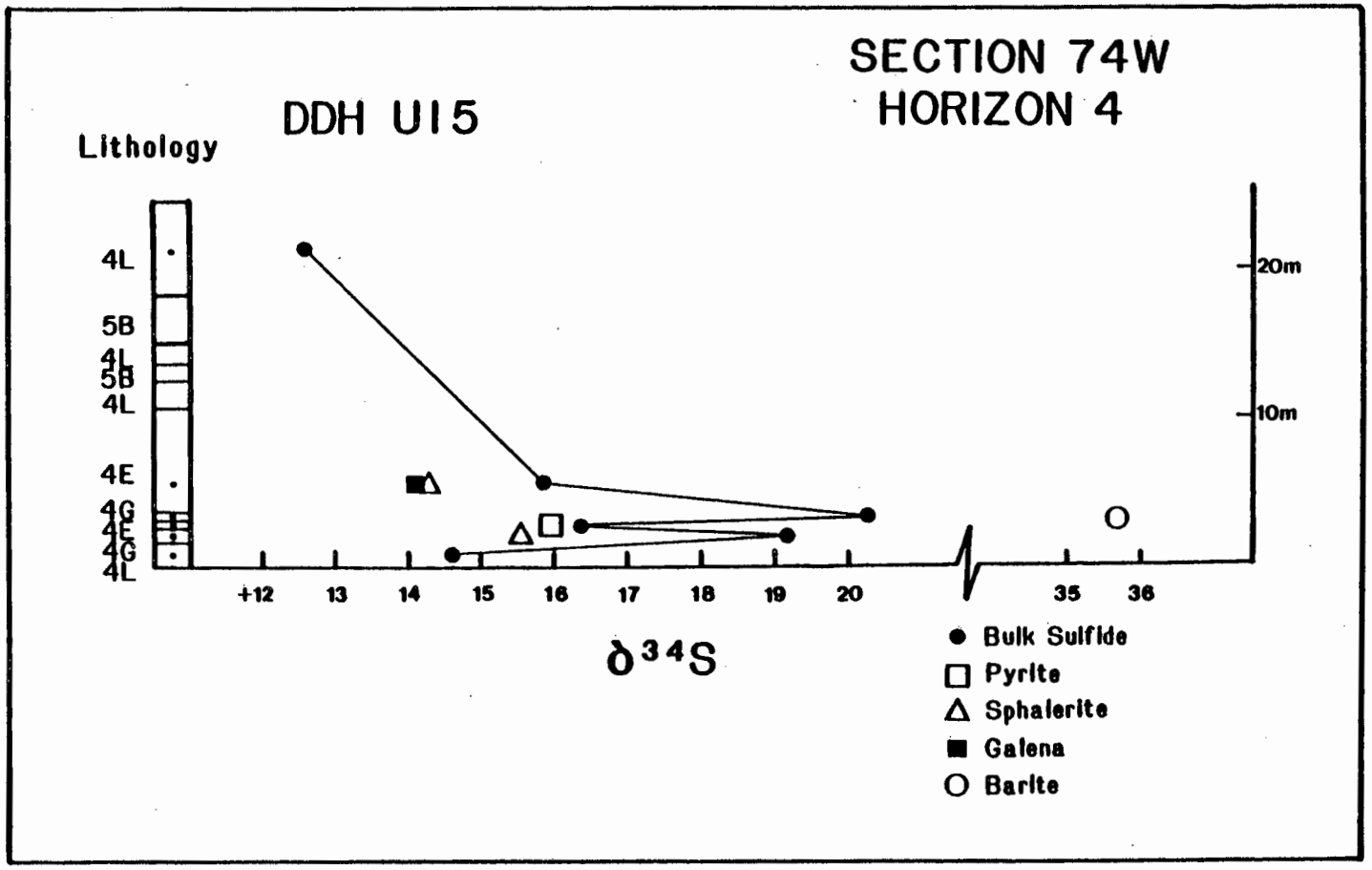
SECTION 74W
HORIZON 4
DDH U15
Lithology
4L
5B
4L
5B
4L
4E
4G
4E
4G
4L
20m
10m
+12
13
14
15
16
17
18
19
20
35
36
δ34S
Bulk Sulfide
Pyrite
Sphalerite
Galena
Barite

Fig. 31.

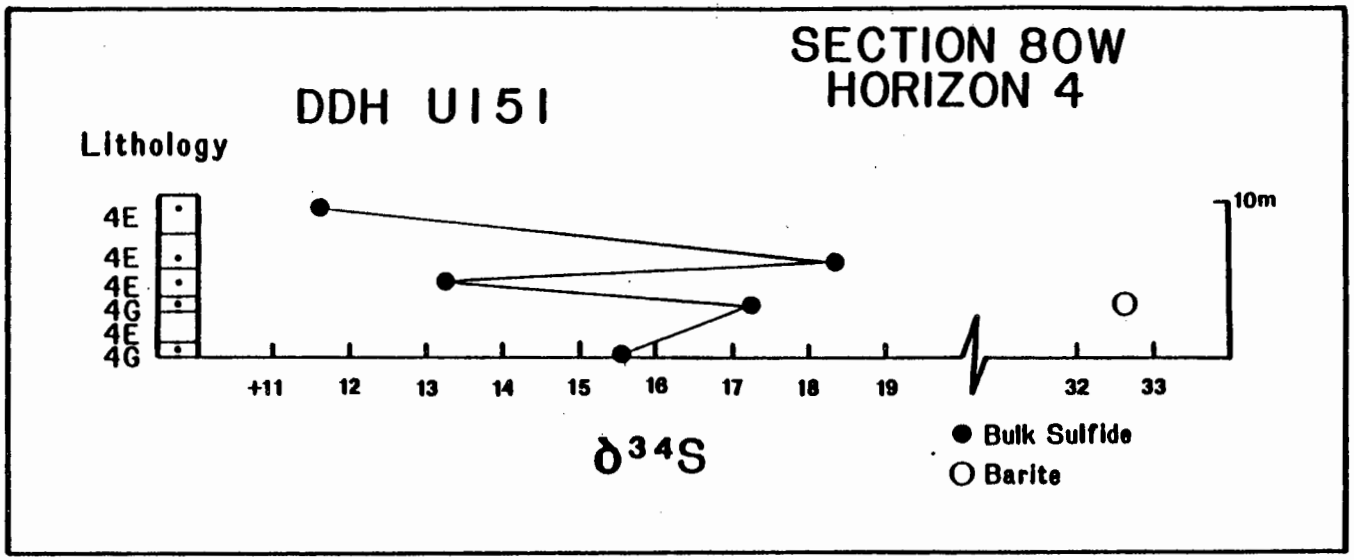
SECTION 80W
HORIZON 4
DDH U151
Lithology
4E
4E
4E
4G
4E
4G
10m
O
+11
12
13
14
15
16
17
18
19
32
33
δ34S
Bulk Sulfide
Barite

Fig. 32.

TABLE 5. Sulfur isotope geothermometry for mineral pairs from the Grum deposit.

Sample #	Δba-py	T°C	Δpy-sl	T°C	Δpy-gn	T°C	Δsl-gn	T°C
A24-331.8	--	--	1.49	178	3.39	276	1.90	344
A24-328.9	--	--	0.94	294	2.36	384	1.42	440
A24-341.4	--	--	--	--	--	--	1.25	487
A24-337.1	--	--	1.09	254	2.18	411	1.09	541
A24-343.5	--	--	--	--	--	--	0.48	954
U151-1.8	--	--	--	--	--	--	0.74	988
U15-24.7	--	--	--	--	--	--	0.16	1852
U142-122.7	15.52	428	--	--	--	--		
A99-142.1	15.09	438	--	--	--	--	--	--
A99-153.5	12.33	513	--	--	--	--	--	--

DISCUSSION

REGIONAL GEOLOGICAL ENVIRONMENT OF DEPOSITION

The Grum deposit occurs within the Selwyn depositional basin which has lateral dimensions in excess of 100 km, is characterized by thick sequences of clastic sediments deposited during a long period of relative crustal stability, and is bounded by fault controlled hinge zones. These are characteristics of "first order basins" according to concepts developed by Krebs (1979) for the European Variscan Trough which contains Rammelsberg and Meggen, and they apply also to basins that contain McArthur River, Mt. Isa and Sullivan (Large, 1980). The Selwyn Basin-Mackenzie Platform hinge zone is the locus of a shale-carbonate facies transition and is marked by a decrease in sediment thickness shelfward. The Selwyn Basin-Pelly Cassiar Platform hinge zone is also marked by facies changes which could have been controlled by basement faulting at the time of Anvil ore deposition. Subsequent deformation along this boundary, including the much later Tintina fault, indicates that it is a major zone of weakness. Such hinge zones have been postulated to be pathways for mineralizing hydrothermal fluids.

The Anvil deposits occur at a regional change in depositional regime: that of noncalcareous to calcareous pelitic sedimentation. Other similar deposits are associated with a change in regional sedimentary facies. Tom occurs at a stratigraphic change from turbidite facies to a thick sequence of carbonaceous shales (Carne, 1979). The stratigraphic setting of the Sullivan deposit coincides with the onset of quartz greywacke turbidite deposition (Thompson and Panteleyev, 1976).

Rammelsberg and Meggen are associated with a marine transgression of pelagic sediments over shelf sediments (Krebs, 1978). It is postulated that such regional changes reflect basin subsidence owing to tectonic activity along marginal faults (Large, 1980; Krebs, 1978).

"Second order basins", measured in tens of kilometers, have been identified in the vicinity of the Rammelsberg, McArthur River and Tom deposits (Large, 1980; Carne, 1979). Complex deformation of the western Selwyn Basin has obscured original sediment thickness variations making it difficult to determine if the Anvil deposits were deposited within a second order basin.

Detailed mapping, petrographic and geochemical examination of the Variscan Trough shale facies have revealed the existence of small depressions, "third order basins", in association with the Rammelsberg and Meggen deposits. Third order basins (100 m to 10 km) in the Variscan Trough are characterized by increased thicknesses of fine grained sediments, increased organic carbon content, presence of diagenetic pyrite and increased amounts of fine turbidite deposits (Krebs, 1978). These third order basins could have acted as morphological traps for exhaled hydrothermal fluids and resultant anoxic environments could have promoted sulfide localization.

Although the kind of detailed work required to delineate third order basins in not always possible, particularly for metamorphosed deposits, sedimentary exhalative deposits are invariably associated with carbonaceous shales, siltstones or micrites which indicate development of reducing conditions. The Anvil sulfide deposits are commonly surrounded by discontinuous lenses of graphitic metapelite, and graphite

is interbedded with quartz and sulfides in the ribbon-banded ore. It is likely that the Anvil sulfides were localized along with carbonaceous material in anaerobic depressions analogous to the third order basins of Rammelsberg and Meggen. The unfolded extent of the Grum deposit is roughly one square kilometer, giving minimum third order basin dimensions. Superposition of the four sulfide horizons of the Grum deposit separated by Mt. Mye and Vangorda Formation lithologies suggests periodic development of anoxic conditions, possibly due to episodic brine venting.

The Mt. Isa and McArthur River deposits are closely associated with gypsum and anhydrite or carbonate pseudomorphs after evaporite minerals, and evidence of evaporites exist in the general sequence of other stratiform sediment-hosted deposits (Gustafson and Williams, 1981). Where evaporites are present in the sequence, they could be important as a source of sulfur and/or of the high salinity ore fluids. Evaporites have not been observed in close association with Grum or with the Anvil deposits in general. However, Cyprus Anvil geologists have suggested that rift related evaporites and continental redbeds could be present in Proterozoic basement sequences beneath Anvil deposits. Heated subsurface waters could have become saline by circulation through the evaporites and the resulting brines could have leached metals from the continental redbeds before exhalation onto the seafloor.

Volcanic activity in the Anvil Range commenced with deposition of the ore deposits and increased volumetrically up section, climaxing in the Menzie Creek volcanics. Cyprus Anvil geologists suggest two end member models for the relationship between volcanism and ore gene-

sis: (1) basaltic magmatism, including postulated intrusives at depth, supplied the heat to drive fluid migration, or (2) volcanics merely reflect active extensional tectonics which released geothermally heated fluids upwards along deep seated faults.

It is thought that high heat flow is necessary for the development of convective circulation of metal bearing fluids within the sedimentary pile, and igneous activity contemporaneous with stratiform sedimentary sulfide deposits could reflect such heat flow. For example, prominent tuffaceous marker beds occur throughout the upper Mt. Isa Group and tuff occurrence in the McArthur Group reaches a maximum in the H.Y.C. Pyritic Shale Member (Mathias and Clark, 1976; Lambert, 1976). Rammelsberg is associated with more than twenty tuff horizons which are felsic to intermediate in composition and up to 3 meters thick. Four similar tuff horizons occur in association with the Meggen deposit (Krebs, 1978). The Sullivan deposit, which has no associated volcanics, is underlain by intrusive sills indicative of high heat flow (Thompson and Panteleyev, 1976).

MINERALIZATION

METAMORPHISM AND DEFORMATION OF ORES

Textures within the Grum ores result from metamorphism and deformation imposed upon the orebodies and the surrounding host rocks during the Mesozoic. Metamorphosed massive sulfide deposits characteristically display granoblastic textures, complex and paragenetically inconsistent grain boundary relationships, porphyroblastic growth of minerals like pyrite, re-equilibration of other minerals under metamorphic conditions,

and migration of some minerals in a stress field (Kalliokoski, 1965). These textural features are superimposed upon original depositional and diagenetic features and have delayed recognition of the syngenetic origin of some deposits.

Recrystallization

One of the major effects of thermal metamorphism of sulfide ores is recrystallization of existing minerals. The forms that sulfide minerals take during metamorphism are expressions of a crystalloblastic series (Stanton, 1972). Based on relative tendencies toward idiomorphism of different minerals and considerations of interfacial free energies, Stanton (1972) proposed a general silicate-oxide-sulfide crystalloblastic series comprising, in order of decreasing tendency to idiomorphism, garnet, magnetite and arsenopyrite, pyrite, dolomite, tremolite, muscovite, chlorite, pyrrhotite, sphalerite, chalcopyrite, and galena.

The metamorphic growth of pyrite porphyroblasts in massive sulfide ores can be compared to the growth in metasediments of silicate minerals with high form energy such as garnet and staurolite (Vokes, 1969). Pyrite grains in the Grum deposit show completely euhedral outlines, partially developed crystal faces (subhedral outlines), embayed outlines and sieve or poikilitic textures. These are textures commonly ascribed to metamorphic recrystallization. Embayed pyrite grains do not necessarily imply replacement by the invading mineral but can merely represent metamorphic growth (Vokes, 1969). Retention of rounded inclusions within poikilitic pyrite grains has been ascribed to lack of orienta-

tion effects and to lack of differences in interfacial energies between positions within and at the grain boundary of the host mineral (Stanton, 1972). If any framboidal pyrite originally existed in the Grum deposit it has been destroyed by metamorphic recrystallization.

Sphalerite, galena, chalcopyrite, pyrrhotite and tennantite-tetrahedrite occur interstitially to pyrite metacrysts in the Grum deposit. These are minerals which commonly display less tendency to idiomorphism and recrystallize as matrix sulfides along grain boundaries of euhedral sulfides (Vokes, 1969). Stanton (1972) finds that etching of such matrix sulfides reveals fine-grained aggregates which show polygonal outlines and 120° triple junctions as do etched portions of Grum sphalerites.

What appears in Grum ores to be a paragenetic sequence of magnetite and arsenopyrite, pyrite, sphalerite, galena (plus chalcopyrite, pyrrhotite, tennantite-tetrahedrite) is actually due to metamorphic recrystallization.

Grain Size

A second thermal effect is coarsening of grain size. In general, progressive regional metamorphism seems to create a coarsening of sulfide grain size and to a certain extent, grain size of sulfides can be linked to the metamorphic grade of the host rocks (Vokes, 1969). Amphibolite grade host rocks surround the Faro deposit which has an average grain size of 1.25 mm (Campbell and Ethier, 1974). Metamorphic grade at Grum is lower greenschist and average sulfide grain size is 0.15 mm. Metamorphic grade of the Swim deposit is lower still and

average sulfide grain size is 0.1 mm (Campbell and Ethier, 1974).

Mineral Assemblage

The effect of thermal events on sulfide mineral assemblages is less than the effect upon silicate assemblages. However, because pyrite is not the only iron sulfide in equilibrium with sedimentary environments, yet is the most abundant and widespread iron sulfide in low grade massive sulfide deposits, some post-depositional changes in iron sulfide mineral assemblage probably took place.

Metamorphic transformation of pyrite to pyrrhotite is often cited to explain increasing pyrrhotite:pyrite ratios associated with increasing grades of metamorphism. At 10 bars pressure, the pyrite to pyrrhotite transformation occurs at 743°C and increasing pressure raises the temperature (Kullerud and Yoder, 1959). For this breakdown to take place during metamorphism, something must lower the temperature of reaction. Experimental investigations suggest that the transformation could take place at metamorphic temperatures in the presence of organic materials with absorbed water and gases which would lower the sulfur fugacity (Lambert, 1973).

Pyrrhotite in the Grum deposit is less common than in the contact metamorphosed Faro deposit, where pyrrhotite abundance decreases away from the adjacent intrustion (Campbell and Ethier, 1974). Occurrences of pyrrhotite in the Grum deposit are more localized and not so clearly a metamorphic effect. Most occurrences of pyrrhotite in Grum are in sections of high grade massive pyritic sulfide and in the sericitized alteration phyllites. Pyrrhotite is rare in the ribbon-banded graphitic

ore but occurs occasionally in quartzitic ores. The pyrrhotite in the Grum deposit could be of metamorphic origin but primary pyrrhotite or an early diagenetic transformation of primary iron sulfide phases to pyrrhotite is also likely.

Cracked euhedral grains of magnetite, invaded by sulfides and gangue in the Grum ores, appear to be primary but are probably metamorphically recrystallized. One magnetite bearing sample of baritic ore showed all stages of mutual replacement textures between magnetite and pyrite. Consequently, presence of magnetite in the primary mineral assemblage cannot be proven. There does seem to be a stratigraphic restriction of magnetite to the baritic and massive ore though some quartzitic ore contains magnetite. Also, horizon 4 contains more magnetite than horizon 2. Perhaps these stratigraphic restrictions of magnetite reflect local variations in fO_2 and/or fS_2 during deposition. Primary sedimentary magnetite is known to occur in the Thetis Deep, Red Sea (Shanks, 1976).

Muscovite in the Grum ores could be recrystallized detrital clay particles. Quartz in the quartzitic ores could represent recrystallized hydrothermal chert as suggested by Cyprus Anvil geologists. This is reasonable considering the paucity of detrital quartz in the surrounding phyllites. In fact, occasional relict chert can be observed in the quartzitic and other ore facies from the Grum deposit (Plate 19).

Retrograde metamorphic effects could perhaps account for alteration of pyrrhotite to marcasite along grain boundaries (Stanton, 1972).

Deformation

Most sulfide deformation associated with D_1 and D_2 was erased by

thermal recrystallization. Deformation effects can be seen in the preferred orientation (roughly // S_2) of barite, quartz, mica and rarely of pyrite. Quartz grains show undular extinction and strain foliation especially when in contact with euhedral pyrite crystals. Twinning in etched sphalerite grains could be deformation twinning (Plate 11). Some post-thermal event deformation is evident: granulation of pyrite in intergranular areas was observed in one sample of ore not megascopically brecciated and zones of sulfide breccias are associated with fault zones and gouge. Remobilization of "softer" sulfides into zones of less stress is evidenced by healing of fractured brittle sulfides and oxides (pyrite, arsenopyrite and magnetite) by chalcopyrite, sphalerite, galena, and pyrrhotite, by minor remobilized chalcopyrite veinlets, and by coarsening of sphalerite and galena grain size in axial regions of S_2 folds.

Banding and Lithofacies Variation

Controversy still surrounds the origin of banding in massive sulfide deposits. Often the banding is parallel regional metamorphic foliation surfaces but bedding is frequently transposed parallel to foliation as well. Present consensus is that banding in sedimentary sulfide ores is primarily a sedimentary fabric related to variations in type and relative amounts of phases precipitated on the seafloor, and only slightly modified by later metamorphism (Vokes, 1969). The banding in Grum ores, as in all Anvil deposits, is probably related to sedimentary processes. Lithofacies variations within Anvil Cycles are certainly related to sedimentary processes.

ELEMENT ZONATION

Copper values in the Anvil deposits are thought to be higher in the pyritic quartzitic ore facies which occurs near the stratigraphic footwall. Chalcopyrite was widespread in thin sections of the pyritic quartzite from the Grum deposit. Copper mineralization within sedimentary exhalative deposits is commonly localized as epigenetic feeder zone mineralization in footwall sediments and diminishes laterally and vertically through the deposits. This is true for Rammelsberg, Tom and Mt. Isa (Krebs, 1978; Carne, 1979; Mathias and Clark, 1975; Large, 1980).

Iron sulfides, primarily pyrite, are abundant without apparent zonation throughout the Anvil deposits, including Grum. Iron content is high throughout most sedimentary exhalative deposits. Notable iron variations are the central pyrrhotite zone of the Sullivan deposit, more abundant iron near the footwall of Rammelsberg, a lateral increase in iron in the McArthur River deposit, and paucity of iron in the Howard's Pass deposits (Thompson and Panteleyev, 1976; Krebs, 1978; Large, 1980; Morganti, 1979).

An upward increase in Pb:Zn ratio has been noted in the Anvil deposits (D.S. Jennings, personal communication) and preliminary indications are that zonation in Grum is similar. Horizon 4 is lead rich relative to zinc whereas horizon 2 is zinc rich. Rammelsberg shows a similar vertical increase in the Pb:zn ratio whereas Tom, Sullivan, McArthur River, and Mt. Isa show a lateral decrease in Pb:Zn. Silver in the Anvil ores tends to be more abundant near the top of the Anvil Cycle whereas gold concentrates near the footwall.

FOOTWALL ALTERATION

Like other Anvil district deposits, Grum is inconsistently surrounded by a sericitized and variably mineralized halo. Horizon 2 in the Grum deposit is underlain by well developed sericitic alteration. Horizons 1, 3 and 4 tend to be underlain by thin and discontinuous zones of alteration. All horizons occasionally show sericitic alteration in the hangingwall. Because this alteration is sometimes best developed in the footwall of Anvil sulfide deposits, and because mineralization discordant to $S_1//S_0$ has been observed, Cyprus Anvil geologists suggest that the alteration is related to ore fluid influx.

Hydrothermally mineralized or altered ore fluid conduits, equivalent to stockwork or stringer zones in volcanogenic deposits, exist in footwall sediments of some sedimentary exhalative deposits. Extensive footwall brecciation at Sullivan, a silicified, copper-zinc-lead mineralized "kniest" below Rammelsberg, similar alteration below Meggen, a copper, lead and silver rich, silicified and sideritized breccia zone below Tom, cross cutting copper mineralization beneath McArthur River, and possibly the brecciated copper-rich "silica-dolomite" of Mt. Isa represent epigenetic mineralization related to influx of fluids which precipitated overlying syngenetic stratiform sulfides (Krebs, 1978; Carne, 1979; Finlow-Bates, 1979; Large, 1980).

The absence of brecciation and strongly developed epigenetic mineralization beneath the Anvil ore could indicate deep water (Finlow-Bates and Large, 1978). By modification of studies by Haas (1971), they suggest that brecciated and copper-mineralized hydrothermal conduits result from boiling of the ore fluids. They relate boiling within

the conduit to water depth of the basin. If water depth is less than 500 meters the hydrostatic pressure will be such that an ore fluid of 270°C and 5% NaCl will boil in the conduit. For a brine (25% NaCl) of the same temperature, boiling would occur in the conduit if water depth is less than 350-400 meters. At some point during boiling the solubility of copper sulfides will be exceeded so that cross cutting copper mineralization will be precipitated. If the conduit is capped, as proposed by Carne (1979) for Tom, the vapor pressure will increase until it exceeds the total confining pressure plus the mechanical strength of the rock. Phreatic explosion and brecciation will result. If water depth exceeds 500 meters (or 350 meters for a 25% NaCl brine) boiling will not occur in the conduit and stratiform mineralization without an associated epigenetically mineralized and brecciated feeder zone will result (Finlow-Bates, 1980). The fine-grained pelagic nature of the Mt. Mye and Vangorda lithologies reflect quiescent deposition consistent with deep marine conditions.

Two factors which must be considered for interpretation of the alteration zones, however, are the existence of hangingwall alteration and the metamorphic history of the ores. It is possible that chemical reactions caused by later metamorphic fluids could be involved in the alteration. However, hangingwall alteration could be the result of normal marine sedimentation into a residual brine pool during the waning stages of an exhalative episode.

LEAD ISOTOPES

Barry Ryan, formerly of the University of British Columbia, has

measured lead isotope ratios of the various Anvil deposits. The leads show no relationship to mantle leads but rather a strong crustal signature, plotting in a field of enclosed basin lead related to sandstone and shale (Ryan, preliminary informal talk at Faro).

SULFUR ISOTOPES

Distribution of $\delta^{34}S$ values for some sedimentary exhalative deposits is shown in Figures 33 and 34. In general, sulfides and sulfates in Paleozoic deposits (for which the seawater sulfate curve is known) straddle the value of contemporary seawater sulfate. Rammelsberg and Meggen sulfides average approximately 10 $^{o}/_{oo}$ lighter than seawater and sulfates are equal to and slightly heavier than contemporaneous seawater (Fig. 33). The shale-hosted Howard's Pass and Vulcan deposits contain sulfides which average about 5 $^{o}/_{oo}$ below contemporary seawater (Fig. 34).

Preliminary data (Shanks, personal communication) indicate that $\delta^{34}S$ values from the DY deposit, Anvil Range, resemble those in the Grum deposit; sulfide minerals about 15 $^{o}/_{oo}$ lighter than sulfate minerals, which are approximately equal to or slightly heavier than contemporary seawater. However, an earlier sulfur isotope study of the Faro deposit, Anvil Range, gave $\delta^{34}S$ values for sulfides approximately 5 $^{o}/_{oo}$ heavier than those for Grum (Campbell and Ethier, 1974). Two explanations for this difference are possible. Either the subbasin in which Faro sulfides accumulated differed from DY and Grum, or sulfur isotope values became lighter during the contact metamorphism related to the adjacent intrusion. The range of sulfide $\delta^{34}S$ values

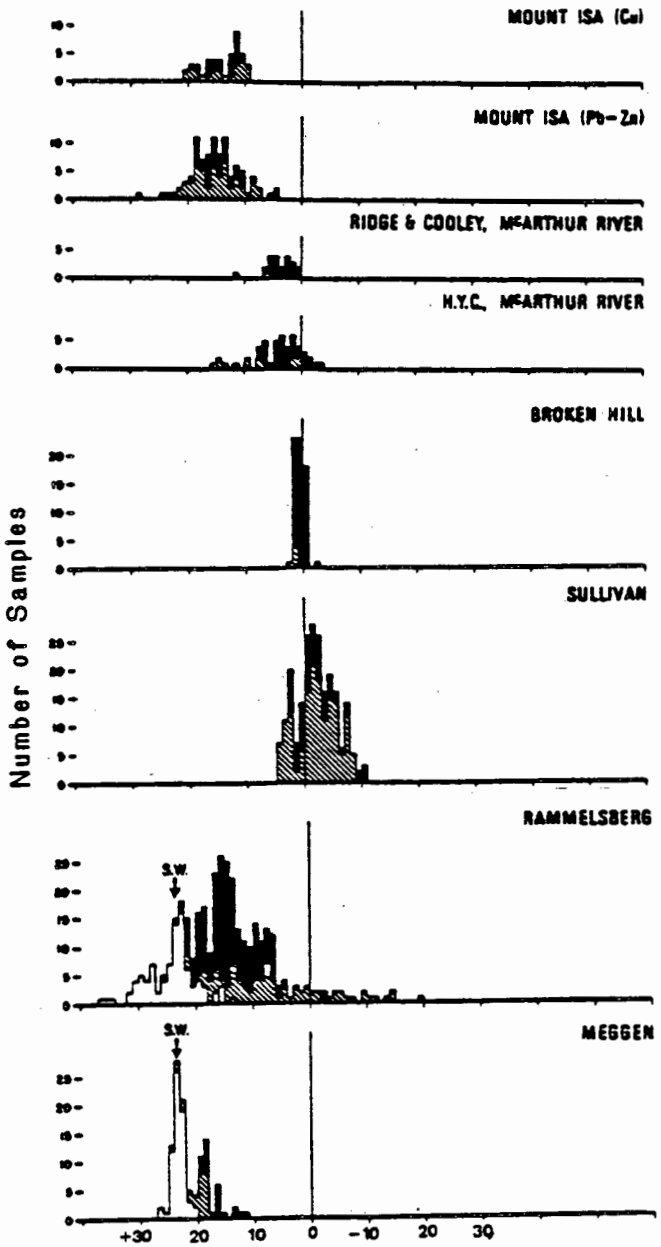

Fig. 33. Frequency distributions of $\delta^{34}S$ from McArthur River, Mt. Isa, Broken Hill, Sullivan, Rammelsberg and Meggen. S.W. is contemporaneous seawater sulfate. Seawater sulfate curve for the Proterozoic is not well known. Solid squares are base metal sulfides; barred squares are pyrite; open squares are barite (modified after Gustafson and Williams, 1981).

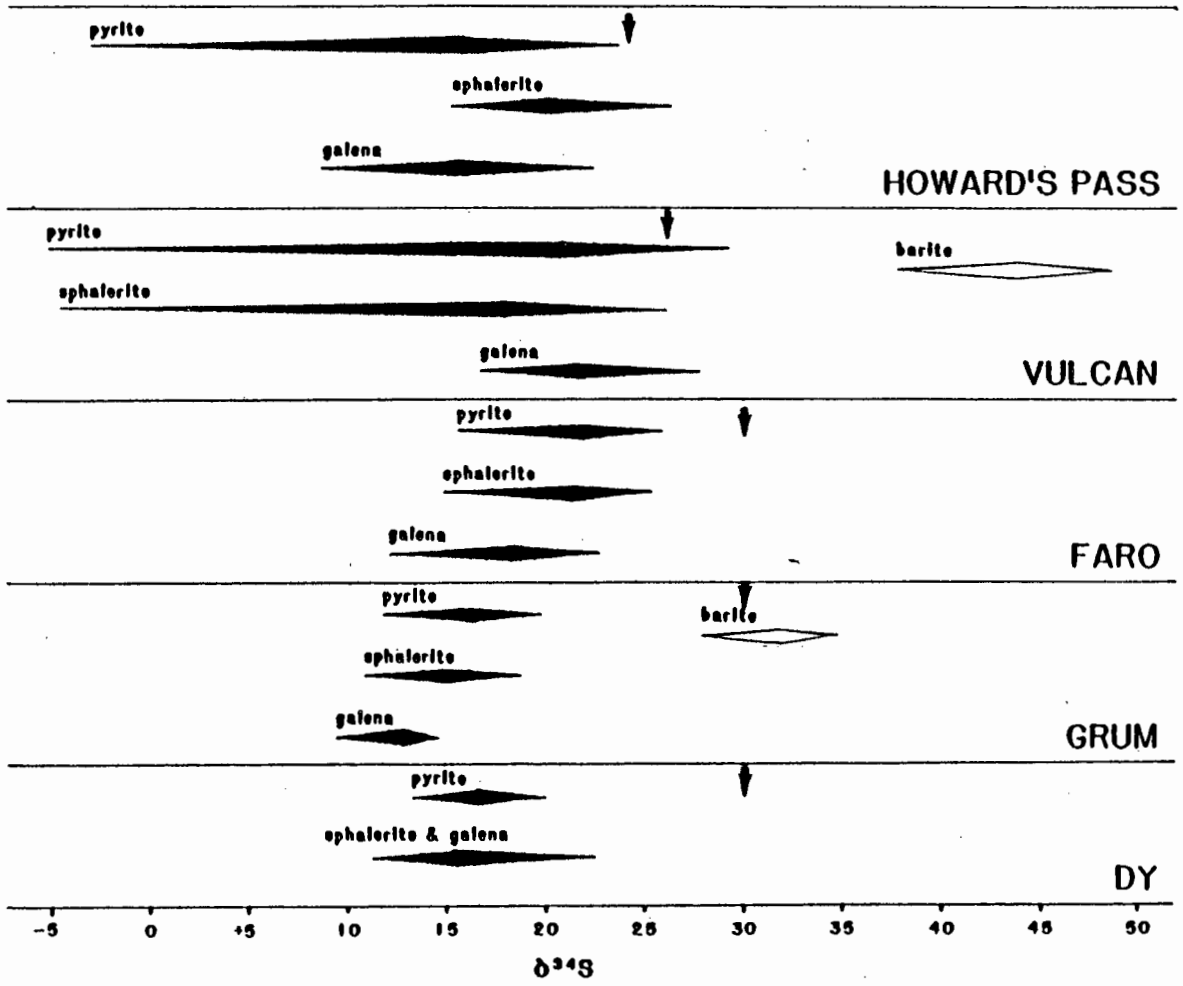

Fig. 34. S-isotopic distributions of Selwyn Basin shale-hosted deposits. Range and mean are depicted by the spread and maximum thickness of the field. Number of analyses is not depicted. Arrow denotes contemporaneous seawater sulfate. References: Howard's Pass (Morganti, 1979); Vulcan (Mako, 1981); Faro (Campbell and Ethier, 1974); Grum (this study); DY (Shanks, in progress).

from Faro is approximately as narrow as the spread of values from Grum. Rammelsberg, McArthur River, Vulcan and Howard's Pass show much wider ranges extending into negative values (Figs. 33 and 34).

Sulfur isotopic data for Grum suggest a stratigraphic increase in $\delta^{34}S$ from the quartzitic to massive to baritic ore facies. Stratigraphic increases have been documented in deposits such as McArthur River, Kupferschiefer, Howard's Pass and Rammelsberg (Table 6). Some of these trends have been explained by biogenic reduction of seawater sulfate in a third order basin closed to influx of fresh seawater sulfate, leading to an increasingly reduced environment through time. As the S_r/S_o ratio increases (fO_2 decreases), the $\delta^{34}S$ of precipitating sulfides increases.

There is no evidence for biogenic reduction of sulfate in the Grum deposit. The range of $\delta^{34}S$ values is fairly narrow; pyrite values are not significantly different from sphalerite and galena values, and the average isotope values of sulfide minerals are only 15 per mil lighter that contemporaneous seawater. In addition, the repetitive nature of Anvil Cycles seem more consistent with episodic venting of sulfide bearing fluids.

Assuming that reduced sulfur is brought with the exhaled fluids, an upward increase in $\delta^{34}S$ can be explained by increasing temperature of the exhaled fluids through the Anvil Cycle. The effect of increasing temperature is to facilitate inorganic sulfate reduction thereby increasing the $H_2S/SO_4^{=}$ ratio which increases the $\delta^{34}S$ of H_2S and precipitating sulfide minerals.

Cyprus Anvil geologists have speculated that the Windermere Grit

TABLE 6. Stratigraphic sulfur isotope variations in volcanogenic and sediment-hosted stratiform sulfide deposits.

McArthur River	$\delta^{34}S$ values of pyrite increase stratigraphically from -3.9 to +14.3; $\delta^{34}S$ values of sphalerite and galena vary irregularly between -1.2 and +5.7.
Kupferschiefer	$\delta^{34}S$ values range between -50 and -30 increasing stratigraphically upward.
Rammelsberg	$\delta^{34}S$ values of pyrite vary irregularly between -15 and +25; $\delta^{34}S$ values of sphalerite and galena increase stratigraphically from +8 to +22.
Howard's Pass	$\delta^{34}S$ values for sphalerite increase from about +15 to about +25 stratigraphically upward through depositional cycles.
Kuroko	$\delta^{34}S$ values decrease from +8.0 in the footwall siliceous ore to +3.0 in the hangingwall baritic ore.
Sullivan	$\delta^{34}S$ values decrease by about 4 per mil from the center to the top of the ore horizon.

References: McArthur River (Smith and Croxford, 1973); Kupferschiefer (Ohmoto and Rye, 1979); Rammelsberg (Anger et al., 1966); Howard's Pass (Morganti, 1979); Kuroko (Lambert and Sato, 1974); Sullivan (Campbell et al., 1978).

Unit could have acted as a sandstone aquifer or resevoir beneath an impermeable Mt. Mye shale cap. Extensional faulting could have breached the shale cap releasing geothermally heated brines to the seafloor. Perhaps, to explain sulfur isotope variation, after breaching of the impermeable cap, deeper (and therefore hotter) fluids were tapped through time, or perhaps the conduit heated up with time. If the subsurface fluids had leached sulfate from evaporites in the Helikian basement or contained recirculated seawater sulfate and if sulfate reduction occurred inorganically within the sediment pile, the exhalation of higher temperature fluids would cause precipitation of heavier sulfides.

The existence of barite at the top of the Anvil Cycle must be considered in conjunction with the upward increasing sulfur isotope values. For solutions containing more than 1 m NaCl, barite solubility increases with temperature (Holland and Malinin, 1979) so that precipitation could occur by simple cooling. However, mixing of a reduced Ba-rich fluid with a more oxygenated fluid could also cause barite precipitation. Mixing of the ore fluid with oxygenated seawater is usually invoked, along with cooling, to explain the occurrence of barite near the top or margins of deposits such as Rammelsberg, Tom, Meggen and Kuroko.

If sulfate reduction of the Grum ore fluid had taken place at elevated temperatures within the sediment pile, mixing with seawater, which will increase the fO_2 within the basin and therefore affect mineral stability fields, is not likely to cause re-equilibration of $\delta^{34}S$ because mixing will cause cooling more rapidly than dilution. Conse-

quently, the appearance of barite, an oxidized phase, is not inconsistent with increased $\delta^{34}S$ values of sulfide sulfur. In fact, if the model of increasing temperature of exhaled fluids through the Anvil Cycle is correct, the hotter fluids could have become bouyant enough to mix with sulfate-bearing seawater overlying an anoxic basin and thus cause precipitation of barite. A 5 m NaCl fluid will become less dense then seawater at about 225°C and temperature fluctuations as small as 10-15°C could control the behavior of a fluid exhaled into an anoxic basin (Phillips et al., 1981).

The occurrence of the sulfides within graphite-rich metapelite and the massive nature of much of the mineralization implies that an anoxic basin was indeed developed. Preliminary data indicate that $\delta^{34}S$ values from trace sulfides in unmineralized phyllites surrounding the DY deposit are very similar to values from mineralized samples (Shanks, personal communication). Such a correlation further substantiates the development of an anoxic basin with sulfides concentrating in a sub-basin and minor dispersion of sulfide minerals into the remainder of the anoxic basin.

If mixing did cause isotopic re-equilibration, the chemical changes in the fluid could be plotted on an fO_2/pH diagram showing Fe-S-O mineral stability fields superimposed on $\delta^{34}S$ contours (Fig. 35). Mineral stability boundaries are calculated for 0.001 and 0.1 moles of total sulfur/kg H_2O at 250°C. If the total sulfur content of the fluid approximates seawater (2600 ppm SO_4 or 0.027 moles S/kg H_2O) the pyrrhotite/pyrite phase boundary would fall between the two calculated boundaries. The coexistence of pyrrhotite and pyrite in the Grum deposit

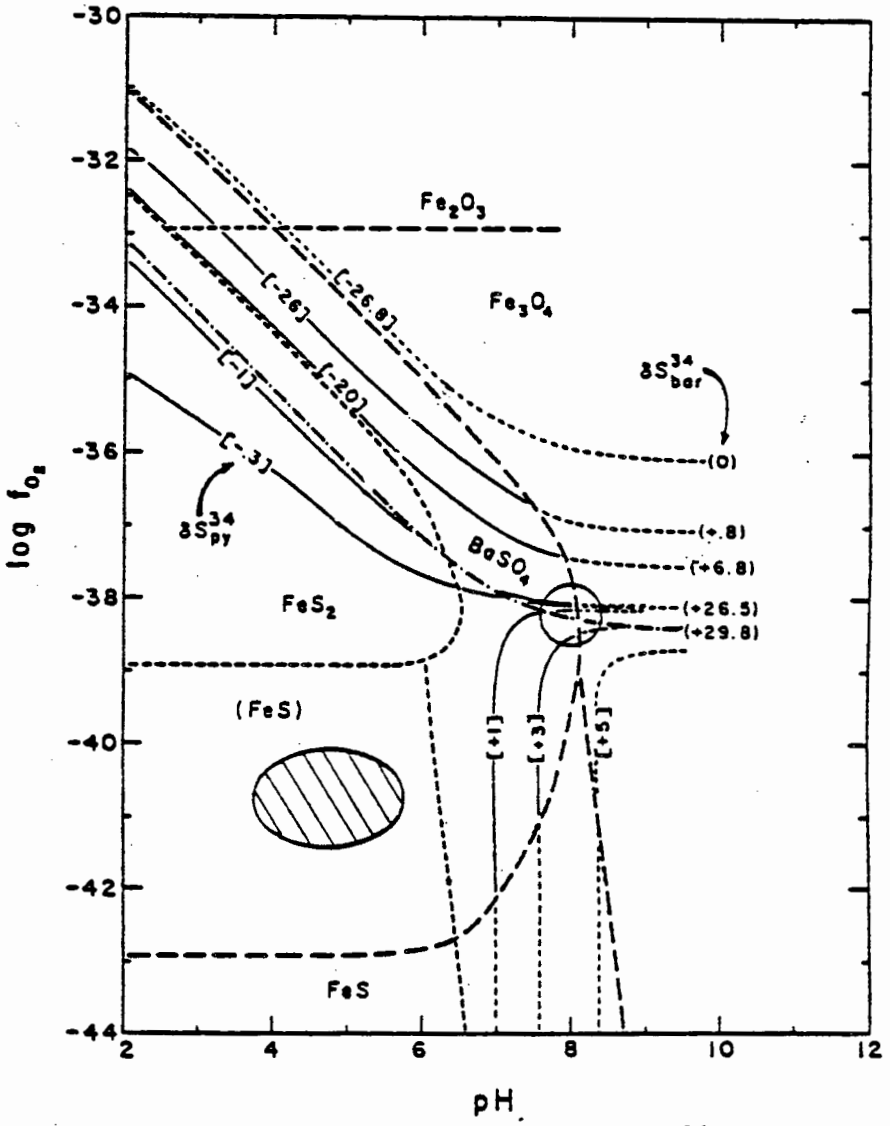

Fig. 35. Comparison of the positions of $\delta^{34}S$ contours with the stability fields of Fe-S-O minerals and barite. T=250°C and I=1.0 (modified after Ohmoto, 1972). Heavy dashed lines = Fe-S-O mineral boundaries at ΣS=0.1 moles/kg H_2O. Light dashed lines = Fe-S-O mineral boundaries at ΣS=0.001 moles/kg H_2O. Dash-dot line = barite soluble-insoluble boundary at $m_{Ba^{2+}} \cdot m_{\Sigma S} = 10^{-4}$. Ruled field represents approximate composition of Grum ore fluid assuming a ΣS content intermediate to the two shown so that the fluid plots near the pyrrhotite-pyrite boundary. Circled field represents approximate seawater composition. Mixing of the ore fluid with seawater would correspond to increasing $\delta^{34}S$ of pyrite as shown by the contours.

implies that the fluid composition was near an intermediate pyrrhotite/pyrite boundary with a pH somewhat less than seawater (Fig. 35). Seawater has a pH of about 8 and lies along the barite soluble-insoluble boundary (Fig. 35; circled field). Dilution of the fluid with seawater would drive the fluid composition toward the composition of seawater. $\delta^{34}S$ of pyrite in equilibrium with the fluid would increase as shown by the contours. Furthermore, the fluid composition would be driven into the barite stability field allowing precipitation of barite. Such a path, which could also intersect the magnetite stability field, would be consistent with the occurrence of minor magnetite in the massive and baritic ore facies. An anoxic basin would preclude precipitation of large amounts of magnetite and other iron oxides.

SUMMARY

The area of the Grum deposit accumulated thick sequences of trailing margin clastic wedge and miogeoclinal sediments during the Late Proterozoic. Uplift of the Pelly Cassiar Platform to the southwest during renewed rifting, isolated the Selwyn Basin. Fine-grained pelagic sediments filled this epicontinental basin until Middle Devonian time.

Extensional faulting in western Selwyn Basin created depressions within the basin. Smaller anaerobic basins accumulated organic rich muds in the Lower Cambrian. Convectively overturned, geothermally heated subsurface waters leached salts, sulfate and metals from underlying evaporites and immature sediments. Metal ions were most likely

transported as chloride complexes in the migrating fluids (Barton and Skinner, 1979). Inorganic sulfate reduction occurred during circulation of brines within the sedimentary pile beneath an impermeable shale cap. Deep seated fault zones breached that cap and tapped the metal-rich brines. Transport of large quantities of fluid accompanied movements along these faults (Sibson et al., 1975).

Hot brines reached the seafloor where they ponded into anaerobic organic-rich basins. Sulfides and silica gel precipitated from the hot brines near the margins of the basins at a rate slow enough that detrital clay and silt sized sediments, and organic material became interlaminated with the hydrothermal sediments. Near the center of the basin, precipitation of chert and sulfides predominated. As deeper and hotter fluids were tapped or as the conduit heated up, the proportion of reduced to oxidized sulfur increased as did the $\delta^{34}S$ of reduced sulfur. Massive quantities of sulfide were precipitated. Hotter fluids became bouyant enough to mix with overlying seawater, causing barite precipitation. A trajectory of increasing fO_2 and pH owing to mixing of the ore fluid with seawater is consistent with increasing $\delta^{34}S$ and the appearance of barite.

* * * * *

The ore textures in the Grum deposit are textures of metamorphic recrystallization related to Mesozoic metamorphism. Euhedral, subhedral, poikilitic and embayed metacrysts of pyrite are surrounded by less abundant matrix sulfides and are occasionally annealed and foliated. Framboidal pyrite is absent. Pyrrhotite and magnetite were pos-

sibly part of the primary mineral assemblage. Some relict chert occurs in the recrystallized quartz of quartzitic ore. Barite is recrystaltalized and annealed.

REFERENCES

Anger, G., Nielsen, H., Purchelt, H. and Ricke, W., 1966, Sulfur isotopes in the Rammelsberg oredeposit (Germany): Econ. Geol., v. 61, p. 511-536.

Anonymous, 1980, Mineral development accelerates in Yukon: Mining Journal, Feb. 8, 1980, p. 108.

Barton, P.B. and Skinner, B.J., 1979, Sulfide mineral stabilities, in H.L. Barnes, ed., Geochemistry of Hydrothermal Oredeposits, (2nd ed.): New York, Wiley, p. 278-403.

Brock, J.S., 1976, Recent developments in the Selwyn-Mackenzie zinc-lead province, Yukon and Northwest Territories: Western Miner, March 1976, p. 9-16.

Brock, J.S., 1973, Geophysical exploration leading to the discovery of the Faro deposit: Can. Mining Metallurgy (C.I.M.) Bull., Oct. 1973, p. 97-116.

Campbell, F.A., Ethier, V.G., Krouse, H.R. and Both, R.A., 1978, Isotopic composition of sulfur in the Sullivan ore body, British Columbia: Econ. Geol., v. 73, p. 246-268.

Campbell, F.A. and Ethier, V.G., 1974, Sulfur isotopes, iron content of sphalerites, and ore textures in the Anvil ore body, Canada: Econ. Geol., v. 69, p. 482-493.

Carne, R.C. and Cathro, R.J., 1980, Metallogeny and national significance of "sedimentary exhalative" zinc-lead-silver deposits of the Selwyn Basin: draft copy of paper presented at the C.I.M. Annual General Meeting, Toronto, Ontario, April 23, 1980, 21 p.

Carne, R.C., 1979, Upper Devonian stratiform barite-lead-zinc-silver mineralization at Tom claims, MacMillan Pass, Yukon Territory: unpbl. M.S. thesis, Univ. of Brit. Col., 149 p.

Carson, D.J.T., 1977, Geological and mineralogical investigations of the metallurgy of the Grum ore body, Yukon Territory: Geological assessment report, Toronto, 48 p.

Claypool, G.S., Holser, W.T., Kaplan, I.R., Sakai, H. and Zak, I., 1980, The age curves of sulfur and oxygen isotopes in marine sulfate and their mutual interpretation: Chem. Geol., v. 28, p. 199-260.

Coney, P.J., Jones, D.L. and Monger, J.W., 1980, Cordilleran suspect terranes: Nature, v. 288, p. 329-333.

Cyprus Anvil Mining Corporation, 1980, The Grum deposit: in-house report, 18 p.

Dawson, K.M., 1977, Regional metallogeny of the northern Cordillera: Report of activities, Part A: Geol. Surv. Can., Paper 77-1A, p. 1-4.

Douglas, R.J.W., Gabrielse, H., Wheeler, J.O., Stott, D.F. and Belyea, H.R., 1970, Geology of western Canada, in R,J,W, Douglas, ed. Geology and Economic Minerals of Canada: Geol Surv. Canada Econ. Geol. Report No. 1, p. 365-488.

Eisbacher, G.H., 1980, Sedimentary tectonics and glacial record in the Windermere Supergroup, Mackenzie Mountains, Northwestern Canada: Geol. Surv. Can., Paper 80-27, 40 p.

Finlow-Bates, T., 1980, The chemical and physical controls on the genesis of submarine exhalative orebodies and their implications for formulating exploration concepts, a review: Geol. Jahrb., Reihe D, Heft 40, p. 131-168.

----, 1979, Chemical mobilities in a submarine exhalative hydrothermal system: Chem. Geol., v. 27, p. 65-83.

Finlow-Bates, T. and Large, D., 1978, Water depth as a major control on the formation of submarine exhalative ore deposits: Geol. Jb., D. 30, p. 27-39, Hanover.

Gabrielse, H., 1976, Environments of Canadian Cordillera depositional basins, in Circum-Pacific Energy and Mineral Resources: Am. Assoc. Petr. Geol. Mem. 25, p. 492-502.

----, 1972, Younger Precambrian of the Canadian Cordillera: Amer. Jour. Sci., v. 272, p. 521-536.

----, 1967, Tectonic evolution of the Northern Canadian Cordillera: Can. Jour. Earth Sci., v. 4, p. 271-298.

Gustafson, L.B. and Williams, N., 1981, Sediment-hosted stratiform deposits of copper lead and zinc, in B.J. Skinner, ed., Seventy-fifth Anniversary Volume: Econ. Geol., p. 139-178.

Haas, J.L., 1971, The effect of salinity on the maximum thermal gradient of a hydrothermal system at hydrostatic pressure: Econ. Geol., v. 66, p. 551-556.

Holland, H.D. and Malinin, S.D., 1979, The solubility and occurrence of non-ore minerals, in H.L. Barnes, ed., Geochemistry of Hydrothermal Ore Deposits, (2nd ed.): New York, Wiley, p. 461-508.

Jennings, D.S., Jilson, G.A. and Pigage, L.C., 1980, Anvil Range Stratigraphy, southcentral Yukon Territory, in Programme and Abstracts, Cordilleran Section: Geol. Assoc. Can., p. 16-17.

Kalliokoski, J., 1965, Metamorphic features in North American massive sulfide deposits: Econ. Geol., v. 60, p. 485-505.

Kaplan, I.R. and Rittenberg, S.C., 1964, Microbiological fractionation of sulfur isotopes: J. Gen. Microbiol., v. 34, p. 195-212.

Krebs, W., 1979, Devonian basinal facies; in House, M.R., Scrittan, C.T., Bassett, M.G., eds., The Devonian System: Spec. Paper in Paleon., No. 23, London, p. 125-139.

----, 1978, Parameters controlling sedimentary stratiform sulphide-baryte deposits in the Rhenohercynic: unpublished lecture notes, 33 p.

----, 1976, Geology of European stratabound lead-zinc-copper deposits: Can. Soc. Petrol. Geol. Seminar, April 7, 8 and 9, 1976, Calgary, Alberta.

Kullerud, G. and Yoder, H.S., 1959, Pyrite stability relations in the Fe-S system: Econ. Geol., v. 54, p. 533-572.

Lambert, I.B., 1976, The McArthur zinc-lead-silver deposit: features metallogenesis and comparison with some other stratiform ores, in K.H. Wolf, (ed.) Handbook of strata-bound and stratiform ore deposits: Amsterdam, Elsevier, v. 2, p. 219-266.

----, 1973, Post-depositional availability of sulfur and metals and formation of secondary textures and structures in stratiform sedimentary sulphide deposits: J. Geol. Soc. Austr., v. 20, p. 205-215.

Lambert, I.B. and Sato, T., 1974, The Kuroko and associated ore deposits of Japan: a review of their features and metallogenesis: Econ. Geol., v. 69, p. 1215-1236.

Large, D.E., 1980, Geological parameters associated with sediment-hosted, submarine exhalative Pb-Zn deposits: an empirical model for mineral exploration: Geol. Jahrb. Reihe D, Heft 40, p. 59-130.

Mako, D.A., 1981, The geology and genesis of the stratiform zinc-lead-barite mineralization of the Vulcan property, Selwyn Basin Northwest Territories, Canada: unpubl. M.S. thesis, Univ. of Wisconsin, 180 p.

Mathias, B.V. and Clark, G.J., 1975, Mount Isa copper and silver-lead-zinc ore bodies--Isa and Hilton mines, in Knight, C.L., ed., Economic Geology of Australia and Papua New Guinea, I. Metals: Australian Inst. Mining Metallurgy Mon. 5, p. 351-372.

Monger, J.W.H., Price, R.A. and Templeman-Kluit, D.J., 1982, Tectonic accretion and the origin of the two major metamorphic and plutonic welts in the Canadian Cordillera: Geology, v. 10, p. 70-75.

Monger, J.W.H. and Price, R.A., 1979, Geodynamic evolution of the Canadian Cordillera - progress and problems: Can. Jour. Earth Sci., v. 16, p. 770-791.

Monger, J.W.H., Souther, J.G. and Gabrielse, H., 1972, Evolution of the Canadian Cordillera: a plate-tectonic model: Amer. Jour. Sci., v. 272, p. 577-602.

Morganti, J.M., 1979, The geology and oredeposits of the Howard's Pass area, Yukon and Northwest Territories: the origin of basinal sedimentary stratiform sulfide deposits: unpubl. Ph.D. thesis, Univ. of Brit. Colum., 327 p.

Mortensen, J.K., 1982, Geological setting and tectonic significance of Mississippian felsic metavolcanic rocks in the Pelly Mountains, southeastern Yukon Territory: Can. Jour. Earth Sci., v. 19, p. 8-22.

Ohmoto, H., 1972, Systematics of sulfur and carbon isotopes in hydrothermal ore deposits: Econ. Geol., v. 67, p. 551-578.

Ohmoto, H. and Rye, R.O., 1979, Isotopes of sulfur and carbon, in Barnes, H.L. (ed.), Geochemistry of Hydrothermal Ore Deposits, (2nd ed.): New York, Wiley, p. 509-567.

Orr, W.L., 1975, Geologic and geochemical controls on the distribution of hydrogen sulfide in natural gas: Geol. Soc. Am. Ann. Mtg. Prog., p. 1220-1221.

Paxton, J. and Po, A.Y., 1978, Geology report of Grum deposit Vangorda Creek area, Yukon Territory: Kerr Addison Mines Ltd., company report, Feb., 1978.

Pazour, D.A., 1979, Cyprus Anvil: Largest mine in the Yukon Territory: World Mining, July, 1979.

Phillips, S.L.,Igbene, A., Fair, J.A., Ozbek, H. and Tavana, M., 1981, A technical data book for geothermal energy utilization: Lawrence Berkeley Laboratory, University of California, Berkeley, 46 p.

Rees, C.E., 1978, Sulphur isotope measurement using SO_2 and SF_6: Geochim. Cosmochim. Acta, v. 42, p. 383-389.

Rye, R.O. and Ohmoto, H., 1974, Sulfur and carbon isotopes and ore genesis: a review: Econ. Geol., v. 69, p. 826-842.

Sakai, H. and Dickson, F.W., 1978, Experimental determination of the rate and equilibrium fractionation factors of sulfur isotope exchange between sulfate and sulfide in slightly acid solutions at 300°C and 1000 bars: Earth Planet. Sci. Letters, v. 39, p. 151-161.

Sangster, D.F., 1976, Sulphur and lead isotopes in stratobound deposits, in Wolf, ed., Handbook of stratabound and stratiform ore deposits: Amsterdam, Elsevier, v. 2, p. 219-266.

----, 1968, Relative sulphur isotope abundances of ancient seas and stratobound sulphide deposits: Geol. Assoc. Can. Proc., v. 19, p, 79-91.

Sato, T., 1972, Behavior of ore-forming solutions in seawater: Mining Geology, v. 22, p. 331-342.

Shanks, W.C., 1976, Geochemical and sulfur isotope study of Red Sea geothermal systems: unpublished Ph.D. thesis, University of Southern California.

Shanks, W.C., Bischoff, J.L. and Rosenbauer, R.J., 1981, Seawater sulfate reduction and sulfur isotope fractionation in basaltic systems: Interaction of seawater with fayalite and magnetite at 200-350°C: Geochim. Cosmochim. Acta, v. 45, p. 1977-1995.

Sibson, R.H., Moore, J.McM. and Rankin, A.H., 1975, Seismic pumping - a hydrothermal fluid transport mechanism: Jour. Geol. Lond., v. 131, p. 653-659.

Sirola, W.M., 1975, The Grum deposit: Western Miner, Dec. 1975, p. 9-13.

Smith, J.W. and Croxford, N.J.W., 1973, Sulfur isotope ratios in the McArthur lead-zinc-silver deposit: Nature, v. 245, p. 10-12.

Stanton, R.L., 1972, Ore Petrology: McGraw Hill, New York, 713 p.

Templeman-Kluit, D.J., 1977, Stratigraphic and structural relations between the Selwyn Basin, Pelly Cassiar Platform and Yukon Crystalline Terrane in the Pelly Mountains, Yukon: Report of Activities, Geol. Surv. Can., Paper 77-1A, p. 223-227.

----, 1972, Geology and origin of the Faro, Vangorda and Swim concordant zinc-lead deposits, central Yukon Territory: Geol. Soc. Can. Bull. 208, 73 p.

Templeman-Kluit, D.J. and Blusson, S.L., 1977, Pelly Cassiar Platform and Selwyn Basin: neither without the other, in Programme and Abstracts: Geol. Assoc. Can., 1977 Ann. Mtg. v. 2, p. 52.

Thompson, R.I. and Panteleyev, A., 1976, Stratabound mineral deposits of the Canadian Cordillera, in Wolf, K.H. (ed.) Handbook of stratabound and stratiform ore deposits: Amsterdam, Elsevier, v. 5, p. 37-108.

Turner, J.S. and Gustafson, L.B., 1978, The flow of hot saline solutions from vents in the sea floor--some implications for exhalative massive sulfide and other ore deposits: Econ. Geol., v. 73, p. 1082-1100.

Vokes, F.M., 1969, A review of the metamorphism of sulfide deposits: Earth Sci. Rev., v. 5, p. 99-143.

Wheeler, J.O., Aitken, J.D., Berry, M.D., Gabrielse, H., Hutchison, W.W., Jacoby, W.R., Monger, J.W.H., Niblett, E.R., Norris, D.K., Price, R.A. and Stacey, R.A., 1972, The Cordilleran structural province, in Price, R.A. and Douglas, J.W. (eds.), Variations in Tectonic Styles in Canada: Geol. Assoc. Can. Spec. Paper No. 11, p. 1-82.

APPENDIX I

LITHOLOGIC CODE

VANGORDA FORMATION

Unit 5	5-A	Variably calcareous, graphitic phyllite
	B	Calcareous muscovite-chlorite$\pm$biotite phyllite
	C	Metabasite
	D	Laminarly banded, variably calcareous, chloritic phyllite
	E	Phyllitic marble and silicated marble
	F	Chloritic phyllite

Modifiers for Unit 5

1	Siliceous
2	Carbonaceous
3	Calcareous
4	Altered, pyritic (white mica envelope)
5	Banded/laminated
6	Non-Calcareous
7	Tuffaceous
8	Chloritic
9	Sulfide-bearing
0	Normal

SULFIDE DEPOSITS

Unit 4	4-A	Sulfide-bearing, ribbon-banded, graphitic quartzite
	B	Pyrite-free quartzite (may contain base metal sulfides)
	C	Base metal-poor, pyritic quartzite
	D	Base metal-bearing, pyritic quartzite
	E	Massive pyritic sulfides
	F	Buckshot facies, massive sulfides (Faro)
	G	Baritic facies, massive sulfides/ sulfates ($>10\%$ $BaSO_4$)
	H	Pyrrhotitic facies, massive sulfides
	J	Non-pyritic, massive sulfides/oxides
	K	Anderite-bearing, massive pyritic sulfides

Modifiers for Unit 4

1	Siliceous
2	Coarse, porphyroblastic pyrite-bearing
3	Fine pyrite/marcasite-bearing
4	Sphalerite and/or galena-bearing
5	Carbonaceous

APPENDIX I (continued)

Modifiers for Unit 4 (continued)

6 Barite-bearing
7 Pyrrhotite-bearing
8 Magnetite-bearing
9 Chalcopyrite-bearing
0 Normal

Unit 4 4-L Muscovite > qtz-chl phyllite (generally sulfide-bearing)

Modifiers for 4L

1 Siliceous
2 Pyrite-bearing
3 Talc-bearing (white mica envelope)
4 Sphalerite and/or galena bearing
5 Carbonate-bearing
6 Chlorite > quartz-muscovite phyllite
7 Pyrrhotite-bearing
8 Magnetite-bearing
9 Chalcopyrite-bearing
0 Normal

MT. MYE FORMATION

Unit 3 3-A Transition zone
B Chloritic phyllite/schist
C Metabasite
D Calc-silicate phyllite/schist
E Graphitic phyllite/schist
F Marble and silicated marble
G Non-calcareous, muscovite-chlorite±biotite phyllite/schist
H Tuffaceous calc-silicate phyllite/schist (assoc. with 3D)
I Graphitic quartzite in non-calcareous phyllite/schist

Modifiers for Unit 3

1 Siliceous
2 Non-calcareous
3 Calcareous
4 Altered, pyritic (white mica envelope)
5 Banded/laminated
6 Sulfide-bearing
7 Tuffaceous
8 Chloritic
9 Carbonaceous
0 Normal

APPENDIX II

GRUM SULFUR ISOTOPE DATA

Sulfur isotope data are reported by cross section and drill hole.

Column headings are explained below:

DDH - diamond drill hole number

Depth - Depth refers to distance between the collar of the hole and the location of the sample. For holes drilled up from the underground workings, depth increases upward. All intersections are presented with the interpreted stratigraphic top up regardless of the real position in space or the angle of the drill hole.

Sample numbers (consisting of the DDH number and the depth) are listed in Appendix III with the corresponding UW file number.

Lithology - Lithologic code is presented in Appendix I.

Assay values - Cu, Pb, Zn and Ag values are from Cyprus Anvil Mining Corporation assays for two meter intervals which encompass the chosen sample. In most cases the assay values are fair approximations of the metal content in the analyzed sample because an attempt was made to choose samples visually representative of the interval.

$S_{T.S.}$ (%) - percent of total sulfide sulfur within the sample calculated from oxidation of bulk sulfide fraction.

S_{py} (%) - percent of sulfide from pyrite within the sample calculated from chemical extraction.

$\delta^{34}S_{py,sl,gn,bs,ba}$ - $\delta^{34}S$ values from pyrite, sphalerite, galena, bulk sulfide and barite reported in per mil relative to Canon Diable Troilite.

Table II-1. Grum--Cross Section 66 West.

DDH	Depth (m)	Lithology	Cu %	Pb %	Zn %	Ag gm/mt	$S_{T.S.}$ %	S_{py} %	$\delta^{34}S_{py}$	$\delta^{34}S_{bs}$	$\delta^{34}S_{ba}$
A99	140.5	4E4	.10	9.50	6.10	137	26.63	12.90	21.87	20.15	---
A99	142.1	4G4	.13	3.40	5.90	62	25.28	6.74	15.52	15.47	30.60
A99	145.3	4E4	.23	3.10	3.70	50	31.24	26.86	13.30	13.41	---
A99	153.5	4G4	.04	0.30	8.30	83	21.70	4.06	19.68	16.53	32.01
A99	154.5	4E8	.24	4.10	3.00	79	40.36	31.27	14.83	15.21	---
A99	157.1	4C0	.28	1.04	0.42	28	27.02	28.95	14.77	14.78	---
A99	162.1	4CE	.24	0.10	0.09	3	15.46	22.37	13.81	13.99	---
A99	169.5	4C7	.28	0.61	0.90	9	32.84	25.04	15.14	15.34	---
A99	178.1	4L4	.08	0.32	0.50	8	12.29	11.51	16.37	16.25	---
A109	136.1	4G4	.04	6.90	10.30	104	21.80	---	---	18.10	32.14
A109	147.8	4E48	.10	16.20	10.30	172	14.22	---	---	16.91	---
A109	149.0	4A3	.09	4.10	4.50	54	10.56	---	---	15.42	---
A109	154.3	4L1	---	---	---	---	5.34	---	---	14.85	---
A109	155.8	4L218	---	---	---	---	14.55	---	---	17.13	---
A135	139.7	4G48	.06	4.50	6.30	68	13.01	---	---	19.01	31.71
A135	146.9	4E0	.19	8.60	6.90	118	25.50	---	---	15.81	---
A135	148.6	4D4	.17	11.60	5.10	145	18.86	---	---	12.87	---
A135	150.8	4C0	.19	1.03	1.11	22	18.19	---	---	17.45	---
A135	152.5	4A31	.19	0.47	0.58	12	10.97	---	---	16.54	---

Table II-2. Grum--Cross Section 74 West.

DDH	Depth (m)	Lithology	Cu %	Pb %	Zn %	Ag gm/mt	$S_{T.S.}$ %	$^{34}S_{py}$	$\delta^{34}S_{sl}$	$\delta^{34}S_{gn}$	$\delta^{34}S_{bs}$	$\delta^{34}S_{ba}$
U15	9.3	4L17	---	---	---	---	6.18	---	---	---	12.54	---
U15	24.7	4E48	.23	3.00	2.70	64	29.96	---	14.28	14.12	15.85	---
U15	27.4	4G4*	.14	6.50	6.20	86	10.29	---	---	---	20.25	35.16
U15	27.9	4E48	.22	7.60	6.30	105	28.57	15.92	---	---	16.37	---
U15	28.8	4G4	.12	11.40	7.00	158	33.43	---	15.51	---	19.17	---
U15	29.3	4L74	.25	3.00	2.80	39	16.90	---	---	---	14.55	---
U28	17.4	4L9	.40	4.10	4.60	61	15.16	---	---	---	15.50	---
U43	22.2	4E46	.08	7.50	14.20	136	30.74	---	---	---	16.66	---
U43	21.6	4AD	.01	6.80	13.10	109	16.74	---	---	---	16.11	---
U43	20.2	4E14	.01	8.40	14.60	144	31.50	---	---	---	14.37	---
U43	18.6	4E4	.10	12.60	32.40	202	28.81	---	---	---	16.53	---
U43	13.4	4E14	---	---	---	---	23.45	---	---	---	15.76	---
U43	11.1	4A4	---	---	---	---	14.95	---	---	---	19.02	---
U43	6.8	4CL	---	---	---	---	14.05	---	---	---	15.95	---

Table II-3. Grum--Cross Section 80 West.

DDH	Depth (m)	Lithology	Cu %	Pb %	Zn %	Ag gm/mt	$S_{T.S.}$ %	S_{py} %	$\delta^{34}S_{py}$	$\delta^{34}S_{sl}$	$\delta^{34}S_{gn}$	$\delta^{34}S_{bs}$	$\delta^{34}S_{ba}$
A24	328.9	4D4	.02	9.50	15.70	125	16.85	3.98	11.77	10.83	9.41	10.52	---
A24	329.5	4G4	.03	2.70	6.00	46	31.85	---	---	---	---	15.98	31.23
A24	330.3	4C0	.06	3.20	6.70	63	27.09	---	---	---	---	15.75	---
A24	331.8	4B4	.05	6.70	15.80	112	19.35	4.85	15.77	14.27	12.37	13.99	---
A24	333.1	4E4	.27	4.60	7.00	75	40.95	---	---	---	---	15.77	---
A24	335.2	4E4	.27	5.80	7.90	91	44.50	42.84	15.26	14.41 (sl+gn)		15.09	---
A24	337.1	4D4	.12	5.60	13.80	111	18.96	5.79	16.64	15.55	14.46	15.88	---
A24	338.6	4E4	.29	6.00	8.80	100	32.70	14.62	16.90	15.29	---	15.74	---
A24	340.8	4A14	.03	4.70	9.10	68	13.70	5.60	14.88	13.38	---	13.59	---
A24	341.4	4E4	.22	5.60	7.80	86	32.55	---	---	13.95	12.70	14.50	---
A24	342.9	4A41	.08	6.30	14.80	132	16.82	12.47	13.53	---	---	13.09	---
A24	343.5	4D4	.08	6.30	14.30	120	30.02	---	---	13.77	13.29	14.08	---
U142	122.7	4G0	.17	3.00	5.40	64	35.72	14.44	19.18	---	---	14.01	---
U142	117.9	4E46	.14	4.70	8.10	91	44.79	36.76	19.57	---	---	15.29	---
U142	108.0	4A0	.20	0.05	0.20	26	30.47	25.82	15.49	---	---	19.34	---
U142	96.5	4L12	---	---	---	---	11.25	7.26	14.04	---	---	19.18	---
U151	18.2	4E4	.20	5.50	6.00	92	---	---	---	15.41	---	---	---
U151	16.4	4DA	.22	9.70	10.90	151	---	---	---	14.39	---	---	---
U151	13.9	4A41	.13	2.90	6.50	56	14.44	---	---	14.11	---	14.27	---
U151	11.3	4A41	.03	2.50	4.40	44	---	---	---	17.52	---	---	---
U151	6.3	4B45	.07	0.12	0.15	6	---	---	---	16.09	---	---	---
U151	5.6	4E4	.04	4.70	5.80	62	---	---	---	16.43	---	---	---
U151	1.8	4E4	.15	6.30	10.80	102	---	---	---	14.32	13.58	---	---

Table II-3 (continued)

DDH	Depth (m)	Lithology	Cu %	Pb %	Zn %	Ag gm/mt	$S_{T.S.}$ %	S_{py} %	$\delta^{34}S_{py}$	$\delta^{34}S_{sl}$	$\delta^{34}S_{gn}$	$\delta^{34}S_{bs}$	$\delta^{34}S_{ba}$
U151	64.2	4KO	.65	7.60	6.20	137	48.03	---	---	---	---	11.56	---
U151	60.6	4E48	.15	13.40	12.30	177	31.89	---	---	---	---	18.34	---
U151	59.0	4EO	.17	3.90	3.40	57	49.11	---	---	---	---	13.24	---
U151	58.0	4G4	.05	10.70	11.10	182	13.79	---	---	---	---	17.20	32.57
U151	55.2	4G4	.13	9.00	8.40	134	18.97	---	---	---	---	15.57	---
U153	41.3	4G4	.29	7.00	9.40	136	35.36	---	---	---	---	15.63	29.48
U153	37.4	4G4	.25	6.10	7.70	115	27.40	---	---	12.20	---	12.94	27.95
U153	33.9	4E41	.07	11.50	19.60	185	30.57	10.99	19.16	18.72	---	18.12	---
U153	32.8	4A4	.20	5.70	7.40	122	26.16	---	---	14.80	---	14.62	---
U153	31.2	4E4	.28	6.00	9.30	103	37.00	---	---	15.88	---	16.04	---
U153	29.8	4EO	.25	1.82	1.78	36	48.90	---	16.28	---	---	15.66	---
U153	27.8	4A41	.13	3.80	7.60	69	12.90	3.44	17.10	14.64	---	15.51	---
U153	25.5	4EO	.27	0.83	1.56	25	35.69	---	---	---	---	16.11	---
U153	21.5	4A41	.11	1.90	4.10	36	8.73	---	---	---	---	15.95	---
U153	19.0	4A41	.03	1.62	4.30	35	15.59	---	---	18.61	---	19.54	---
U153	17.7	4A31	.06	1.63	3.80	38	29.87	---	---	---	---	23.13	---
U153	8.8	4A41	.06	4.80	12.70	82	15.25	---	---	15.81	---	15.54	---

APPENDIX III - SAMPLES REFERENCED IN THESIS

U.W. File No.	Sample No. (DDH and depth)	Type of Speciman[1]
U.W. 1743/1	A99-140.5	pt,rc
2	A99-142.1	pt,rc
3	U15-24.7	pt,rc
4	U15-27.4	pt,rc
5	A24-331.8	pt,rc
6	A24-338.6	pt,rc
7	A24-343.5	pt,rc
8	U151-13.9	pt,rc
9	U151-60.6	pt,rc
10	U153-8.8	pt,rc
11	A38-642	t,rc
12	A117-204.6	t,rc
13	A77-995	t,rc
14	A19-250	t,rc
15	U156-71.7	t,rc
16	U153-40.6	pt,rc
17	U150-138.9	pt,rc
18	U15-115.3	pt,rc
19	U146-38.8	t,rc
20	A11-217	t,rc
21	U143-113	pt,rc
22	U142-61.4	dc
23	A77-972	dc
24	A109-59.0	dc
25	U150-70.3	dc
26	A27-269	dc
27	A121-148.5	dc
28	A79-276	dc
29	A135-157.8	dc
30	U15-114.3	dc
31	U151-3.7	dc
32	A38-1156.5	dc
33	U156-57.7	dc
34	A135-137.1	dc
35	U39-82.5	dc
36	U39-32.7	dc
37	A11-113.3	dc
38	A32-920	dc
39	U150-107.9	dc
40	A79-974.3	dc
41	U153-53.4	dc

[1] pt = polished thin section; t = thin section; rc = rock chip; dc = drill core